

Dottorato di Ricerca in Ingegneria Civile
Graduate School in Civil Engineering

Sede: Facoltà di Ingegneria - Università di Pavia - via Ferrata 1 - 27100 Pavia - Italy

Dottorato di Ricerca in Ingegneria Civile VIII Nuova serie (XXII
Ciclo)

**Using Satellites Systems for
Structural Monitoring:
Accuracy, Uncertainty and Reliability**

Tesi di Dottorato
Ing. Clemente Fuggini

Relatore:
Prof. Fabio Casciati

Controrelatore:
Prof. Andrea Del Grosso

October 2009

To Santino, Mariuccia, Ettore

Dottorato di Ricerca in Ingegneria Civile

| | |
|---|--|
| Settore: Field: | Ingegneria Engineering |
| Sede Amministrativa non consortile: Administrative location: | Università degli Studi di PAVIA University of Pavia |
| Durata del dottorato: Duration: | 3 anni 3 years |
| Periodo formativo estero: Period in foreign organization: | come previsto dal regolamento del Dottorato di Ricerca as required by the school's rules |
| Numero minimo di corsi: Minimum number of courses: | 6 6 |

Recapiti - Adresses



Dipartimento di Meccanica Strutturale
via Ferrata 1 - 27100 Pavia - Italy
Tel. 0382 / 505450 Fax 0382 / 528422



Dipartimento di Ingegneria Idraulica e Ambientale
via Ferrata 1 - 27100 Pavia - Italy
Tel. 0382 / 505300 Fax 0382 / 505589

Coordinatore – Coordinator

CASCIATI Fabio - Professore Ordinario di Scienza delle Costruzioni (ICAR/08)

Dipartimento di Meccanica Strutturale
via Ferrata 1 - 27100 Pavia – Italy Tel. 0382 / 505458 Fax 0382 / 528422
e-mail: fabio@dipmec.unipv.it

Collegio dei Docenti – Teaching Staff

| | |
|--------------------|---------------------------------------|
| CIAPONI Carlo | Professore Straordinario (ICAR/02) |
| DEL GROSSO Andrea | Professore Ordinario, Unige (ICAR/09) |
| FARAVELLI Lucia | Professore Ordinario (ICAR/08) |
| GALLATI Mario | Professore Ordinario (ICAR/01) |
| GOBETTI Armando | Professore Associato (ICAR/08) |
| MOISELLO Ugo | Professore Ordinario (ICAR/02) |
| PAPIRI Sergio | Professore Associato (ICAR/02) |
| SALA Roberto | Professore Associato (ING-IND/08) |
| MARCELLINI Alberto | Dirigente di Ricerca. CNR – Milano |

Organizzazione del corso

Il dottorato di ricerca in *Ingegneria Civile* presso la Scuola di Dottorato in Scienze dell'Ingegneria dell'Università degli Studi di Pavia è stato istituito nell'anno accademico 1994/95 (X ciclo).

Il corso consente al dottorando di scegliere tra quattro curricula: idraulico, sanitario, sismico e strutturale. Il dottorando svolge la propria attività di ricerca presso il Dipartimento di Ingegneria Idraulica e Ambientale per i primi due curricula o quello di Meccanica Strutturale per gli ultimi due.

Durante i primi due anni sono previsti almeno sei corsi, seguiti da rispettivi esami, che il dottorando è tenuto a sostenere. Il Collegio dei Docenti, composto da professori dei due Dipartimenti e da alcuni esterni all'Università di Pavia, organizza i corsi con lo scopo di fornire allo studente di dottorato opportunità di approfondimento su alcune delle discipline di base per le varie componenti. Corsi e seminari vengono tenuti da docenti di Università nazionali ed estere.

Il Collegio dei Docenti, cui spetta la pianificazione della didattica, si è orientato ad attivare ad anni alterni corsi sui seguenti temi:

- Meccanica dei solidi e dei fluidi
- Metodi numerici per la meccanica dei solidi e dei fluidi
- Rischio strutturale e ambientale
- Metodi sperimentali per la meccanica dei solidi e dei fluidi
- Intelligenza artificiale

più corsi specifici di indirizzo.

Al termine dei corsi del primo anno il Collegio dei Docenti assegna al dottorando un tema di ricerca da sviluppare sotto forma di tesina entro la fine del secondo anno; il tema, non necessariamente legato all'argomento della tesi finale, è di norma coerente con il curriculum, scelto dal dottorando.

All'inizio del secondo anno il dottorando discute con il Coordinatore l'argomento della tesi di dottorato, la cui assegnazione definitiva viene deliberata dal Collegio dei Docenti.

Alla fine di ogni anno i dottorandi devono presentare una relazione particolareggiata (scritta e orale) sull'attività svolta. Sulla base di tale relazione il Collegio dei Docenti, "previa valutazione della assiduità e dell'operosità dimostrata dall'iscritto", ne propone al Rettore l'esclusione dal corso o il passaggio all'anno successivo.

Il dottorando può svolgere attività di ricerca sia di tipo teorico che sperimentale, grazie ai laboratori di cui entrambi i Dipartimenti dispongono, nonché al Laboratorio Numerico di Ingegneria delle Infrastrutture.

Il "Laboratorio didattico sperimentale" del Dipartimento di Meccanica Strutturale dispone di:

1. una tavola vibrante che consente di effettuare prove dinamiche su prototipi strutturali;
2. opportuni sensori e un sistema di acquisizione dati per la misura della risposta strutturale;
3. strumentazione per la progettazione di sistemi di controllo attivo e loro verifica sperimentale;
4. strumentazione per la caratterizzazione dei materiali, attraverso prove statiche e dinamiche.

Il laboratorio del Dipartimento di Ingegneria Idraulica e Ambientale dispone di:

1. un circuito in pressione che consente di effettuare simulazioni di moto vario;
2. un tunnel idrodinamico per lo studio di problemi di cavitazione;
3. canalette per lo studio delle correnti a pelo libero.

Course Organization

The Graduate School of Civil Engineering, a branch of the Doctorate School in Engineering Science, was established at the University of Pavia in the Academic Year of 1994/95 (X cycle). The School allows the student to select one of the four offered curricula: Hydraulics, Environment, Seismic Engineering and Structural Mechanics. Each student develops his research activity either at the Department of Hydraulics and Environmental Engineering or at the Department of Structural Mechanics. During the first two years, a minimum of six courses must be selected and their examinations successfully passed. The Faculty, made by Professors of the two Departments and by internationally recognized external scientists, organizes courses and provides the students with opportunities to enlarge their basic knowledge. Courses and seminars are held by University Professors from all over the country and abroad. The Faculty starts up, in alternate years, common courses on the following subjects:

- solid and fluid mechanics,
- numerical methods for solid and fluid mechanics,
- structural and environmental risk,
- experimental methods for solid and fluid mechanics,
- artificial intelligence.

More specific courses are devoted to students of the single curricula.

At the end of each course, for the first year the Faculty assigns the student a research argument to develop, in the form of report, by the end of the second year; the topic, not necessarily part of the final doctorate thesis, should be consistent with the curriculum selected by the student. At the beginning of the second year the student discusses with his Coordinator the subject of the thesis and, eventually, the Faculty assigns it to the student. At the end of every year, the student has to present a complete report on his research activity, on the basis of which the Faculty proposes to the Rector his admission to the next academic year or to the final examination. The student is supposed to develop either

theoretical or experimental research activities, and therefore has access to the Department Experimental Laboratories, even to the Numerical Laboratory of Infrastructure Engineering. The Experimental Teaching Laboratory of the Department of Structural Mechanics offers:

1. a shaking table which permits one to conduct dynamic tests on structural prototypes;
2. sensors and acquisition data system for the structural response measurements;
3. instrumentation for the design of active control system and their experimental checks;
4. an universal testing machine for material characterization through static and dynamic tests.

The Department of Hydraulics and Environmental Engineering offers:

1. a pressure circuit simulating various movements;
2. a hydrodynamic tunnel studying cavitation problems;
3. a micro-channels studying free currents.

Acknowledgments

The author wishes to express all his deep gratitude and appreciation to his advisor, Prof. Fabio Casciati, for his patient guidance, for his scientific knowledge and human experience during the preparation of this thesis.

The author wishes to express all his deep gratitude to Prof. Lucia Faravelli for her constant support and her human experience during the PhD studies.

The author would like to thank Prof. Andrea Del Grosso, for his valuable suggestions in the evaluation of this work.

The fruitful collaboration with Mr. Raed Alsaleh from University of Pavia, which contributed to improve this work, is totally acknowledged by the author.

Acknowledgements are also expressed to the Company Leica Geosystems for providing the sensors installation and the technical support.

Elenco delle tesi – Previous PhD Theses

- Marco Battaini (X ciclo) Sistemi strutturali controllati: progettazione e affidabilità. (February 1998).
- Claudia Mariani (X ciclo) Problemi di ottimizzazione per strutture bidimensionali anisotrope. (February 1998).
- Antonella Negri (X ciclo) Stima delle perdite idrologiche nei bacini di drenaggio urbani. (February 1999).
- Aurora Angela Pisano (XI ciclo) Structural System Identification :Advanced Approaches and Applications. (February 1999).
- Carla Saltalippi (XI ciclo) Preannuncio delle piene in tempo reale nei corsi d'acqua naturali. (February 1999).
- Eugenio Barbieri (XI ciclo) Thermo fluid Dynamics and Topology: Optimization of an Active Thermal Insulation Structure. (February 2000).
- Barbolini Massimiliano (XII ciclo) Dense Snow Avalanches: Computational Models, Hazard Mapping and Related Uncertainties. (February 2000).
- Espa Paolo (XII ciclo) Moti atmosferici generati da forze di galleggiamento: simulazioni numeriche e studio su modello fisico. (February 2000).
- Petrini Lorenza (XII ciclo) Shape Memory Alloys: Modelling the Martensitic Phase Behaviour for Structural Engineering Exploitation. (February 2000).

- Podestà Stefano (XIV ciclo) Risposta sismica di antichi edifici religiosi: una nuova proposta per un modello di vulnerabilità. (February 2002).
- Sturla Daniele (XIV ciclo) Simulazioni lagrangiane di flussi rapidamente variati nell'approssimazione di acque poco profonde. (February 2002).
- Marazzi Francesco (XV ciclo) Semi -active Control of Civil Structures: Implementation Aspects. (February 2003).
- Nascimbene Roberto (XV ciclo) Sail Modelling for Maximal Speed Optimum Design. (February 2003).
- Giudici Massimo (XVI ciclo) Progettazione in regime non lineare di strutture in CAP a cavi aderenti e non aderenti. (February 2004).
- Mutti Matteo (XVI ciclo) Stability Analysis of Stratified Three—phase Flows in Pipes. (February 2004).
- Petaccia Gabriella (XVI ciclo) Propagazione di onde a fronte ripido per rottura di sbarramenti in alvei naturali. (February 2004).
- Casciati Sara (XVII ciclo) Damage Detection and Localization in the Space of the Observed Variables. (February 2005).
- D'Amico Tiziana (XVI ciclo) Ricerca e sviluppo di metodologie diagnostiche per il recupero di edifici monumentali: prove vibroacustiche sul tufo. (February 2005).
- Barco Olga Janet (XVII ciclo) Modeling the Quantity and Quality of Storm Water Runoff Using SWMM. (February 2005).

| | |
|--|--|
| Boguniewicz Joanna (XVIII ciclo) | Integration of Monitoring and Modelling in the Surface Water State Evaluation Process of a Sub-Alpine Lake Watershed. (February 2006). |
| Bornatici Laura (XVIII ciclo) | L'impiego degli algoritmi generici per la risoluzione dei problemi di progetto di reti di distribuzione idrica. (February 2006). |
| Collivignarelli Maria Cristina (XVIII ciclo) | Trattamento di rifiuti liquidi mediante processi biologici aerobici termofili e mesofili e processi avanzati di ossidazione chimica in diversa. (February 2006). |
| Domaneschi Marco (XVIII ciclo) | Structural Control of Cable-stayed and Suspended Bridges. (February 2006). |
| Ráduly Botond (XVIII ciclo) | Artificial Neural Network applications in Urban Water Quality Modeling. (February 2006). |
| Cappabianca Federica (XVIII ciclo) | La valutazione del rischio valanghivo attraverso la modellazione dinamica. (February 2006). |
| Callegari Arianna (XVIII ciclo) | Applicazione di tecnologie di monitoraggio on-line per la gestione dei processi di trattamento reflui. (February 2006). |
| Gazzola Elisa (XVIII ciclo) | Applicazione di processi biologici anaerobici al trattamento di acque reflue e fanghi di depurazione: aspetti tecnici ed energetici. (February 2006). |
| Antoci Carla (XVIII ciclo) | Simulazione numerica dell'interazione fluido-struttura con la tecnica SPH. (July 2006). |
| Giuliano Fabio (XIX ciclo) | Performance Based Design and Structural Control for Cable Suspension Bridges. (February 2007). |
| Maranca Federica (XVIII ciclo) | Valutazione del ciclo di vita (LCA): confronto tra sistemi di trasporto gas via gasdotto. |

- (February 2007).
- Falappi Stefano (XIX ciclo) Simulazioni numeriche di flussi di fluidi viscosi e materiali granulari con la tecnica SPH (February 2007).
- Zanaboni Sabrina (XIX ciclo) Pre-trattamento di rifiuti liquidi industriali mediante ossidazione ad umido. (February 2007).
- Matteo Bruggi (XX ciclo) Topology optimization using mixed finite elements. (February 2008).
- Gian Paolo Cimellaro (XX ciclo) Passive Control of Industrial Structures for Natural Hazard Mitigation: Analytical Studies and Applications. (February 2008).
- Alessandro Abbà (XXI ciclo) Il recupero dei rifiuti speciali nel settore delle costruzioni: studio delle possibilità di recupero e valutazione dei meccanismi di lisciviazione. (February 2009).
- Karim Hamdaoui (XXI ciclo) Experimental Applications on Cu-based Shape Memory Alloys: Retrofitting of Historical Monuments and Base Isolation (February 2009).
- Thomas Messervey (XXI ciclo) Integration of Structural Health Monitorin into the Design, Assessment, and Management of Civil Infrastructure (February 2009).
- Filippo Ubertini (XXI ciclo) Wind Effects on Bridges: Response, Stability and Control (February 2009).

Index

| | |
|---|---------|
| Introduction and main motivation | pag. 1 |
| <i>Motivation and summary</i> | pag. 3 |
| | |
| Chapter 1 | |
| Basic Aspects of GPS Technology | |
| Introduction | pag. 7 |
| 1.1. GPS Overview | pag. 7 |
| 1.1.1. GPS History | pag. 8 |
| 1.1.2. GPS System Overview | pag. 8 |
| 1.2. GPS System Segments | pag. 10 |
| 1.2.1. Space Segment | pag. 11 |
| 1.2.2. Control Segment | pag. 13 |
| 1.2.3. User Segment | pag. 13 |
| 1.3. GPS Signal Characteristics | pag. 17 |
| 1.4. GPS performance | pag. 22 |
| 1.4.1. GPS governing relations | pag. 23 |
| 1.4.2. Differential Global Positioning System | pag. 36 |
| 1.5. Conclusions | pag. 39 |

Chapter 2

Overview of GPS Applications in Civil Engineering

| | |
|--|---------|
| Introduction | pag. 41 |
| 2.1. Overview of full-scale GPS applications | pag. 43 |
| 2.2. GPS-based structural monitoring of long spans bridges | pag. 44 |
| 2.3. GPS-based structural monitoring of tall buildings | pag. 59 |
| 2.4. Conclusions | pag. 71 |

Chapter 3

GPS Precision in Static and Dynamic Tests

| | |
|-------------------------------|----------|
| Introduction | pag. 73 |
| 3.1. The experimental mock-up | pag. 73 |
| 3.2. Experimental results | pag. 76 |
| 3.2.1. Static tests | pag. 77 |
| 3.2.2. Dynamic tests | pag. 97 |
| 3.3. Conclusions | pag. 116 |

Chapter 4

Full scale GPS-Based SHM of an Industrial Steel Building

| | |
|--|----------|
| Introduction | pag. 117 |
| 4.1. Overview of the full scale tests | pag. 118 |
| 4.2. Long duration record results | pag. 121 |
| 4.2.1. Data processing of GPS records | pag. 123 |
| 4.2.2. Resolution | pag. 131 |
| 4.3. Results from short duration records | pag. 134 |

| | |
|---|---------|
| 4.3.1. Short duration records data processing | pag.137 |
| 4.3.2. GPS vs. accelerometers results comparison | pag.138 |
| 4.3.3. Structural identification for impact and deceleration force | pag.147 |
| 4.4. Conclusions | pag.157 |

Chapter 5

Full scale GPS-based SHM of a super tall tower

| | |
|---|---------|
| Introduction | pag.159 |
| 5.1. Experimental configuration of the GNTVT | pag.160 |
| 5.2. Data processing of records during Nuri and Hagupit typhoon events | pag.162 |
| 5.2.1. Data processing: torsional effects | pag.165 |
| 5.3. Data processing in the absence of a significant wind event | pag.175 |
| 5.4. Conclusions | pag.186 |

| | |
|----------------------------------|---------|
| Conclusions and Synthesis | pag.189 |
|----------------------------------|---------|

| | |
|---------------------|---------|
| Bibliography | pag.193 |
|---------------------|---------|

INTRODUCTION AND MAIN MOTIVATION

The potential of a GPS-Based Structural Monitoring is studied within the thesis, with focus on accuracy, uncertainty and reliability.

In the last years, the request of sensors which operate in all wheater conditions independently from temperature variations and able to provide in real time direct measurements of structural tri-axial displacements is growing. To match the constraints listed above many techniques have been developed and studied. One of these, based on Satellite Positioning Systems, is receiving more and more interest by the scientific community.

Since their first military applications on the early 70th, the Global Navigation Satellite Systems (GNSS) are proving to be useful for civil applications, as the ones concerning civil engineering problems, related to monitoring applications of complex structural systems (such as suspension and cable stayed bridges, tall building, skyscraper, etc.).

Among all the Satellite Systems (the Russian Glonass, the future European Galileo, the Chinese BeiDou, and the Japanese QZSS), the America Global Positioning System (GPS) is now an alternative to standard sensors in order to detect the dynamic response of the previous mentioned long-period structures.

This thesis try to go deeper in some characteristics that can make the GPS useful for civil engineering applications. It starts from the basic principles of GPS, shows some recent full-scale applications, analyzes the effectiveness and the reliability of the GPS. Some topic problems, such as the dependence on the satellite constellation configuration, the influence of objects close to the sensors, the ability to detect movements induced by long period actions as well as by short period excitations are addressed.

These aspects are developed and discussed in five chapters:

Chapter 1 presents an overview of the Global Positioning System (GPS) for precise applications. A review of the positioning systems allowed by GPS, their governing relations, as well as the receiver types and receiver tasks are provided

as the basis for the developments of the following chapters. The so called “geometric dilution of precision” is also introduced.

Chapter 2 gives an overview of some recent GPS applications in the field on civil engineering, focusing on the dynamic SHM of long-period structures such as long bridges and tall buildings and describing for each specific application the monitoring system, the sensors network, the accuracy reached in terms of displacements and frequencies detected.

Chapter 3 investigates the reliability and the accuracy of the measurements of dual frequency GPS receivers for experimental static and dynamic tests when the GPS system is made by a fixed reference receiver and a moving one. This chapter provides answers to some questions as the GPS precision, the GPS signal stability, the GPS dependence on the orientation of the line connecting a fixed (reference) with a moving (rover) receiver.

Chapter 4 analyzes the effectiveness of a GPS-Based Structural Monitoring solution in full scale tests. The steel building which hosts the authors laboratory is the case-study within this chapter. Natural (i.e., wind actions) and man made (i.e., internal bridge crane movements) dynamic actions are considered. It is proved the effectiveness of GPS measurements in long duration actions (at low frequencies) as well as in short duration actions (at high frequencies).

Chapter 5, finally, describes the GPS use into a full-scale monitoring system of a super tall flexible structure: the Guangzhou New TV Tower in China. The attention here is mainly paid to the GPS ability to track rotating movements of the upper part of the tower due to strong winds events, such as typhoon, which are very common in that area.

Motivation and summary

To investigate the effectiveness of a GPS-Based Structural Monitoring (SM) solution is the main target of the thesis.

To provide safety and healthy performance to civil infrastructures, a Structural Monitoring System is required. Any possible system has to be designed depending on the type of information one is supposed to record and on the scale at which the structural behavior must be assessed (i.e., global or local level). Indeed accuracy, durability and serviceability are requirements that any monitoring system (Sumitro and Wang, 2005) has to satisfy in order to be regarded as feasible and reliable for long-term monitoring applications. The basis is to collect absolute and relative displacements of critical points across the structural systems. The relative displacements become consequently the key to assess drift and stress conditions in a structure. Furthermore the availability of real-time data is required in view of producing alert messages and modifying the maintenance activities to increase the safety of the structure.

The availability of a monitoring system under negative atmospheric conditions or large temperature variations is also a must. Techniques of terrestrial positioning, like laser displacement sensors, are often unsatisfactory in this respect, as accuracy and functionality decrease with negative wheatear conditions. Indeed the visibility dependence, makes the terrestrial positioning systems prone to be affected by measurements errors.

In the last few years Global Navigation Satellites Systems (GNSS) have been proved to be useful for monitoring applications in structural engineering. They guarantee operability in all weather conditions, offer continuous long term acquisition and provide absolute and relative displacements directly. Among the satellite positioning systems (American, Russian and the future European), the Global Positioning System (GPS) is becoming an alternative to common accelerometers in different type of monitoring application.

GPS sensors have been experimentally tested to measure the dynamic response of long-period structures (Celebi 2000; Nickitopoulou et al. 2003, 2006; Kijewsji-Correa et al. 2006; Li et al. 2006; Psimoulis et al. 2008a); to monitor the wind-induced deformation of tall flexible buildings (Kijewsji-Correa et al., 2003a, 2003b; Campbell et al. 2006; Seco et al. 2007; Hristopulos et al. 2007); to assess the vibrations of suspension and cable-stayed bridges (Xu et al. 2002; Lekidis et al. 2005; Meng et al. 2007), the displacements of high chimneys (Breuer et al. 2002; Cazzaniga et al. 2006) and large dams (Barnes et al. 2006). Many applications were developed by installing GPS receivers at key locations of the structure to capture its static and dynamic displacements in real time and in all weather conditions (Tamura et al. 2002). In other cases, the GPS was incorporated in the monitoring of a major suspension bridge (Wong 2004), or of tall building (Yigit et al., 2008; Psimoulis et al. 2008b; Ni et al. 2009).

The accuracy of such an approach to measure tri-axial displacements have been discussed in the past in (Celebi 2000; Kijewsji-Correa et al. 2006; Cazzaniga et al. 2006; Tamura et al. 2002) and recently in (Psimoulis et al. 2008a; Psimoulis et al. 2008b). The last cited reference, in particular, assesses the potential of GPS for the identification of the dynamic characteristics of civil engineering structures excited by wind or earthquakes loads, being the displacements in the range from 5 to 20mm and frequency of oscillation lower than 4Hz. Yet, in view of a future and permanent GPS-Based Structural Health Monitoring (SHM), the behavior of such technology has to be accurately analyzed for long duration records (wind actions) as well as for short records (impact forces).

This study is mainly devoted to investigate the reliability of a GPS instrumentation first in laboratory tests and then in full scale experiments.

Two kinds of tests were carried out in the laboratory environment in order to collect any possible information in view of assessing the achievable accuracy of the GPS units for long-term precise monitoring applications:

- (i) Static tests;
- (ii) Dynamic tests.

The first kinds of tests were carried out to quantify the background noise in the GPS configuration, and to investigate, the influence of GDOP on the recorded signal. They provide answers to two main questions: a) repeatability of long-period oscillations in both the longitudinal and transversal directions for two consecutive satellite configurations; b) evaluation of the best resolution possible when adopting dual frequencies GPS receivers.

The second set of tests was designed to quantify the range of frequencies and amplitudes that can be successfully tracked by GPS sensors in Civil Engineering applications.

In the full scale tests two buildings have been considered as case studies:

- (i) the steel building which host the authors laboratory;
- (ii) a super tall tower in China (the Guangzhou New TV Tower).

In the case (i) the GPS feasibility was studied for different forces which produce structural movements to be detected: natural (i.e., wind) and man made (i.e., internal bridge crane) dynamic actions are considered. A comparison of the GPS records with those collected by tri-axial accelerometers was conducted when dynamic vibrations were induced into the structure by movements of an internal bridge-crane. Also, different GPS units locations on the roof of the building were conceived to detect any “signal dilution of precision” (DOP). A finite element FE model of the building was realized and the elaborations from the GPS position readings were compared with the results obtained by the numerical simulation. The purpose here was to identify the structural model of the building in view of an automatized damage alert system.

The (ii) case study was chosen to prove the GPS ability to detect complex torsional movements of a super tall structure both in the absence and in the presence of wind excitations. The structural behavior of the tower was investigated through the GPS data recorded at the top level. The way to process these displacement data to detect the torsional effects of wind actions on the tower is the main concern of this part. In addition a comparison with an elaboration of the data recorded by uni-axial accelerometers, placed close to the GPS receivers, was also carried out, to check the accuracy of GPS.

Chapter 1

BASIC ASPECTS OF GPS TECHNOLOGY

Introduction

This chapter presents an overview of the Global Positioning System (GPS) principles for precise applications. A review of the positioning systems allowed by GPS, their governing relations, as well as the receiver types and receiver tasks are provided as the basis for understanding GPS techniques. The accuracies provided by different technique are underlined and the special requirements for GPS receivers are described.

1.1 GPS Overview

The Global Positioning System (GPS) is an earth-orbiting-satellite based navigation system (Kaplan and Hegarty, 2006). GPS is an operational system, providing users worldwide with twenty-four hour a day precise position in three dimensions and precise time traceable to global time standards. GPS is operated by the United States Air Force under the direction of the Department of Defense (DoD) and was designed for, and remains under the control of, the United States military authority, despite the many thousands of commercial and recreational civil implementations. Primarily designed as a land, marine, and aviation

navigation system, GPS applications have expanded to include surveying, space navigation, automatic vehicle monitoring, emergency services dispatching, mapping, geographic information systems and monitoring systems.

1.1.1. GPS History

In the early 1960s, several U.S. government organizations, including the Department of Defense (DOD), the National Aeronautics and Space Administration (NASA), and the Department of Transportation (DOT), were interested in developing satellite systems for three-dimensional position determination. The optimum system was viewed as having the following attributes: (i) global coverage, (ii) continuous/all weather operation, (iii) ability to serve high-dynamic platforms, (iv) high accuracy.

In 1969, the Department of Defense (DoD) established the Defense Navigation Satellite System (DNSS) program to consolidate the independent development efforts of each military service to form a single joint-use system. The DoD also established the Navigation Satellite Executive Steering Group, which was charged with determining the viability of the DNSS and planning its development.

From this effort, the system concept for Navigation Satellite Timing and Ranging (NAVSTAR) Global Positioning System (GPS) was formed. The NAVSTAR GPS program was developed by the GPS Joint Program Office.

Presently, GPS is fully operational and meets the criteria established in the 1960s for an optimum positioning system. The system provides accurate, continuous, worldwide, three-dimensional position and velocity information to users with the appropriate receiving equipment.

1.1.2. GPS System Overview

The satellite constellation nominally consists of 24 satellites arranged in 6 orbital planes with 4 satellites per plane. A worldwide ground control and monitoring network monitors the health and status of the satellites. This network also uploads navigation and other data to the satellites.

GPS can provides service to an unlimited number of users since the user receivers operate passively (i.e., they receive only and do not transmit any signal to the satellites). The system utilizes the concept of one-way “time of arrival” (TOA) ranging, which is the measure of the distance between transceiver and receiver.

Satellite transmissions are referenced to highly accurate atomic frequency standards clocks, which are in synchronism with a GPS time base. The satellites broadcast ranging codes and navigation data on two frequencies called L1 (1,575.42 MHz) and L2 (1,227.6 MHz).

Each satellite transmits on these frequencies, but with different ranging codes than those employed by other satellites. These codes were selected for their low cross-correlation properties. Each satellite generates a short code referred to as the “coarse/acquisition” or C/A code and a long code denoted as the “precision” or P-code.

The navigation data provide the means for the receiver to determine the location of the satellite at the time of signal transmission, whereas the ranging code enables the user’s receiver to determine the transit (i.e., propagation) time of the signal and thereby to determine the satellite-to-user range. Utilizing this technique, to measure the receiver’s three-dimensional location requires that TOA ranging measurements be made from four satellites. If the receivers clocks were synchronized with the satellite clocks, only three range measurements would be required. However, a crystal clock is usually employed in navigation receivers to minimize the cost, complexity and size of the receiver. Thus, four measurements are required to determine user latitude, longitude, height, and receiver clock offset from internal system time.

The GPS system provides two separate services: the Standard Positioning Service (SPS) and the Precise Positioning Service (PPS).

The Standard Positioning Service (SPS) is defined as the standard specified level of positioning and timing accuracy that is available, without restrictions, to any user on a continuous worldwide basis.

The Precise Positioning Service (PPS) is on the contrary defined as the most accurate direct positioning, velocity, and timing information continuously

available, worldwide, from the basic GPS. The Precise Positioning Service is primarily intended for military users and selected government agencies. Access for Civilian users to the PPS position accuracies is controlled through two cryptographic features denoted as “antispoofing” (AS) and “selective availability” (SA). AS is a mechanism intended to defeat deception jamming through encryption of the military signals. SA, that adds intentional time varying errors of up to 100 meters to the available navigation signals, was discontinued on May 1, 2000, and the current U.S. government policy is to maintain it off.

1.2 GPS System Segments

The GPS is constituted of three major segments:

- 1) space segment (SS);
- 2) control segment (CS);
- 3) user segment (US).

The SS consist of the satellite overhead. The satellite constellation is the set of satellites in orbit that provide the ranging signals and data messages to the user receivers.

The CS is a ground system that tracks and maintains the satellites in space. The CS monitors satellite health and signal integrity and maintains the orbital configuration of the satellites. Furthermore, the CS updates the satellite clock corrections and ephemerides¹ as well as numerous other parameters essential to determining user position.

The US comprises the user receivers. It performs navigation and timing positioning.

¹ The satellites ephemerides are a collection of parameters used to calculate the satellites position with time. The ephemerides describe the satellite orbits and clock correction parameters variable over time used for positioning and baseline computations. The ephemerides may be broadcast (projected ahead into time and subject to selective availability) or precise (post-fitted).

1.2.1. Space Segment

The SS is the constellation of satellites from which the users obtain the ranging measurements. The satellites transmit a coded signal for this purpose. This concept makes the GPS a one-way-system with signals transmitted by the satellites while the users are passively receiving the signals which are modulated with data that include information to define the position of the satellites.

The space segment has two principal aspects:

- (a) the constellation of satellites in terms of the orbits and positioning within the orbits;
- (b) the features of the satellites that occupy each orbital slot.

Referring to the American Global Positioning System, the satellites constellation consists of 24 satellites positioned in six Earth-centered orbital planes with four satellites in each plane. The nominal orbital period of a GPS satellite is one-half of a sidereal day or 11 hours, 58 minutes. In this way each satellite makes two orbits each sidereal day, repeating the same ground track each day. The orbits are nearly circular and equally spaced around the equator at a 60° separation with a nominal inclination relative to the equatorial plane of 55° .

Figure 1.1 depicts the GPS constellation. The orbital radius (i.e., nominal distance from the center of mass of the Earth to the satellite) is approximately 26.600km. This satellite constellation provides a 24-hour global user navigation and time determination capability.

Since the GPS original implementation, further satellites have been added to reach actually the number of 31. The additional satellites improve the precision of GPS receiver calculations by providing redundant measurements. With the increased number of satellites, the constellation was changed to a non uniform arrangement. Such an arrangement was shown to improve reliability and availability of the system, relative to a uniform system, when multiple satellites fail. With the actual constellation, about ten satellites are visible from any point on the ground at any one time.

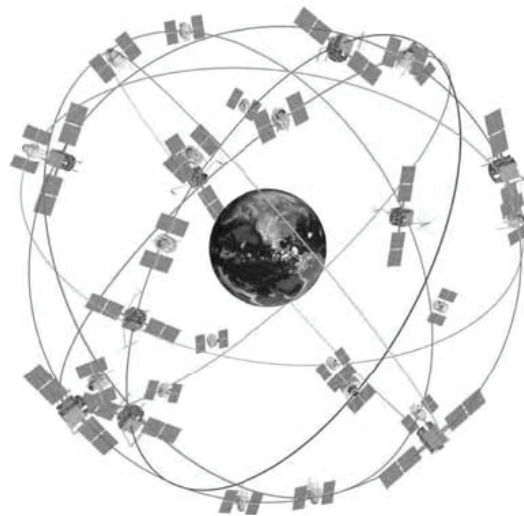


Figure 1.1. GPS satellite constellation

Each satellite broadcasts the navigation signals at two microwave frequencies L1, L2. These two carrier signals are phase modulated by pseudo-random bit streams that spread the carrier frequencies into a broader bandwidth of noise-like, spread-spectrum signals.

In addition to pseudo-random noise (PRN) codes, the signals are modulated with the Navigation Message consisting of a set of orbital (ephemerides) data, satellite clock offset descriptions and other system parameters.

The L1 (1575MHz) signal carries a PRN code that repeats each millisecond and that is unique for each of the thirty one satellites. These coarse acquisition codes (C/A codes) are broadcast at a bit rate of 1.023MHz and are used to identify and acquire each satellite, and to align receiver timing signals with those transmitted by the satellite.

In addition to the C/A code the L1 signal carries the Navigation Message code (at 50Hz) and the P-code. The P-code is a PRN code with a period of seven days that is transmitted at a rate of 10.23MHz.

On the contrary, the L2 signal, also a microwave signal (1227MHz), carries only the P-code and is used for dual frequency ionospheric delay measurements.

1.2.2 Control Segment

The CS is responsible for maintaining the satellites and their proper functioning. This includes:

- (a) maintaining the satellites in their proper orbital positions;
- (b) monitoring satellite's state of health and status;
- (c) updating each satellite's clock, ephemeris and other indicators in the navigation message at least once per day;
- (d) resolves satellite anomalies.

The CS is made of three different physical components: (a) the master control station (MCS); (b) monitor stations; (c) the ground antennas.

The MCS, located in Colorado Springs, provides the central command and control of the GPS constellation. Specifically:

- (a) monitoring and maintaining satellite's state of health and orbits
- (b) estimating and predicting satellite clock and ephemeris parameters;
- (c) generating GPS navigation messages;
- (d) maintaining GPS timing service and its synchronization;
- (e) monitoring the navigation service integrity;
- (f) verifying and logging the navigation data delivered to the GPS user.

To perform the navigation tracking function, the CS has a dedicated, globally distributed monitor station network: Ascension Island, Diego Garcia, Kwajalein, Hawaii, Colorado Springs and Cape Canaveral. Each monitor station operates under the control of the MCS and consists of the equipment and computer programs necessary to collect satellite-ranging data, satellite status data, and local meteorological data. The data are forwarded to the MCS for their processing.

1.2.3 User Segment

The user segment (US) is typically composed by a GPS unit receiver, which processes the L-band signals transmitted from the satellites to determine the user tri-dimensional position.

While positioning determination is the most common use, receivers are designed for other applications, such as timing source.

GPS receivers are embedded in many of the items one uses daily . These items include for example cellular telephones and satellite navigation systems for orientation maps.

Selection of a GPS receiver depends on the user's application (i.e., civilian versus military, platform dynamics, shock and vibration environment).

GPS receivers may include an input for differential corrections, using the RTCM (Radio Technical Commission for Maritime Services)² SC-104 format.

Many GPS receivers can relay position data to a PC or other device using the NMEA 0183 protocol³. Although this protocol is officially defined by the NMEA, references to the protocol have been compiled from public records, allowing open source tools to read the protocol without violating intellectual property laws. Other proprietary protocols exist as well. Receivers can interface with other devices using methods including a serial connection, USB or Bluetooth.

In general, each GPS receiver is composed of five principal components as shown in Figure 1.2. In particular:

- (i) an antenna tuned to the frequencies transmitted by the satellites;
- (ii) a receiver;
- (iii) a processor with a highly-stable clock (often a crystal oscillator);
- (iv) an input/output (I/O) and control display unit;
- (v) a power supply.

² The Radio Technical Commission for Maritime Services defines a differential data link to relay GPS correction messages from a monitor station to a field user. RTCM SC-104 recommendations is the standard for differential GPS correction transmission. It defines the correction message format and 16 different correction message types.

³ NMEA 0183 is a combined electrical and data specification for communication between marine electronic devices such as echo sounder, sonars, anemometer (wind speed and direction), gyrocompass, autopilot, GPS receivers and many other types of instruments. It has been defined by, and is controlled by, the U.S.-based National Marine Electronics Association (NMEA).

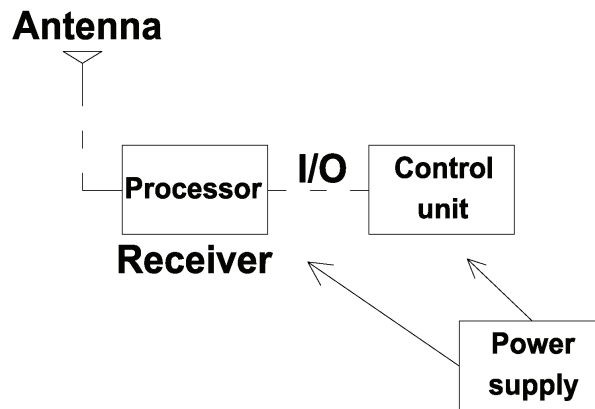


Figure 1.2. GPS receiver components

The antenna is the part of the system which receives the satellite signals. The antenna is polarized and provides near hemispherical coverage. Any antenna typically detects any satellite the horizontal angle of which is more than 15° (the so called “cut-off angle”). Below 15° , in fact the gain of the antenna is usually negative. Furthermore any GPS software allows the user to decide the value of the angle which, depending on the position on the receiver on the earth surface (i.e., low or high latitude), can be switched to 10° , but also to 20° .

The more precise antennas are designed to work with dual frequency GPS receivers and so are designed to operate at both L1 and L2.

Furthermore, when computing position with a GPS receiver, one estimates the position of the electrical phase center of the antenna. There is both a physical and an electrical realization of this phase center. The electrical phase center is often not collocated with the physical phase center and may vary with the direction of arrival of the received signal, this leads to a variation of centimeters between the electrical and physical phase. A data calibration is therefore required for high-accuracy applications.

The antennas are connected by/without wires to the GPS receiver.

Actually two basic types of receiver exist: (i) those that track L1 C/A code and P-code on L1 and L2 and (ii) those that only track C/A code. In light of the GPS modernization effort, these are referred to as “legacy” receivers. The new

generation of GPS receiver will also track the new L5 GPS frequency: they are being designed as three band receivers to achieve ionospheric compensation and increased interference immunity. The L5 frequency (1176.45 MHz) has been proposed for use as a civilian safety-of-life (SoL) signal.

In any receiver, a processor is then generally required to control and command the receiver through its operational sequence, starting with channel signal acquisition and followed by signal tracking and data collection.

In addition an input/output (I/O) device is used as an interface between the GPS set and the user. I/O devices are of two basic types: integrated or external.

Finally the last component of a GPS units is the power supply which can be either integrated, external, or a combination of the two. Typically, alkaline or lithium batteries are used for integrated or self-contained implementations, such as handheld portable units; whereas an existing power supply is normally used in integrated applications, such as a board-mounted receiver installed on a server to provide accurate time. Airborne, automotive, and shipboard GPS set installations normally use platform power but typically have built-in power converters (ac to dc) and regulators.

Actually many GPS receivers can be cheaply bought in the market and more than 100 manufactures produce different types of GPS receivers. Leica Geosystems (www.leica-geosystems.com), Trimble (www.trimble.com), Garmin (www.garmin.com) and Topcon (www.topcon.com), among the others, have many different products ranging from handhelds to automobile and aircraft navigators to complex survey receivers (Kaplan and Hegarty, 2006) .

In a so wide range of GPS units (i.e., receiver plus antenna), their selection is strongly dependent on the user application. The intended application influences the receiver design, the construction and the capacity.

For each application, several environmental, operational, and performance parameters must be examined.

Since the precision, the sampling rate and the stability of the signal are aspects to be checked, choosing one receiver instead of another leads to different performance in the applications.

This also applies to the scientific community which developed a large number of applications (some of them in the field of civil engineering, as reported in Chapter 2), showing different results just changing the receiver produced with the same receiver specifications. In addition even if receivers for precise application are sold for sampling rate up to 100Hz, one has to be careful while sampling at a so high frequency (normally precise GPS receiver sampling rate is not higher than 20Hz).

Just to give an idea of the main parameters which must be checked before toward a GPS units for precise applications, a brief list of them is provided:

- (i) shock and vibration requirements;
- (ii) temperature and humidity extremes;
- (iii) single or dual frequency operability;
- (iv) multipath mitigation;
- (v) type of dynamic conditions (e.i., acceleration and velocity) for operability;
- (vi) Differential Global Positioning System (DGPS) capability;
- (vii) interference rejection capabilities;
- (viii) power consumption.

1.3 GPS Signal Characteristics

The GPS satellites transmit navigation signals on two carrier L-band frequencies called L1 (1575MHz), the primary frequency, and L2, the secondary frequency (1227MHz).

The receiver can distinguish the signals from different satellites because GPS uses a code division multiple access (CDMA) spread-spectrum technique where the low-bit rate navigation data message (50Hz) is encoded with a high-rate pseudo random noise (PRN) sequence that is different for each satellite.

The receiver knows the PRN codes for each satellite and can use this to reconstruct the actual message data.

The L1 and L2 frequencies, known as carrier frequencies, are so modulated by spread spectrum codes with unique PRN sequences associated with each satellite and by a common navigation data message. All satellites transmit at the

same carrier frequencies. In order to track one satellite in common view with several other satellites, a GPS receiver must generate the same PRN sequence and carrier signal of the desired satellite.

A block diagram, representative of the signal structure for L1 ($154f_0$) and L2 ($120f_0$), is plotted in Figure 1.3 (being f_0 the fundamental frequency equal to 10.23MHz). In the diagram the C/A code is shown as transmitted at a chip rate of $f_0/10=1.023$ MHz, while the P-code has a chip rate of $f_0=10.23$ MHz.

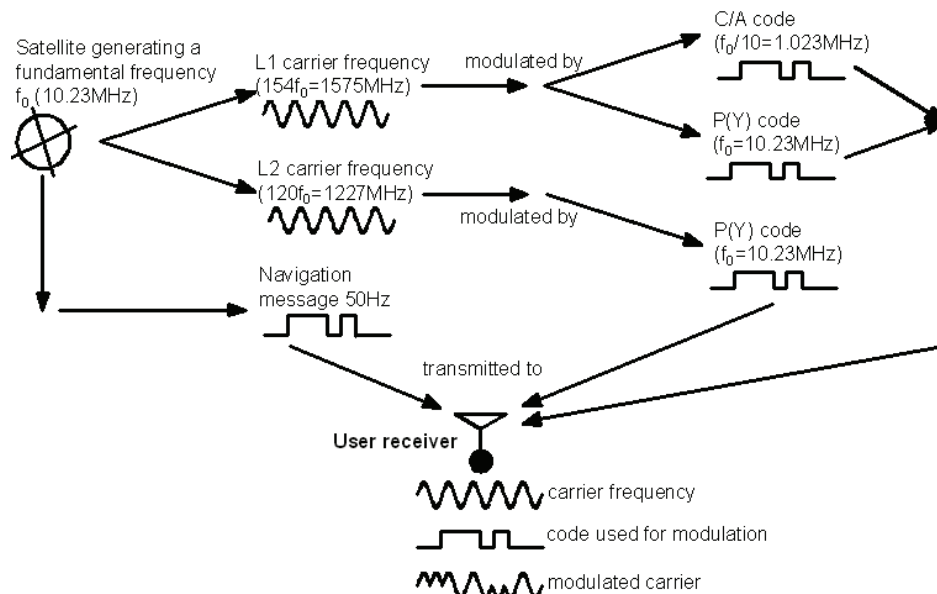


Figure 1.3. GPS signal structure

In figure 1.3, the P-code is indicated as P(Y) code. It derives from considering the anti-spoofing (AS) mechanism in the satellite signals. In fact, when the AS is activated the P code is encrypted to form what is known as the Y-code. The Y-code has the same rate as the P code. Thus, the acronym often used for the precision (encrypted) code is P(Y) code.

As shown in Figure 1.3, the L1 frequency is modulated by two PRN codes, the C/A code, and the P(Y) code. On the contrary the L2 frequency is modulated by only one PRN code at a time.

The P(Y) code is available to precise positioning (PP) users but not to standard positioning (SP) users since the CS normally configures an anti-spoofing (AS) mode in the satellite.

The PP users (in the past only available to military users, now to any user with precise receivers) have access to the cryptographic keys and algorithms used in the AS process. On the contrary, the SP users (i.e., users with a standard navigation receiver, as those mounted on cars) do not have access to the cryptographic algorithms used in the AS process and as consequence do not have access to the P(Y) code.

In addition to the AS, the control of U.S. government on the GPS signal was in the past realized by subjecting both the C/A code and the P(Y) code, as well as the L1 and L2 carrier frequencies, to an encrypted time-varying frequency offset plus an encrypted ephemeris offset error known as selective availability (SA). SA denied the full accuracy of GPS to the stand-alone SPS users. However, SA has been switched off since May 2000.

Table 1.1 summarizes the GPS signal structure on L1 and L2 frequency.

Table 1.1. GPS signal structure

| <i>Signal priority</i> | <i>Primary</i> | <i>Secondary</i> |
|--------------------------------|-----------------------------|----------------------------|
| <i>Signal frequency</i> | L1 | L2 |
| <i>Carrier frequency (MHz)</i> | 1575 | 1227 |
| <i>PRN codes (MHz)</i> | P(Y)=10.23 and C/A=1.023 | P(Y)=10.23 or C/A=1.023 |
| <i>Navigation message (Hz)</i> | 50 | 50 |

As derives by looking at Table 1.1, both the C/A code and P(Y) code signals are modulated with the 50Hz Navigation message. The data contained in the Navigation message provide the user with the information necessary to compute the precise locations of each visible satellite and time of transmission for each navigation signal. The data also include a significant set of auxiliary

information that may be used to assist the equipment in acquiring new satellites, to translate from GPS system time to the Universal Time Coordinated (UTC)⁴, and to correct for a number of errors that affect the range measurements.

In practice, a GPS receiver must first generate the same PRN code that is transmitted by the satellite being acquired by the receiver; then it must shift the phase of this replica code until it correlates with the satellite PRN code.

To clarify the latter point:

(i) the GPS satellite transmissions utilize the so called “direct sequence spread spectrum” (DSSS) modulation. DSSS provides the structure for the transmission of ranging signals and essential navigation data, such as satellite ephemerides and satellite health. The ranging signals are PRN codes that modulates the satellite carrier frequencies. These codes look like and have spectral properties similar to random binary sequences (see Figure 1.4). These codes have a predictable pattern, which is periodic and can be replicated by a suitably equipped receiver.

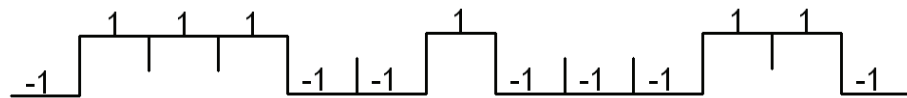


Figure 1.4. PRN code sequence

(ii) each GPS satellite broadcasted two types of PRN ranging codes: a “short” coarse/acquisition (C/A) code and a “long” precision (P) code.

(iii) to determine a user receiver’s position with respect to a coordinate system origin, one has to calculate the distance from the user receiver to the satellites. This distance is computed by measuring the propagation time required

⁴ The UTC is the uniform atomic time system as deduced directly from observations of stars and the fixed numerical relationship between Universal and Sidereal Time, corrected for polar motion and for seasonal variation in the earth's rotation rate. It is maintained by the U.S. Naval Observatory.

for a satellite-generated ranging code to transit from the satellite to the user receiver antenna.

The propagation time measurement process is illustrated in Figure 1.5, where it is shown a specific code phase generated by the satellite at time t^* which arrives at the receiver at time t' . The propagation time required is then represented by Δt . Within the receiver, an identical coded ranging signal is generated at time t , with respect to the receiver clock. This replica code is shifted in time until it achieves correlation with the received satellite-generated ranging code.

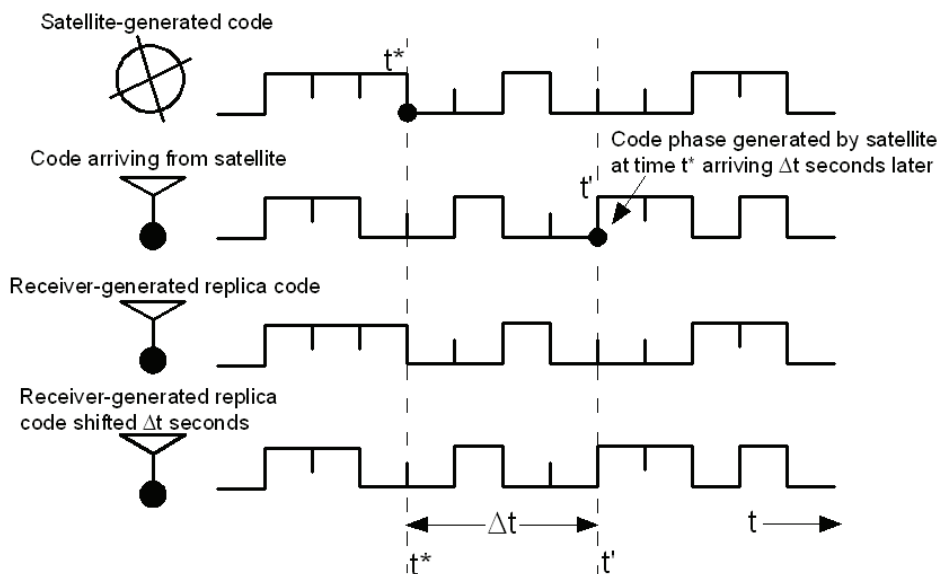


Figure 1.5. Propagation time measurement process

If the satellite clock and the receiver clock were perfectly synchronized, the correlation process would yield the true propagation time. By multiplying this propagation time, Δt , by the speed of light, the true (i.e., geometric) satellite-to-user distance can be computed.

However, as reported in next section 1.4.1, the satellite and receiver clocks generally are not synchronized, because the receiver clock is typically offset

from system time. Thus, the range determined by the correlation process is called “pseudo-range” because it is the range determined by multiplying the signal propagation velocity by the time difference between two non-synchronized clocks (i.e., the satellite and the receiver clock).

1.4 GPS performance

The accuracy with which an user receiver can determine its position depends on the complicated interaction of several factors.

In general, the GPS accuracy performance depends on the quality of the pseudo-range and carrier phase measurements as well as on the broadcast navigation data.

In addition, the way to reproduce by means of physical models the effects of some parameters (such as the ionospheric and tropospheric delays) involved in the calculation of the GPS receiver position has to be considered.

Furthermore, the accuracy to which the satellite clock offsets relative to GPS system time are known to the user, or the accuracy to which satellite-to-user propagation errors are compensated, are important. Relevant errors are also induced by the control, space, and user segments.

To analyze the effect of such errors on the accuracy of the measurements, a fundamental assumption is usually made: the error sources can be allocated to individual satellite pseudo-ranges and can be modelled as effectively resulting in an equivalent error of the pseudo-range values. The effective accuracy of the pseudo-range value is called the equivalent range error. For a given satellite it is considered to be the sum of the contributions from each of the error sources associated with that satellite. Usually, the equivalent range error for a satellite is assumed to be independent and identically distributed for any satellite.

Concluding, the accuracy of the position/time solution determined by GPS can then be viewed as the product of a geometry factor and a pseudo-range error factor.

Based on this assumption the GPS measurement error can be estimated by the following expression:

$$GPS\ error = pseudo\text{-}range\ error * geometry\ factor.$$

Where the pseudo-range error factor corresponds to what previously is mentioned as equivalent range error, while the geometry factor on the contrary expresses the effect of the satellite vs. user receiver geometry configuration on the GPS solution error. It is generically known as the “signal geometric dilution of precision” (GDOP).

1.4.1 GPS governing relations

GPS positions are calculated using the concept of triangulation. This refers to using distances from several known locations to compute the coordinates of an unknown location. In this case the known locations are the positions of GPS satellites. The known position of overhead satellites allows one to determine the “unknown” position of a GPS receiver/antenna pair on the Earth (Figure 1.6).

Each satellite continuously transmits the current time kept by its atomic clock, as well as its current position x^j, y^j, z^j along its orbital path. The distance r_i^j of the j^{th} satellite to the unknown position of the receiver on the Earth, x_i, y_i, z_i is computed by measuring the propagation time (Δt_i^j) required to move from the satellite to the user receiver antenna.

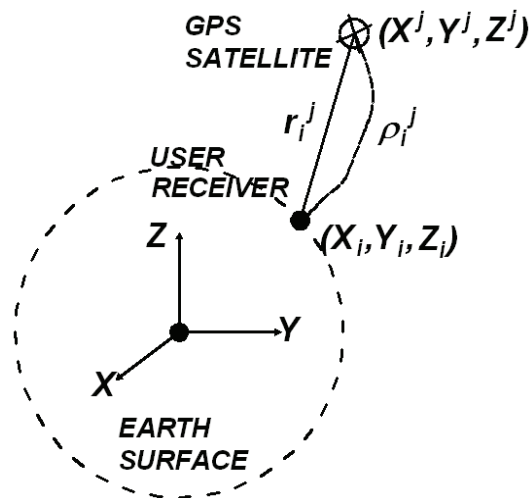


Figure 1.6. Satellite – Receiver distance

For an ideal case, the true (i.e., the geometric) satellite-to-receiver distance can be computed by multiplying the propagation time Δt_i^j by the speed of the light ($c=290,000$ km/s). The distance r_i^j for any j ($j=1,2,\dots,N_{sat}$) can be written as:

$$r_i^j = c\Delta t_i^j = c(T_i - T^j) \quad (1.1)$$

where T_i represents the time at which the signal reaches the receiver, and T^j is the time at which the signal left the receiver.

However, as previously mentioned, the satellite and receiver clocks are generally not synchronized, since the receiver clock generally has a bias error from the time of satellite atomic clocks.

Thus, the range one obtains is denoted as “pseudo-range” ρ_i^j as it contains (i) the geometric satellite-to-receiver range, (ii) an offset due to the difference between system time and the receiver clock. The pseudo-range can be written as:

$$\rho_i^j = c[(T_i + \delta t_i^j) - (T^j)] = c(T_i - T^j) + c\delta t_i^j = r_i^j + c\delta t_i^j \quad (1.2)$$

where δt_i^j represents the offset of the receiver clock from the system time.

Equation (1.2) can be expanded into a set of equations (with $j=1,2,\dots,N_{sat}$) in the unknowns x_i, y_i, z_i and δt_i^j :

$$\rho_i^j = \sqrt{(x^j - x_i)^2 + (y^j - y_i)^2 + (z^j - z_i)^2} + c\delta t_i^j = f(x_i, y_i, z_i, \delta t_i^j) \quad (1.3)$$

These nonlinear equations can be solved for the unknowns by employing either (i) closed form solutions, (ii) iterative techniques based on linearization, or (iii) Kalman filtering (Xu, 2007; Kaplan and Hegarty, 2006).

Solving Equation (1.3) by adopting the linearization technique means introducing a correction ($\Delta x_i, \Delta y_i, \Delta z_i$) of the approximate position ($\underline{x}_i, \underline{y}_i, \underline{z}_i$), i. e., an offset of the true position (x_i, y_i, z_i).

Actually both the unknown receiver position and clock offset are written as the sum of an approximate component and an incremental component:

$$x_i = \underline{x}_i + \Delta x_i; \quad y_i = \underline{y}_i + \Delta y_i; \quad z_i = \underline{z}_i + \Delta z_i; \quad \delta t_i^j = \underline{\delta t}_i^j + \Delta t_i^j \quad (1.4)$$

Therefore in Equation (1.3) one can write:

$$f(x_i, y_i, z_i, \delta t_i^j) = f(\underline{x}_i + \Delta x_i, \underline{y}_i + \Delta y_i, \underline{z}_i + \Delta z_i, \underline{\delta t}_i^j + \Delta t_i^j) \quad (1.5)$$

Equation (1.5) can be expanded at ($\underline{x}_i, \underline{y}_i, \underline{z}_i, \underline{\delta t}_i^j$) using a Taylor series:

$$\begin{aligned} f(\underline{x}_i + \Delta x_i, \underline{y}_i + \Delta y_i, \underline{z}_i + \Delta z_i, \underline{\delta t}_i^j + \Delta t_i^j) = \\ f(\underline{x}_i, \underline{y}_i, \underline{z}_i, \underline{\delta t}_i^j) + \frac{\partial f(\underline{x}_i, \underline{y}_i, \underline{z}_i, \underline{\delta t}_i^j)}{\partial \underline{x}_i} \Delta x_i + \\ \frac{\partial f(\underline{x}_i, \underline{y}_i, \underline{z}_i, \underline{\delta t}_i^j)}{\partial \underline{y}_i} \Delta y_i + \frac{\partial f(\underline{x}_i, \underline{y}_i, \underline{z}_i, \underline{\delta t}_i^j)}{\partial \underline{z}_i} \Delta z_i + \frac{\partial f(\underline{x}_i, \underline{y}_i, \underline{z}_i, \underline{\delta t}_i^j)}{\partial \underline{\delta t}_i^j} \Delta t_i^j + \dots \end{aligned} \quad (1.6)$$

By truncating the expansion after the first-order (to eliminate nonlinear terms), the partials derivatives are evaluated as follows:

$$\begin{aligned}
\frac{\partial f(x_i, y_i, z_i, \delta t_i^j)}{\partial x_i} &= -\frac{x^j - x_i}{r_i^j} \\
\frac{\partial f(x_i, y_i, z_i, \delta t_i^j)}{\partial y_i} &= -\frac{y^j - y_i}{r_i^j} \\
\frac{\partial f(x_i, y_i, z_i, \delta t_i^j)}{\partial z_i} &= -\frac{z^j - z_i}{r_i^j} \\
\frac{\partial f(x_i, y_i, z_i, \delta t_i^j)}{\partial \delta t_i^j} &= c
\end{aligned} \tag{1.7}$$

Substituting Equation (1.6) and (1.7) into Equation (1.3) yields:

$$\rho_i^j = \underline{\rho}_i^j - \frac{x^j - x_i}{r_i^j} \Delta x_i - \frac{y^j - y_i}{r_i^j} \Delta y_i - \frac{z^j - z_i}{r_i^j} \Delta z_i + c \Delta t_i^j \tag{1.8}$$

and rearranging Equation (1.8) yields:

$$\underline{\rho}_i^j - \rho_i^j = \frac{x^j - x_i}{r_i^j} \Delta x_i + \frac{y^j - y_i}{r_i^j} \Delta y_i + \frac{z^j - z_i}{r_i^j} \Delta z_i - c \Delta t_i^j \tag{1.9}$$

Introduce now a set of new variables a^{xj}, a^{yj}, a^{zj} , which denote the direction cosines of the unit vector pointing from the approximate receiver position to the j^{th} satellite:

$$a^{xj} = \frac{x^j - x_i}{r_i^j}; \quad a^{yj} = \frac{y^j - y_i}{r_i^j}; \quad a^{zj} = \frac{z^j - z_i}{r_i^j} \tag{1.10}$$

Equation (1.9) can be rewritten as:

$$\Delta\rho_i^j = \underline{\rho_i^j} - \rho_i^j = a^{xj} \Delta x_i + a^{yj} \Delta y_i + a^{zj} \Delta z_i - c\Delta t_i^j \quad (1.11)$$

By solving Equation (1.11), written for at least four satellites, for $j=1,2,\dots,N_{sat}$, the four unknowns Δx_i , Δy_i , Δz_i , and Δt_i^j can be eventually evaluated.

Equation (1.11) can be rewritten in matricial form as:

$$\Delta\rho = H\Delta x \quad (1.12)$$

where

$$\Delta\rho = \begin{bmatrix} \Delta\rho_i^1 \\ \Delta\rho_i^2 \\ \vdots \\ \vdots \\ \Delta\rho_i^{N_{sat}} \end{bmatrix} \dots H = \begin{bmatrix} a^{x1} & a^{y1} & a^{z1} & 1 \\ a^{x2} & a^{y2} & a^{z2} & 1 \\ \vdots & \vdots & \vdots & \vdots \\ \vdots & \vdots & \vdots & \vdots \\ a^{xN_{sat}} & a^{yN_{sat}} & a^{zN_{sat}} & 1 \end{bmatrix} \dots \Delta x = \begin{bmatrix} \Delta x_i \\ \Delta y_i \\ \Delta z_i \\ -c\Delta t_i^j \end{bmatrix}$$

which, for $N_{sat} = 4$, has the solution:

$$\Delta x = H^{-1} \Delta\rho \quad (1.13)$$

Once the unknowns are computed, the receiver's coordinates x_i , y_i , z_i and the receiver clock offset δt_i^j are obtained using Equation (1.4).

The true receiver-to-satellite measurements are corrupted by independent errors such as measurement noise, deviation of the satellite path from the reported ephemeris, and multipath (Kaplan and Hegarty, 2006).

Let $\boldsymbol{\varepsilon}_i^j$ be the vector containing the pseudo-range measurement errors. These errors become errors ε_{xi} in the components of the vector $\Delta\mathbf{x}$:

$$\boldsymbol{\varepsilon}_{xi} = \mathbf{H}^{-1} \boldsymbol{\varepsilon}_i^j \quad (1.14)$$

The error ε_{xi} can be minimized by collecting the measurements from the maximum number of visible satellites, which will result in an overdetermined solution set of equations similar to Equation (1.13).

Each of these redundant measurements will generally contain independent error contributions. Redundant measurements can be processed by least squares estimation techniques that obtain improved estimates of the unknowns. In particular if $N_{sat} > 4$, Equation (1.12) represents a system with more equations than unknowns. Generally, the system will be inconsistent in that errors such as the value of $\Delta\boldsymbol{\rho}$ will preclude any value of $\Delta\mathbf{x}$ from exactly solving the system.

Assume the $N_{sat} > 4$ are visible and for each of them the pseudorange measurements are available. Also assume that the linear connection matrix \mathbf{H} and the vectors $\Delta\boldsymbol{\rho}$ are known. For any particular value of $\Delta\mathbf{x}$, the quantity $\boldsymbol{\eta} = \mathbf{H}\Delta\mathbf{x} - \Delta\boldsymbol{\rho}$ is called the residual vector.

$\Delta\mathbf{x}$ has to be calculated so that the residuals are small. The ordinary least square solution is defined as the value of $\Delta\mathbf{x}$ that minimizes the square of the residual vector, where the square of a vector is defined as the inner product of the vector with itself. Therefore one pursues the minimization of the sum of the squares of the single components in the residual vector.

Let R_{SE} be the square of the residual vector:

$$R_{SE}(\Delta\mathbf{x}) = (\mathbf{H}\Delta\mathbf{x} - \Delta\boldsymbol{\rho})^2 \quad (1.15)$$

Given \mathbf{H} and $\Delta\boldsymbol{\rho}$, the least squares problem is formulated as: find the value of $\Delta\mathbf{x}$ which minimizes R_{SE} . Since:

$$R_{SE} (\Delta \mathbf{x} + d\mathbf{x}) = R_{SE} (\Delta \mathbf{x}) + d\mathbf{x}^T \mathbf{H}^T \mathbf{H} d\mathbf{x} \quad (1.16)$$

the minimization of R_{SE} demands that the product $\mathbf{H}^T \mathbf{H}$ has to be nonsingular, i.e., the columns of matrix \mathbf{H} must be independent each of the others. As the j -th column of matrix \mathbf{H} contains the terms a^{xj}, a^{yj}, a^{zj} , which are written in function of an offset from the true position (x_i, y_i, z_i) , the offsets in computing the true position must be independent one of the others.

Thus the minimization of the residuals implicitly incorporates the minimization of the measurement errors emphasized in Equation (1.14) in the case of $N_{sat} = 4$.

The latter terms can also be regarded as the result of a further global time offset δt_D , which is split in the sum of several contributions:

$$\delta t_D = \delta t_{atm} + \delta t_m + \delta t_r \quad (1.17)$$

where: δt_{atm} represents the delays due to atmosphere, (i.e., ionospheric effects, and tropospheric delay); δt_m the multipath offset and δt_r the receiver noises and hardware offset (see Figure 1.7).

Equation (1.2) is then rewritten as:

$$\rho_i^j = r_i^j + c(\delta t_i^j + \delta t_D) \quad (1.18)$$

with δt_D given by Equation (1.17). Equation (1.18) allows one to elaborate separately, as independent sources, the pseudo-range errors in Equation (1.14).

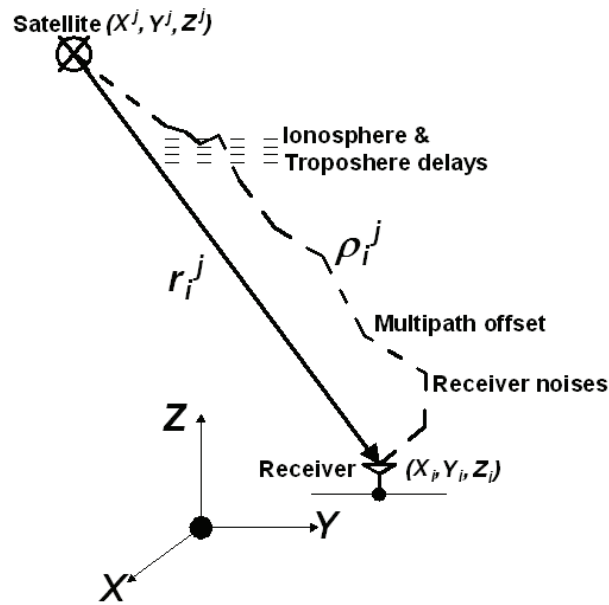


Figure 1.7. GPS measurements offsets

Inconsistencies of atmospheric conditions affect the speed of the GPS signals as they pass through the Earth's atmosphere. These effects are smallest when the satellite is directly overhead and become greater for satellites nearer the horizon since the path through the atmosphere is longer. Once the receiver's approximate location is known, a mathematical model can be used to estimate and compensate for these errors.

The atmospheric effects, summarized in Equation (1.17) as δt_{atm} can be computed by separating its two components: the ionospheric delay and the tropospheric delay.

Varying in density and thickness due to solar pressure and geomagnetic effects, the ionosphere can delay the GPS signals by as much as 300 nanoseconds, corresponding to around 100 meters (Klobuchar, 1982). The diurnal (24-hour) changes in the ionosphere cause the largest variations in delay. At night the delay is at a minimum and the thinner and higher night-time

ionosphere is more easily modeled than the less dense and thicker layer during the day.

The ionospheric delay of the GPS signal depends on its frequency. This phenomenon is known as dispersion and can be calculated from measurements of delays for two or more frequency bands, allowing delays at other frequencies to be estimated. Since the ionospheric delay is frequency dependent, it can be removed by exploiting dual-frequency (L1 and L2, where L1 and L2 are the two carrier frequencies of the GPS signal) GPS receivers.

The effects of the ionosphere generally change slowly, and can be averaged over time. Those for any particular geographical area can be easily calculated by comparing the GPS-measured position to a known surveyed location. This correction is also valid for other receivers in the same general location.

The ionospheric error is also strictly related to the adopted baseline (distance reference-rover): when the two antennas are close (say some meters) each to the other, the ionospheric delay is the same for the reference and the rover, and hence the error can be neglected.

From a mathematical point of view the ionospheric delay can be expressed in function of an index of refraction n . The index of refraction for a medium is defined as the ratio of the wave's propagation speed in free space (c) to that in the medium (v): $n=c/v$.

The path length difference due to ionospheric refraction (i.e., the difference between measured and geometric range), is defined as:

$$\Delta I_i^j = \int_j^i n ds - \int_j^i dl \quad (1.19)$$

where:

$$I_{i \text{ geom}}^j = \int_j^i dl \quad \text{represents the line-of-sight (i.e. geometric) range}$$

$I_{i\text{ meas}}^j = \int_j^i nds$ represents the measured range

In addition to the ionospheric delay, the GPS signal delays through the troposphere which is the layer of atmosphere usually associated with changes in weather (from ground level up to 8 to 13 kilometers).

The tropospheric effects are more localized and subject to local conditions, change more quickly than the ionospheric effects and are difficult to model.

The tropospheric delay, on the contrary of the ionospheric one, is not frequency dependent and its effects can only be reduced by considering some computational model as the Hopfield scheme (Hopfield, 1969).

The tropospheric delay is a function of the tropospheric refractive index, and its path is defined by:

$$\Delta T_i^j = \int_j^i (n-1)ds \quad (1.20)$$

which is analogous to the ionospheric Equation (1.19).

The path length difference can be also be expressed by:

$$\Delta T_i^j = 10^{-6} \int_j^i Nds \quad (1.21)$$

where $N=10^6(n-1)$ is the refractivity.

Hopfield in 1969 showed the possibility of separating N into a dry N_d and a wet N_w component ($N=N_d+N_w$).

While N_d can be predicted very accurately, N_w is more difficult to predict due to uncertainties in the atmospheric distribution.

$$\begin{aligned}
(\Delta T_i^j)_d &= 10^{-6} \int_j^i N_d ds \\
(\Delta T_i^j)_w &= 10^{-6} \int_j^i N_w ds \\
\Delta T_i^j &= 10^{-6} \int_j^i N_d ds + 10^{-6} \int_j^i N_w ds
\end{aligned} \tag{1.22}$$

Hopfield has empirically found a representation of the dry refractivity, as function of the receiver height h above the surface:

$$N_d(h) = N_{d,0} \left[\frac{h_d - h}{h_d} \right]^4 \tag{1.23}$$

where $N_{d,0}$ is the dry refractivity component at standard sea level and h_d is the upper extent of the dry component of the troposphere referenced to standard sea level.

Similarly the wet refractivity is determined by:

$$N_w(h) = N_{w,0} \left[\frac{h_w - h}{h_w} \right]^4 \tag{1.24}$$

where h_w is the extent of the wet component of troposphere.

The path length difference when the satellite is at zenith and the receiver is at sea level is from Equation (1.21) and can be written as:

$$\Delta T_i^j = 10^{-6} \int_{h_0}^{h_d} N_{d,h} dh + 10^{-6} \int_{h_0}^{h_w} N_{w,h} dh \tag{1.25}$$

The evaluation of Equation (1.23), using the expression of Equations (1.24) and (1.25) yields:

$$\Delta T_i^j = \frac{10^{-6}}{5} [N_{d,0} h_d + N_{w,0} h_w] \quad (1.26)$$

Equation (1.26) is computed by numerous model (Hopfield, Modified Hopfield, Saastamoinen, etc....) because of the difficulty to model the wet refractivity component (Hopfield, 1969; Saastamoinen, 1972) . The Hopfield model is considered in all the GPS applications along this thesis, as it produce the most reliable results in the calculation of the pseudo-range distance (Satirapod and Chalermwattanachai, 2005).

The multi-path error (which is difficult to remove within urban zones) is the result of a signal arriving at the receiver with a slight delay δt_m because it was reflected off by objects, that are obstructing the line-of-sight from the satellite to the receiver.

These delayed signals can cause inaccuracy. A variety of techniques have been developed to mitigate multipath errors. For long delay multipath, the receiver itself can recognize the wayward signal and discard it. To address shorter delay multipath from the signal reflecting off the ground, specialized antennas (i.e., choke ring antenna) may be used to reduce the signal power as received by the antenna. Short delay reflections are harder to filter out because they interfere with the true signal, causing effects almost indistinguishable from routine fluctuations in atmospheric delay.

Based on these consideration to mitigate the multipath effects attention has to be paid on the antenna placement, antenna design and the use of materials that absorb GPS radio-frequency signals which can decrease the potential multipath interference. In many applications, above all in urban environments, one has to deal with the multipath errors, which can be reduced but not completely removed. In particular the multipath produces long period distortions (i.e., noises at low frequency) in the GPS 3D positions. The error

interferes with the accuracy of the measurements and can be removed by adopting traditional band-stop filtering technique (Kijewski-Correa and Kochly, 2007) or wavelet-based decomposition (Chen et al., 2001).

The last term in Equation (1.17) typed as δt_r , refers to the receiver noises and hardware offset. They are the results of thermal noise effects and vibration-induced oscillation on the receiver hardware stability. To be general, the δt_r are marked as time-dependent, although in practice their effects change slowly and can be averaged over time (Leick, 1995).

Summarizing, the positions of the GPS antennas have to be chosen to satisfy some requirements:

- (i) the antennas must have a clear view of the sky above to track as much as possible of the orbiting satellites;
- (ii) the reference and the rover should be in close proximity to minimize baseline errors.

In addition the quality of GPS position estimates depends on the number and the geometric distribution of the available satellites.

The error terms ε_i^j (a single value for any receiver), for which the time delay representation in Equation (1.17) has been introduced, turn out to be time dependent during a single day since the satellites are not geo-stationary.

This suggests to estimate the target position from records of length one day or more.

But also the repetition day after day is affected by uncertainties and this further aspect is known in the literature (Xu, 2007; Kaplan and Hegarty, 2006; Leick, 1995) as "signal geometric dilution of precision" (GDOP), which is mainly due to a deviation from the idealized geometric distribution of the satellites.

The GDOP is modelled by a geometric factor which describes the effect of the actual geometric satellite distribution on the accuracy of the target position. It provides an indication of how geometry affects accuracy.

When visible GPS satellites are close together in the sky, the GDOP value is high; when far apart, the GDOP values is low. Thus low GDOP value represents a better GPS positional accuracy due to a wider separation between the satellites used to calculate a GPS receiver position.

From an analytical point of view, this GDOP factor introduce an amplification of the standard deviation of the measurement errors.

In others words, the standard deviation (σ) of the “pseudo-range” (ρ_i^j) is replaced by the corrected standard deviation of the “pseudo-range” $\bar{\sigma}(\rho_i^j)$:

$$\bar{\sigma}(\rho_i^j) = \sigma(\rho_i^j) * GDOP \quad (1.27)$$

GDOP is inherent in the satellite technology and can be removed only by adding further satellites.

1.4.2 Differential Global Positioning System

As a stand alone GPS receiver user can only attain an accuracy of around 1m, which does not meet the requirements for a precise positioning system, augmentation in the number of the receiver and in their way to track a satellite and to reduce signals errors are required.

For precision positioning applications, a *Differential Global Positioning System* (DGPS) mode is required.

In general, the coordinates x_i , y_i , z_i , of a static or moving receiver can be obtained in a static mode (a GPS antenna is fixed in a certain position and receives the information sent by a number of tracked satellites) or in a differential kinematic mode. In the latter case, the signal recorded by a moving receiver (rover) is corrected, in real time or in post processing, by a stationary receiver (reference) fixed in a nearby position. This GPS positioning is, as previously mentioned, called *Differential Global Position System* (DGPS) (Dana, 1997).

The DGPS is so a method to improve the positioning or timing performance of GPS using one or more reference stations at known locations, each equipped

with at least one GPS receiver. The reference station provides information to the end user via a data link that may include:

- (i) corrections to the user's pseudo-range measurements;
- (ii) corrections to GPS satellite-provided clock and ephemeris data;
- (iii) integrity data (i.e., "to use" or "not to use" indications for each visible satellite, or statistical indicators of the accuracy of provided corrections);
- (iv) auxiliary data including the location, health, and meteorological data of the reference sensor.

The DGPS (see Figure 1.8) can be seen as a kinematic technique (it is in fact often indicated as *Real Time Kinematic* (RTK) DGPS)⁵, based on a reference receiver, that computes the coordinate differences between the GPS-derived position and the surveyed location: these differences are then transmitted to the rover receiver.

By DGPS, a significant reduction of the GPS pseudo-range errors is achieved, mainly when the rover receivers are close enough to the reference receiver such that the signal paths from the satellite to the rover and the reference are essentially identical. Indeed, the errors from all sources, except multipath and those internal to the receiver, are fully correlated (Kaplan and Hegarty, 2006).

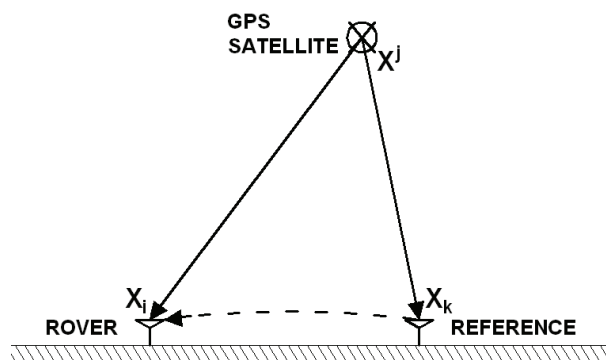


Figure 1.8. DGPS concept

⁵ A RTK is a real-time *Differential Global Positioning System* (DGPS) method that uses carrier phase measurements for greater accuracy.

Since the reported position of the j^{th} satellite is x^j, y^j, z^j and the k^{th} reference receiver is surveyed in at position x_k, y_k, z_k , the pseudo-range measurements consist of Equation (1.18) for the reported position and:

$$\rho_k^j = r_k^j + c(\delta t_k^j + \delta t_D) \quad (1.28)$$

for the reference receiver. Focus the attention on the differential correction:

$$\Delta \rho_k^j = \rho_k^j - r_k^j = c(\delta t_D + \delta t_k^j) \quad (1.29)$$

and subtract it in Equation (1.28):

$$\rho_i^j - \Delta \rho_k^j = r_i^j = c[(\delta t_D + \delta t_i^j) - (\delta t_D + \delta t_k^j)] \quad (1.30)$$

For the most part, the rover's pseudo-range error components will be identical to those experienced by the reference with the exception of multipath and receiver noise. The corrected pseudo-range can be expressed as:

$$\rho_{i,corr}^j = r_i^j + c(\delta t_{residual} + \delta t_{combined}) \quad (1.31)$$

where $\delta t_{residual}$ represents the residual error delay and $\delta t_{combined}$ is the combined clock offset. Actually, Equations (1.18) and (1.30) produce results at discrete instants of time, say t_j and t_k . Therefore, to enable the rover to compensate for this motion, the reference transmits a pseudo-range rate correction $\Delta \rho_k^j(t_k)$, which must be adjusted by the rover into:

$$\Delta\rho_k^j(t_i) = \Delta\rho_k^j(t_k) + \Delta\rho_k^j(t_k)(t_i - t_k) \quad (1.32)$$

The corrected rover pseudo-range is then calculated as

$$\rho_{i,corr}^j(t_i) = \rho_i^j(t_i) + \Delta\rho_k^j(t_i) \quad (1.33)$$

1.5 Conclusions

Within this chapter an overview of the GPS characteristics is presented. Attention is focused on the process to derive the user receiver position from the GPS signal generated by the overhead satellites.

The time correlation process, the signal modulation as well as the sources of errors inherent in the global positioning system are examined in detail.

The characteristics of a differential global positioning system (DGPS) technique are explained, underlining how it can maximize the accuracy of estimated acquired by GPS.

Chapter 2

OVERVIEW OF GPS APPLICATIONS IN CIVIL ENGINEERING

Introduction

An overview of some recent GPS applications in the Structural Health Monitoring (SHM) of civil engineering infrastructures, such as long bridges and tall buildings, is presented in this chapter.

Trough the description of some applications developed in the last two decades, this chapter tries to underline the successful use of GPS sensors in the structural monitoring of long periods structures and to examine the main results achieved in terms of GPS effectiveness, accuracy and resolution.

The state of art of GPS applications is here reported as it is needed to understand towards which direction the scientific research is going on and to explain the features adopted in chapters 3, 4 and 5 of this thesis.

In the last two decades in fact the number of research projects focused on the GPS use in the civil engineering domain is increasing due to both experimental laboratory tests and full-scale dynamic applications. Most of these works try to asses the effectiveness and reliability of satellite positioning systems in the dynamic monitoring of long period structures (Celebi, 2000; Cheng et al., 2002;

Ogaja et al., 2007), such as long bridges and tall buildings, which may vibrate during wind events (typhoons), temperature variations, load changes and earthquakes.

Further, these studies underline the GPS effectiveness in comparison with traditional sensors such as accelerometers, laser sensors and velocimeters.

As these methods present some disadvantages (among the others: temperature dependence, integration data process, visibility of the monitored object, etc.), the GPS is catching the attention of the scientific community as alternative or combined sensor for SHM, for both static and dynamic applications as it can overcome the limitations of climate variations and visibility. On the other sites the limitation of GPS in tracking high frequency motions, conduced many researchers to focus on integrated GPS – accelerometers systems (Chan et al., 2006; Meng et al., 2003; Li, 2004; Roberts et al., 2004) or GPS – fiber optics systems (Ge et al., 2002).

Apart from discussing the principles of the GPS technologies and approaching at well known problems in adopting a GPS solution (such as signal distortions and interferences in urban environments), the studies presented in the following try to answer to several challenging questions:

(i) Which combination of minimum displacement and maximum frequency can the GPS records?

(ii) Is the GPS accuracy dependent on the sampling rate used to record data?

(iii) In which range can the accuracy varies depending on the variation of the sampling frequency from 5 up to even 50Hz (actually the maximum achievable)?

(iv) Is the GPS accuracy dependant on the orientation (towards the North or the East) of the user receiving when adopting a differential global positioning system mode?

(v) Which is the influence of the geometric dilution of precision on the supposed accuracy?

(vi) Finally, is the GPS consistent with the requirements of a dynamic structural monitoring of long period structures?

The latter question, which may include all the above questions, involves the problem of defining which are the needed requirements for GPS applications and setting their range of variations. From the reported reference papers one derives that the consistency of GPS can be assessed by defining the maximum accuracy in measuring three-dimensional displacements (i.e., East, North and vertical components) and the highest detected frequency of motion.

Related to the first aspect, one can assert that the order of sub-centimeters of precision is achievable for horizontal movements (i.e., East and North components), while is around ten times worst for the vertical ones. On the other side for that concerns the frequencies, one can state that the highest frequency which can be detected is less than 10Hz and, in particular, is close to 5Hz.

Based on these considerations, it is possible to conclude that, in terms of displacement and frequency, the GPS technology may have limitations when very small displacements and very high frequencies measurements are required, but also that this limitations are not at all constraining in the monitoring of flexible (i.e., long period) structures, such as long span bridges and tall building.

The description of some applications is so presented with the aim to show and clarify these remarks.

2.1 Overview of full-scale GPS applications

Within the following sections a complete list of some cases study is provided.

Some GPS applications, developed in the last twenty years, into the field of the structural monitoring of civil engineering infrastructures are presented divided in two areas of applications:

- (i) tall building (towers and skyscrapers);
- (ii) long-span bridges (suspension and cables stayed bridges).

and, for each one of these two areas, in a chronological order.

Both the applications concern the dynamic monitoring process of long period structures, while the use of GPS as sensor for tracking static slow deformations (dams, embankments) is beyond the scope of this chapter and in general of the thesis.

A series of scientific studies, which are considered the most significant, is reported below divided into two previously mentioned fields: long span bridges, tall buildings. The purpose in describing them is to explain their contribution in the developing of the GPS unit in the structural monitoring and to show the approach followed in the use of the sensors for a dynamic monitoring of long period structures.

The chronological order is the way chosen to present those studies within this chapter.

2.2 GPS-based structural monitoring of long span bridges

In this section some structural monitoring applications based on GPS sensors are presented referring to long span bridges, as suspension and cables stayed bridges.

Since the first study case in 1996, it was clear that, due to the flexibility of such structures, the GPS could be an useful method to measure deck or cables displacements, to detect frequencies and mode shapes of these structures. It is also worth noting that sometimes the GPS was not the only kind of sensors used, but was integrated with other sensors. This was done for three main purposes:

(i) to prove the GPS accuracy in measuring the 3D movements of the bridges if compared to the results derived from others traditional sensors (most of the times, they were accelerometers);

(ii) to analyze the GPS data in terms of displacements and frequencies when the structure is excited by different sources of actions, such a winds, traffic loads, temperature variations;

(iii) to combine the GPS information with those of others sensors to get the dynamics of the bridge.

Some of the first applications were conceived in the United Kingdom and involved the Institute of Engineering Surveying and Space Geodesy (IESSG) of

the University of Nottingham, which become initially a sort of reference institution in this field, trying to approach at different GPS applications and referring to different GPS problems inherent in the technology. The first attempt can be considered the one studied by Ashkenazi et al. in 1996, when the real-time GPS monitoring of the Humber Bridge in the United Kingdom was realized.

One year after, in the United State of America, Duff and Hyzak (Duff and Hyzak, 1997) were probably the first to measure the short-term motion of a suspension bridge under wind and traffic loading with the GPS technology. They considered two cases study: the Hartman Bridge in Houston and the Blackwater River Bridge in Florida. To detect the bridge deformations induced by the traffic load, they conceived a kinematic global positioning system.

In the same year, in the United Kingdom, Ashkenazi et al. (Ashkenazi et al., 1997) analyzed the use of a Real Time Kinematic (RTK) GPS for monitoring the movements of large bridges detected in real-time. Successful tests were carried out at key points on three different bridges: the Humber Bridge, the Nottingham Clifton Bridge and the Dee Bridge.

Among the others, the Humber bridge has been the first case of GPS application to monitoring of long-span bridges. As mentioned, this bridge was monitored using a RTK GPS. The bridge, located across the Humber estuary on the East coast of England, consists of three sections, in an approximately North-South direction. It spans 2220m and it supported by two towers 155m high. The real-time monitoring of the bridge was carried out by putting individual GPS antennas on strategic points on the bridge deck (mid-span) and the support towers (Ashkenazi and Roberts, 1997). The reference receiver, by which the measurements of the rover receivers were corrected in real time, was situated 1.5km away from the bridge. In addition to the rovers dual-frequency GPS receivers, a pair of telemetry links and a real-time processing software were also considered. The objectives of the study was to monitor the displacement of the bridge deck at mid-span in the axial directions of the bridge, and the

displacement of support tower in the North-South, East-West and vertical directions.

In 1999, the California Department of Transportation (Caltrans) launched a GPS-based project on three strategic bridges: the Vincent Thomas Bridge in Los Angeles Harbour, the San Francisco Bay Bridge and the Golden Gate Bridge in San Francisco. The purpose was to evaluate the feasibility and capability of GPS technology for monitoring long span bridges (Turner, 2003). The project demonstrated that a network of RTK-GPS receivers could be a good tool for monitoring relative displacements, which are the key to indicate potential problems in the structural behavior. Following this first effort, a new project focused on the Carquinez Bridge in California, was launched in early 2004 for monitoring real-time displacements under traffic, wind and seismic loads.

The Japan, which has many long span bridges, started its researches for the monitoring of suspension bridges only at the beginning of the 21th century.

In 2000, Fujino et al. realized the GPS based monitoring system for the Akashi Kaikyo Bridge (the longest bridge of the world). Nakamura (Nakamura, 2000) then compared the GPS results to wind velocities and acceleration data of suspension bridge girder displacements under wind forces. The field measurements were carried out on the main span (1991m in length) of the bridge during a strong wind season, and the displacements of the girders obtained agreed well with the numerically-predicted values and wind tunnel test results (Yamada et al., 2006). An advanced SHM system (Fujino et al., 2000), composed of three GPS receivers, several seismometers, accelerometers, and anemometers, was designed in 1999 and it is still operational since that time, having as objective to ensure the traffic safety and the structural soundness of the bridge. Two GPS antennas were mounted on the tall bridge towers at both ends of the bridge, and the third is at the midpoint of the bridge. The system was designed to determine the three-dimensional coordinates at these three key points. The evaluation of bridge configurations under temperature changes was made using GPS. In addition to GPS measurement, temperature was also

measured at the corresponding points to obtain the relationship of temperature and displacement. Through the continuous measurements of bridge positions, temperatures at representative points, and other sensory data, the bridge performance is till now monitored in real-time, and a network of GPS reference stations enables a level of accuracy of sub-centimeter.

In 2000, at around the same period of the installation of GPS sensors on the Akashi Kaikyo Bridge, the Tsing Ma Bridge, the major suspension rail bridge of the world, was chosen as reference case to install a network of over 700 hundred sensors (of different types: anemometers, temperature sensors, dynamic weigh-in-motion sensors, accelerometers, displacement transducers, level sensing stations, and strain gauges) and 31 GPS receivers (Wong et al., 2001). The bridge, with a clear span of 1377m, is part of the Lantau Link, which comprises the Tsing Ma suspension bridge, viaducts crossing Ma Wan and the Kap Shui Mun cable-stayed bridge. Inside the Wind and Structural Health Monitoring System (WSHM) for the bridge, the GPS receiver system, referred to as "the real-time GPS On-Structure Instrumentation System (GPS-OSIS)", was designed to monitor the motions of the main suspension cables, decks and bridge towers.

The GPS SHM system (Wong, 2004), which is still working, is composed of four subsystems: the GPS surveying system; the information and collection system; the information processing and analyses system; the control system. Within the system, the GPS receivers (with a sampling rate of 10Hz) were located mainly on the two sides of the bridge body and the top of the bridge tower. The three-dimensional coordinates obtained were achieved by the real time kinematic (RTK) GPS technique and then transferred to the information processing and analyses system synchronously by the information collection system. The system had the purpose of monitoring the instantaneous displacements of the bridge body and the bridge tower in real time (during natural events or the trains crossing), and further calculated the stress of main structures, assessing the carrying capability, working status and enduring capability.

Also in Brazil some trials have been conducted since 2001 (Schaal and Larocca, 2002; Larocca, 2004; Larocca and Schaal, 2005). Larocca, in 2004, presented the results of the monitoring test campaign of the dynamic behavior under traffic load of the Hawkshaw Cable-stayed Bridge, in New Brunswick, Canada (main span of 217m, towers height of 36m) . Two L1 (single-frequency) GPS receivers were installed at the bridge mid-span, recording data with a sampling rate of 5Hz, and one reference over a gravel mountain near the bridge. The GPS data were processed by using a differential positioning technique. The mid-span of the bridge, under truck loading presented vertical displacement values of around 2.5cm, with frequency of 0.57Hz. The amplitude and the frequency of these displacements were correctly detected by single-frequency GPS receivers.

The detection of the bridge movements was then presented in Larocca and Schaal (2005), where they used a methodology, where there is no data adjustment and bridge oscillations can be seen directly using the data collected from two satellites, one close to the zenith and the other in the direction of the horizon. Within this methodology, the reference satellite was chosen according to the direction of bridge movements (e.i., close to horizon for vertical oscillations). However, this innovative and promising technique showed the constraint of requiring both the highest and the lowest satellite visible in the satellite constellation configuration. Even if this limitation can be overcome with proper trial planning, it is worth noting that this methodology cannot be applied to continuous real-time monitoring applications, as it requires a strong post-processing data elaboration and correction.

At the University of Nottingham, in collaboration with the University of New South Wales, several studies ranging from GPS to accelerometer integrations (Roberts et al., 1999, 2004, 2006b) to GPS-pseudolite integrations were realized (Meng et al., 2007, Dodson et al., 2003). A GPS integration with others measurements sensors (in the specific case topography pseudolite sensor) was studied at the University of New South Wales, Australia (Barnes et al., 2003, 2005).

Among the others, the trials on Wilford Suspension Footbridge in Nottingham (Barnes et al., 2003; Cosser et al., 2004) and the Parsley Bay Suspension Footbridge in Sydney (Barnes et al., 2005) demonstrated that pseudolite augmentation could be one of the possible solution when the geometry of the satellite constellation is so weak that for the GPS is difficult to track the minimum required satellites number. The pseudolites are ground-based transmitters of GPS-like signals, which can be optimally located to provide additional ranging information, and therefore improve the positioning precision.

Barnes et al., in 2002 developed an innovative carrier phase single-epoch software that can process both GPS and pseudolites data. They demonstrated that, when GPS is augmented with pseudolites, similar positioning precision (sub-cm) can be obtained for both the horizontal and vertical components. Due to the location of the pseudolites their trail on the Wilford Suspension Footbridge, the best improvements in precision were in the East and Vertical components by 41% and 31% respectively, and least in the North component (6%). The main drawbacks was due to the multipath errors which induced constant biases in the pseudolite measurements (up to 5cm) and which could not be removed from the solution. In Chapter 4 the issue of multipath errors will be examined and a filtering procedure by removing the low frequency trends from the position time series will be considered.

Dodson et al, in 2003 presented new results of the monitoring campaign on the Wilford bridge for providing a more robust system evaluation. By addressing to the problem of the implications of the GPS satellite constellation for precise engineering applications, simulations of the relationship between GDOP values and geographical locations were carried out. They revealed that the northern GDOP values were worst than the eastern GDOP in the areas with latitudes between 20° and 70°. The consequences were analyzed with the real bridge deformation data. The necessity of augmenting GPS with ground-based pseudolites was underlined by showing that the accuracy of the GPS positions can be significantly improved with the introduction of the pseudolites corrections. The experimental GPS results, as recorded in situ, were compared with the simulated GPS data, which produced around 40% positioning precision

improvement in both eastern and vertical coordinates. By such approach the researcher were able to demonstrate that millimeter level of precision can be achieved. The issue of the GDOP, the authors referred to in their study, will be discussed in Chapter 3 and its implications will be considered in a simulated application in Chapter 5.

New tests campaign was conducted in 2007 by Meng et al., when the structural response measurements of GPS and accelerometers to different excitations such as forced vibration, ambient vibration and decayed free motion from the Wilford suspension footbridge were used to extract the motion amplitude and corresponding vibration frequencies. It was found that the maximum frequency discrepancies due to different excitation methods were less than 3%. Frequencies under 5Hz (the Nyquist frequency of 10Hz GPS data), with a dominant peak at 1.73Hz, were clearly detected by the GPS sensors. In the analysis of structural dynamics, GPS coordinate time series were differenced to output accelerations and these values matched well with those of real acceleration data from the accelerometer. On the contrary, relative displacements estimated through acceleration double integral, compared with those from direct GPS coordinates, showed a good agreement. The results pointed out that both amplitude and natural frequencies could be precisely determined by GPS, indicating an high reliability for tracking very small vibration amplitudes (few millimeters).

In 2003, Lekidis et al., studied the applications of GPS sensors to detect the dynamic characteristics of the Evripos cable-stayed bridge in Greece, by comparing the experimental recorded data with those derived from numerical analysis. The Evripos Bridge is cable-stayed bridge measures with a mid-span of 215m and side-spans of 90m each. Four Javad dual-frequency GPS receivers were used, two employed as references located on bedrock, on pillars about 300m away from the bridge, and two positioned on the middle of two spans of the bridge where large displacements can be experienced. The use of two reference stations improved the geometry and the reliability of the solution. Observations were carried out at 10Hz sampling rate during sessions of 4 hours.

Additionally, a robotic total station (Leica TCA 1800) was employed to provide independent observations of the motion of the key points. From the recorded time histories of the two rover receiver, a frequency analysis was conceived. The GPS spectrum indicated one peak at 0.5Hz and more power peaks at low frequencies (from 0 to 0.2Hz) caused by the long wavelength biases of the solutions, such as multipath (probably caused by the steel cables of the bridge) and by a weak satellite geometry. The frequency content related to those effects was consistent with what presented by other studies for similar situations and suggested once again to use suitable filtering approach to remove noises at low frequencies caused by multipath (see Chapter 4) and by geometric signals dilution of precision (see Chapter 3).

Lekidis et al., concluded that the GPS measurements can offer additional information to common accelerometers data and can obtain more precise characteristics of the signal vibration, when the structural oscillations are in a frequency range of 0.1-2Hz. However they pointed out that the GPS was not well suited for high precision monitoring and proposed a direct integration of the GPS and total station data to provide an optimized solution combining the high frequency GPS data with the lower frequency, but more precise total station data.

In July 2004, the researchers of the University of Nottingham conducted further tests to assess the performance of GPS receivers for short baseline (i.e., short distance between a rover and a reference receiver) (Roberts et al., 2004). The tests were designed to investigate the use of high rate carrier phase GPS receivers (Javad JNS100, dual frequency, 100Hz sampling rate receiver) for deflection monitoring of structures. Static trials have been conducted to assess the precision of such a receiver, as well as the potential applications of such a high data rate. Trials were carried out in a controlled environment monitoring, making a comparison between a the 100Hz dual-frequency GPS receiver and a 10Hz single-frequency receiver.

The results showed that the 10Hz receivers performed slightly better than the 100Hz in the static trials. Even if the purpose of the authors was to show that a

100Hz receiver can perform better than a standard 10Hz receiver, this result was not completely achieved. Furthermore, choosing a single frequency receiver to demonstrate that the 100Hz receiver could work better seems to be contradictory. The limitations of a single-frequency GPS receiver are in fact well known (i.e., its precision is affected by the Ionospheric delay) into the research and industrial world, so the tests led to not completely useful information. In addition it is important to point out that the limitation of the sampling rate for the GPS receiver is a problem and it is still now an open discussion within the research community. For what concern this thesis, a very simple approach is adopted to show how the GPS precision degrades with the increasing of the sampling rate (see Chapter 3).

In 2004, Smyth et al., proposed a data fusion of relatively slow-sampled GPS displacement measurements with fast-sampled acceleration measurements as a means of significantly reducing measurement noise and circumventing double integration of the acceleration to obtain displacement estimates for large scale bridges. The motions of the suspended spans and towers of a suspension bridge (main span 1298m) located near New York City were monitored, through the data recorded during the 2004 New York City Marathon, where over 30,000 runners cross the bridge in less than half an hour. Displacements were monitored during that period by using three highly sensitive GPS receivers, two rovers placed on the bridge (one on the upper deck and one on the top of the tower) and one reference located at a fixed position near the structure (on the roof of a building). A sample rate of 5Hz was chosen for all the receivers. The combination of the high-sample rate accelerations data with relatively low sample rate GPS data was shown to be useful to estimate displacements from noise contaminated measurements.

In 2005 a Real Time Kinematic Global Positioning System (RTK-GPS) was used to monitor the response of the Bosphorus Bridge in Turkey (Erdogan et al., 2007) under loads such as pedestrian running which are not usually considered in the design of a suspension bridge. The bridge (completed in 1973) has a

1074m main span. The deck is a hollow box construction and inclined hangers ensure the suspension of the deck. The Eurasia Marathon on October 2005 was a good occasion to monitor the bridge response by GPS sensors during expected loads which produce rhythmic, systematic and random movements of the structure at very low frequencies (0.00036-0.01172Hz). The monitoring set-up was constituted by a rover GPS receiver placed on a middle point of the deck (where the maximum vertical movement was expected) and a reference on a building approximately 1Km away from the bridge. A 2Hz sampling rate was chosen for these observations. The bridge response, analyzed in both time and frequency domain, was clearly detected by GPS due the very high amplitude of the displacements (from -390mm below the mean deck level to 159mm above this level) and to the very low range of frequencies (from 0.00036Hz to 0.01172Hz). A comparison with the results obtained by a FE model was also carried out. This work showed once again the effectiveness of the GPS solution in monitoring long period structures with high induced displacements, even when the kind of action inducing these oscillations has random components.

In 2005 a GPS deflection monitoring trial was conducted on the West Gate Bridge in Melbourne (Raziq and Collier, 2007). The results were compared to the estimated frequencies and movements from the design of the bridge. The frequency information derived from the GPS results were also compared to frequency data extracted from an accelerometer installed close to a GPS receiver. GPS results agreed closely to the historical results and recent accelerometer trials for key modal frequencies, indicating the suitability of GPS receivers to monitor engineering structures that exhibit small movements. The West Gate Bridge is a cable-stayed box girder bridge where the amplitude of deck deflections is in the order of a few centimeters under ambient traffic and wind loading. Four Leica dual frequency GPS receivers were used (sampling at 10Hz), three mounted on the bridge (centre, quarter span and tower, respectively) and the fourth one, working as reference, on a building near the bridge. Data recorded by a RTK technique were processed, filtering the low frequency content of the signal spectrum, and analyzed showing that the GPS

tracked the frequency corresponding to the 1st symmetrical vertical bending (0.34 Hz), but not others two frequencies at 1.02Hz and 0.78Hz which were identified by the accelerometers. In the GPS signal spectrum these two latter frequencies were presented but hidden by noises as the amplitude of the movements related to these frequencies was quite small. The time domain analysis revealed that the deflection along the longitudinal axis of the bridge, recorded by GPS was around 1.5cm, while across the longitudinal direction of the bridge the deflection was around 1cm (which was just in the detectable range for the dual-frequency receivers adopted). Being the displacements of centimeters level, they were both detected by the GPS sensors.

In 2006, Roberts et al., performed a deflection monitoring trials on the Forth Road Bridge in Scotland. The Bridge consists of 3 spans, the main of around 1Km. Forty-six hours of GPS data were gathered upon the bridge at 7 locations; 5 on the deck and two on the southern tower, using both single and dual frequency Leica receivers. The data were post-processed in an On The Fly (OTF)⁶ manner relative to the reference receiver located adjacent to the Bridge. An Adaptive Filtering was also used to mitigate multipath. During the trials, the traffic and the wind loading were monitored. The results illustrated the amplitude (up to 40cm) and frequency (around 0.1Hz) of the deflections compared with those of a Finite Element Model (FEM) modal analysis of the Bridge, showing a good agreement. Unfortunately, the use of a post-processing data elaboration technique and the large amplitude of the oscillations are the drawbacks of this study.

As the interest in the GPS based SHM is growing in China, can be seen from one of the many cases studies, the Jiangyin Yangtze River Highway Bridge, which spans more than one kilometer (Leica, 2007). It is the longest steel box

⁶ The OTF method establishes a search space using differential phase and pseudo-range positioning. The correct solution within the search space is identified using least-squares search or ambiguity covariance methods. These methods are generally limited to short and medium baselines

girder suspension bridge in China, and the fourth longest in the world, built along the national key trunk route crossing the Yangtze River, between Jiangyin and Jingjiang in Jiangsu Province.

A Leica-Geosystems GPS monitoring system which focuses on the monitoring of the girder geometric form and the displacement of the bridge towers was conceived in 2005. The system provided a cost-effective and innovative solution for delivering three-dimensional positioning information at a sampling rate of 20Hz from several GPS sensors, including an advanced analysis application software (Leica, 2007). With the use of a RTK technology, the accuracy at the 1cm level was achieved. The sensor mock-up consisted of one reference station installed on the roof of building close to the bridge and eight GPS rover sensors installed at key monitoring points of the bridge to assess the dynamics characteristics of the bridge. The rover receivers were placed at the two bridge towers, at the maximum flexibility points of the main span, and at the four quartile points, at the one-fourth, middle and three-fourth points of the bridge. Based on transformation parameters provided by the user, the system implemented provided three dimensional dynamic displacements results within the bridge's coordinate system.

In addition to the Jiangyin Yangtze River Highway Bridge, the Humen suspension bridge is a further suspension bridge in China with main span of 888m and global length of 15Km. A GPS based SHM system (Xu et al., 2002; Guo et al., 2005) was installed for monitoring the bridge working status in real time under the typhoons, traffic loads and temperature variations. A GPS reference station, equipped with a double-frequency GPS receiver, was located on the top of the building of the control centre (located in an open space and within 300m of the bridge) whose 3-D coordinate were previously determined by conventional static GPS methods. Eight GPS rover receivers were located on the position of middle, one fourth and one eighth of the bridge span and two on the bridge towers. The sampling rate was chosen to be 5Hz, consistent with the bridge main frequency. A RTK sensors communication was adopted via an optical fibers network, which avoided potential signal loss caused by large

vehicles blocking GPS signal paths. The recorded data were then processed by means of a suitable signal analysis techniques to obtain modal parameters from the wind-induced response. In the GPS power spectra, frequency peaks at 0.095, 0.134, 0.446Hz were clearly identified, corresponding to the first lateral sway mode, to the first vertical sway mode and to the torsional mode respectively.

Lately in 2008 in China a SHM was implemented and 179 sensors were installed on the Yonghe Bridge (Kaloop and Li, 2009). Among the others GPS and accelerometers sensors were used to collect the lateral displacements, acceleration and torsion displacements data of the bridge towers. Three GPS sensors were adopted: one reference installed near the bridge and two rovers installed at the top of the two bridge towers. GPS (sampled at 10Hz) and accelerometers (sampled at 100Hz) data were collected for wind events on January 2008. The displacement of the southern tower is the along wind direction were between -20.02 and 28.91mm with an average value of 1 mm, whereas it was found to be between -13.02 and 23.38mm with average value of 0.80mm in the transversal direction. By adopting a wavelet analysis the power spectral density in the horizontal displacements were calculated showing a greater level of energy in the along wind direction (frequency of 0.3Hz) than in the transversal one (frequency of 1.1Hz).

Once again the researchers pointed out that the GPS was able to measure movements at low frequencies while, due to its signals errors, GPS could not measure the high frequency of dynamic behavior of tower. The analysis of the test results revealed that the noises of GPS signals are high (above all at low frequencies) but that the GPS is an useful tool for characterizing the dynamic behavior of low frequency bridges.

Table 2.1 summarizes all the above mentioned reference cases.

Table 2.1. State of the art of GPS applications for long span bridges

| Frequency range | Around 0.1Hz | | | | From 0.095Hz to 0.446Hz | From 1.73Hz to 5Hz |
|---------------------------------|---------------------------------|---------------------------------------|-----------------------------------|-------------------------------|--|--------------------|
| Displacements range | Sub-centimeter | | From -200mm to +200mm | From -150mm to +150mm | Sub-centimeter | |
| Type of excitation | Ambient vibrations | Wind events | Natural events Trains crossing | Typhoons Traffic loads | Ambient vibrations | |
| GPS technique and sampling rate | Real Time Kinematic | Real Time Kinematic | Real Time Kinematic (10Hz) | Real Time Kinematic (5Hz) | GPS + pseudolites | |
| Number of sensors | One reference Several rovers | One reference Three rovers | Thirty-one receivers | One reference Eight rovers | Two reference Twelve rovers | |
| Type of structure | Humber Bridge | Akashi Kaikyo Bridge | Tsing Ma Bridge | Humen suspension bridge | Wilford Suspension Footbridge | |
| Authors | Ashkenazi et al., 1997 | Fujino et al., 2000 Nakamura, 2000 | Wong et al., 2001 | Xu et al., 2002 | Barnes et al., 2002 Meng et al., 2007 | |

| | | | | | |
|-----------------------|-----------------------------|------------------------------|-------------------------------|-----------------------------|---------------------------------|
| From 0.3Hz to 0.5Hz | Around 2.8Hz | Around 0.5Hz | Around 0.1Hz | From 0.00036Hz to 0.01172Hz | Between 1cm and 1.5cm |
| From 4mm to 1mm | From -250mm to +50mm | Around 2.5cm | Up to 40cm | From -390mm to 159mm | From 0.34Hz to 1.02Hz |
| Ambient vibrations | Runners crossing the bridge | Truck loading | Traffic loads Wind actions | Runners crossing the bridge | Ambient traffic Wind loading |
| DGPS (10Hz) | DGPS (5Hz) | DGPS (5Hz) | On the fly kinematic (10Hz) | Real Time Kinematic (2Hz) | Real Time Kinematic (10Hz) |
| Two references | One reference | One reference | One reference | One reference | One reference |
| Two rovers | Two rovers | Two rovers | Seven rovers | One rover | Three rovers |
| Evrinos bridge | New York City bridge | Hawkslaw Cable-stayed Bridge | Forth Road Bridge | Bosporus Bridge | West Gate Bridge |
| Leikidis et al., 2003 | Smyth et al., 2004 | Larocca and Schaal, 2005 | Roberts et al., 2006 | Erdogan et al., 2007 | Raziq and Collier, 2007 |

| | | |
|---|-------------------------------|------------------------------|
| | | From 0.3Hz to 1.1Hz |
| | Around 1cm | From -20.00mm to +28.91mm |
| Ambient vibrations | Wind actions Traffic loads | |
| Real Time Kinematic (20Hz) | Post-processing (10Hz) | |
| One reference Eight rovers | One reference Two rovers | |
| Jiangyin Yangtze River Highway Bridge | Yonghe Bridge | |
| Leica, 2007 | Kalooop and Li, 2009 | |

2.3 GPS-based structural monitoring of tall buildings

In this section some applications of GPS sensors in the structural monitoring of tall buildings and towers are presented.

The first studies in this field started a couple of years before the ones on long span bridges.

A great difference with the GPS applications for bridges was due to the typical environmental conditions of tall buildings. Most of them in fact, on the contrary of long span bridges, arise in urban environments which are full, and not free, of electronic and magnetic interferences and are the main factor which make the GPS signal prone to multipath effects. In fact the presence of buildings near the one to be monitored can obstruct the view of satellites and can produce a deviation of the signal from the ideal line (i.e., a multipath), which represents a constraint which influences the GPS measurements in urban environment and which has consequently to be overcome. Most of the studies presented in the following had to deal with this problem by limiting, with appropriate algorithms, its influence on the GPS accuracy, through the application of signal filtering procedures, or by choosing a preferable sensors locations, to finally prove the GPS effectiveness in the monitoring of tall building.

The main interest in this field was to detect the dynamic behavior of the buildings while subjected to wind actions or to earthquakes, sometimes in comparison with traditional sensors.

In Calgary (Canada) a first attempt on the Calgary Tower (160m high) in 1993, was probably the earliest test where GPS sensors were applied for the dynamic monitoring of a tall structure under wind loading. Lovse et al. (Lovse et al., 1995) outlined the GPS results while the tower oscillations, at a low frequency (around 0.3Hz), were caused by a 60–100km/h wind. The monitoring set-up consisted of one reference GPS receiver located on the roof of a building situated approximately 1km North of the tower and two GPS rover receivers on the tower (at the height of 160m). Among the others, one data acquisition test conducted on November 1993, at the sampling rate of 10Hz, showed that the frequency of North-South and East-West movement was about 0.3Hz, the North-South amplitude approximately ± 15 mm and the East-West amplitude ± 5 mm. These results underlined that the GPS could be a feasible sensor for long period structures, with low natural frequencies (0.3Hz) and amplitude of displacements vibrations of the order of sub-centimeters.

In 1997, a similar experiment was carried out in China. Guo and Ge described the use of GPS to measure the displacements and frequencies of the Diwang Tower (79 stories, 325m high) in Shenzhen City, under wind loading such as the York typhoon (the strongest typhoon in the region since 1983). The sensors set-up consisted of a rover receiver located on the top of the building (at the height of 325m) and a reference one placed on a lower building about 500m away on the South-West direction. The OTF (Ambiguity Resolution On The Fly) kinematic method was adopted to acquire the GPS signals sampled at 20Hz. The dynamics displacements and vibration frequencies were measured by GPS and accelerometers while the building was subjected to the York typhoon. The study showed that the GPS data could be useful to assess the amplitude and frequency of the tower deflections (0.17Hz) due to the 90km/h winds caused by the typhoon, with an accuracy of around ± 5 mm. In addition it was shown that

the GPS results matched, in both time and frequency domain, the ones acquired by an accelerometer placed close to the GPS rover sensor.

In California, a well known area for seismic risk, researchers at the US Geological Survey (USGS) successfully tested the feasibility of using GPS technology to monitor the dynamic response of buildings to earthquakes (Celebi et al., 1999). Since the occurrence of Northridge (1994) and Kobe (1995) earthquakes, several studies of damage detection of tall buildings under earthquakes were realized. Early studies by USGS scientists in California have discussed concepts and the technical feasibility of using GPS technology to monitor the response of buildings to such earthquakes (Celebi et al., 1999). Simulation studies with a model structure demonstrated the technical feasibility of GPS receivers on tall buildings. In particular Celebi in 2000 showed that sampling at 10Hz with GPS units provided an accurate displacement response history from which drift ratios and dynamic characteristics can be derived. Despite the small displacements (around 1cm) and low signal noises, the dynamic frequencies were identified thus indicating that during larger displacements, better identification of the dynamic characteristics as well as drift ratios could be made with higher confidence. From the data recorded on the model structure, the fundamental frequencies were identified (0.245 and 0.296Hz) and a damping percentage of approximately 2% was extracted.

In 2002, Celebi and Sanli described the developmental work in which two GPS receivers were deployed on two 44-stories buildings in Los Angeles and one 34-stories building in San Francisco. The buildings were also instrumented with accelerometers to allow comparison of GPS measured displacements with the displacements calculated from acceleration measurements. For the 44-stories building ambient vibrations were measured with a GPS unit deployed on its roof. A reference GPS unit was located within 500m of the building. The signals were very noisy and amplitudes very small. Despite this the detected frequency (around 0.3Hz) appeared to be reliable when compared with the 0.23Hz frequency calculated from accelerations records. The results showed the great potential for GPS applications to monitor long period structures (such as

tall buildings, tall chimney, long span suspension and stayed cable bridges) during earthquakes and wind-induced deformations of, as the dynamic characteristic (frequencies and damping) could be identified.

Since 1996, in Singapore, the Republic Plaza Building has been instrumented with accelerometers and anemometers in order to measure its response to earthquakes and wind forces (Brownjohn et al., 2003b, 2004). The Republic Plaza (66 floors and 280m tall) was built with earthquake proof features and designed to improve its stability to wind loading. In February 2000 a pilot experiment was carried out to test the feasibility of incorporating GPS to the existing monitoring system (Ogaja et al., 2001, 2003). Both the GPS and accelerometer data successfully captured the building response to strong winds. Brownjohn et al. (Brownjohn et al., 2003a) also looked into the challenges of implementing GPS and fibre optics for the continuous monitoring of the building. The RTK-GPS system of the Republic Plaza was designed to provide, to sub-centimeter accuracy at a rate of up to 10Hz. The system consisted of a dual-frequency reference receiver, installed at the Leica Singapore headquarters, about 10 km from the monitored building, and two dual-frequency rover receivers, sampled at 8Hz, on the roof of the building. During sudden strong wind and earthquake events there were clear and systematic GPS displacement signals of quasi-static movement or dynamic response.

In 2004, Hristopulos et al., investigated the feasibility of using the above described GPS network for determining the response of the Republic Plaza Building to wind loading and to study the correlation properties of the GPS signal. The authors proposed a filtering procedure that removes from the GPS signal singular pulses due to loss of lock between the receiver and the satellite or receiver tracking problems, as well as the low-frequency noise. They validated the GPS measurements by comparison with accelerometers data. The applied procedure enabled to model the stochastic and systematic components of the GPS displacement time series for extracting the weak structural response from the dominant noise. The spectrum of the building response obtained from the filtered GPS data exhibited a dominant peak at 0.19Hz, which was in agreement with the accelerometers spectrum. This result, obtained by applying a

suitable filter to remove the low-frequency noise from the GPS signal spectrum, revealed the GPS effectiveness in detecting the building response to wind loading.

Investigators at the Tokyo Polytechnic University and the University of New South Wales (Australia), described a series of tests on a 108m steel tower in Tokyo using GPS, accelerometers and optical fibre sensors (Tamura et al., 2002; Li, 2004; Li et al., 2005, 2006). Data collected during typhoons and earthquakes (Tamura et al., 2002; Li, 2004) were analyzed in both time and frequency domains, showing the benefits of sensor integration. From the evaluation of the applicability of a RTK-GPS measurement system the researchers achieved some interesting conclusions: RTK-GPS can measure the total displacement, not only its dynamic component but also the static component; the GPS is available for response measurements when natural frequencies are smaller than 2Hz and displacement larger than 2cm; the characteristics of vibrations can be estimated not only for accelerometer signal but also for RTK-GPS signals; the deformation of the tower caused by heat stress was measured to be about 4cm.

Tamura et al, in 2002 analyzed the efficiency of this RTK-GPS solution. In their study accelerometers have been used for field measurements of wind-induced responses of buildings. However, as wind-induced response consists of a static component, which is difficult to measure by accelerometers, and a dynamic fluctuating component, detected by accelerometers, GPS sensors were adopted to measure the displacements due to the static component of the wind-induced response. In their in situ tests, a rover GPS receiver was set on the top of the 108m high steel tower (close to an accelerometer) and a reference receiver was set on the top of a rigid 16m high reinforced concrete building located next to the tower (110m far). The GPS data was the sum of the static displacement of about 4 cm and the fluctuating component with a dominant frequency equal to the lowest natural frequency of the building (0.57Hz). The acceleration record seems to correspond closely to the fluctuating component of the displacement recorded by the RTK-GPS network. The power spectral

density of the GPS displacement time series showed almost constant energy at the lower and higher sides of the natural frequency, which could be attributed, as also underlined in others studies here presented, to the background noise of GPS measurements (multipath and GDOP).

Further tests, with the same sensors set-up of Tamura et al., 2002, were carried out in 2003 by Li et al. (Li et al., 2005; 2006), and in 2006 by Tamura and Yoshida, with the aim of validating the system reliability in comparison with the results of accelerometers and of a Finite Element model (FEM) of the building. The GPS signals, sampled at 10Hz, once recorded were filtered to remove the effects of GPS noises which were evidenced also in Tamura et al., 2002. The comparison was made considering the structural response to two different kind of actions: wind action during a typhoon and seismic action due to an earthquake event. The spectrum of the time series data recorded during the typhoon for both GPS and accelerometers indicated the same frequency peak at 0.57Hz (see also Tamura et al., 2002). A further peak at 2.16Hz, confirmed by the FE model analysis, was detected by both sensors. The earthquake data were recorded for a limited period of 300s in order to see both the P and S waves clearly. The S waves, causing a more than 6 cm peak vibration of the tower in both horizontal directions, were detected by the GPS unit, on the contrary the P waves were detected only by accelerometers. This was because the magnitude of P waves is 2–3 times smaller than the S waves and hence could be buried in the GPS noise.

Based on the results the researchers concluded that the GPS could pick up signals at the low frequency (from 0 to 0.2Hz), probably affected by GPS-specific noise such as multipath, while the accelerometer could easily record high frequency signals (from 2Hz). The two sensors were so complementary having an overlapping capability in the frequency range between 0.2 and 2Hz. Furthermore, even if the GPS could not detect the P waves components of the seismic action, it could record the static and quasi-static response components induced by winds, which were missed from the accelerometers data.

In 2002, Breuer et al., evaluated the accuracy of the measurements using GPS sensors to detect small movements of the Stuttgart TV tower due to weak wind events. Several tests were conducted by changing the baselines length connecting the rover (on the TV tower) and the reference receivers, showing that accuracy was independent of the distance between reference and rover unit. Only the number of available satellites and their geometric distribution were responsible for the achieved precision of position. The responses of the tower due to ambient vibrations and wind actions were analyzed. The rover GPS unit was placed on the level above the platform for visitors (155m above the ground level) on the TV tower and the reference sensor was located about 450m away from the building. The displacements of the tower, 4cm in the cross-wind direction and 2.5cm in the along-wind direction, were clearly identified by the GPS sensors. Also the first natural frequency of 0.2Hz was detected.

In 2003, Kijewski-Correa et al. (Kijewski-Correa et al., 2003a, 2003b) described a comprehensive full-scale GPS configuration and validation tests in Chicago where the instrumentation was deployed on three tall buildings, including high-accuracy GPS, accelerometers and anemometers. Through the Chicago full-scale monitoring program, the first ever systematic comparison of tall buildings response against Finite Element and wind tunnel models used in their design was made. The program was led in 2003 by the NatHaz Modeling Laboratory at the University of Notre Dame in conjunction with the Boundary Layer Wind Tunnel Laboratory at the University of Western Ontario and Skidmore, Owings & Merrill in Chicago. The purpose of the program was to emphasize the need of calibrating and experimentally validating any GPS sensor before installation in full-scale, so that displacement tracking limitations and resolutions can be accurately benchmarked. As the accuracy of GPS continuously fluctuates throughout the day due to the position and availability of satellites, some reliability measure were also provided, to quantify the geometric dilution of precision (GDOP). High-accuracy GPS units were integrated with traditional sensors. Each building was equipped with force-balance accelerometers, mounted in orthogonal pairs at opposite corners of the

highest possible floor, to capture both sway and torsional responses. Ultrasonic anemometers were also mounted at opposite corners of the rooftop to measure the wind field characteristics above Chicago. The observed responses were compared to predictions from wind tunnel tests and analytic models developed in the design phase.

In detail building [1] is a steel tube comprised of exterior columns, spandrel ties, and additional stiffening elements to achieve a near uniform distribution of load on the columns across the flange face, with very little shear lag; building [2] is reinforced concrete building, with shear walls located near the core to provide lateral load resistance; building [3] is a framed tubular system fundamentally behaving as a vertical cantilever fixed at the base to resist wind loads. The system is comprised of closely spaced, wide columns and deep spandrel beams along multiple frame lines. As common accelerometers could only detect the resonant and not the quasi-static component of the wind-induced displacements response (see Tamura et al., 2002; Li et al., 2006), a GPS unit was also installed on the top of the buildings allowing to track dynamic displacements with high accuracy at sampling rates of 10Hz. A differential GPS (DGPS) was adopted by using a rover receiver on the top of building [1] and a reference receiver installed on a building 1290m away. Significant wind events were considered for the full-scale comparison of GPS data with accelerometers and Finite Element results in detecting the dynamic characteristics of the building (i.e., natural frequencies and damping). The November 24, 2003 wind events was chosen as case study. The recorded GPS displacements were filtered through the use of band-pass filter, and the comparison was restrained to the dominant fundamental sway responses along the N-S and E-W axes of the building. The issues of multipath interference was also addressed as it was seen that the GPS displacements showed a long period distortions (i.e., noises at low frequency) which were obviously caused by multipath (expected in a such dense urban zone). These errors interfered with the ability to accurately determine background wind-induced response. They could be removed by adopting traditional band-stop filtering technique (Kijewski-Correa and Kochly, 2007) or wavelet-based decomposition (Chen et al., 2001).

The calibration program demonstrated that at sufficiently large amplitudes of the displacements ($> \pm 2\text{cm}$), GPS performance is independent of the frequency of motion, however, for low amplitude motions ($< \pm 2\text{cm}$), the GPS tracking ability is superior at lower frequencies, motivating its application to the monitoring of flexible civil structures. This was further demonstrated in the tracking of simulated motions of tall buildings under the action of wind, where GPS performance produced errors of less than 10%. However in the full-scale tests on one of the three tall buildings in Chicago, an excellent correlation between GPS and accelerometers in detecting the structural dynamic response was underlined.

In 2005, Campbell et al., conducted a series of measurements tests of the wind-induced response of a high-rise building in Hong Kong during the Damrey typhoon. The building, a 256m tall reinforced concrete structure, was instrumented with accelerometers and a GPS unit to characterize both the high frequency modal response (by accelerometers) and the slowly-varying, quasi-static response (by GPS). The maximum measured peak resultant accelerations were approximately 5.1mg in the core and approximately 5.3mg at the wing, while the maximum recorded displacements was 36mm. Accelerations calculated from the GPS displacement measurements (sampled at 20Hz) were compared with accelerations measured by accelerometers. A band-pass filter (from 0.1 to 0.5Hz) was applied to the accelerations calculated from GPS recorded displacements to capture contributions from the first three modes of the structure and to remove noises. Outside of this frequency range, the spectral powers of modal frequencies contributed less than 1% to the overall acceleration response of the building. The comparison of a record of one hour acceleration time histories, as recorded from accelerometer and as calculated from GPS data, showed a good agreement between the two sensors. However, the peak acceleration estimated from GPS displacements was approximately 80% of that measured by accelerometers. For torsional motion measurements from GPS and accelerometers were approximately 5% different.

In Australia, in 2006, a full-scale monitoring program was conceived on the Latitude Tower in Sydney (Rizos et al., 2008). It is a 45-story office building in the Sydney Central Business District, completed in late 2004, standing at a height of 192m above street level. The tower is a composite structure, consisting of reinforced concrete and structural steel components. Core construction is reinforced concrete, with steel beams and a composite slab spanning to the perimeter columns, which consist of concrete-filled steel hollow sections. The floor plan is approximately rectangular, with small rectangular sections of the floor plan removed in the north-east and south-west corners of the tower. A test bed was set up by the University of New South Wales in collaboration with the University of Sydney to study the structural response of the building to local wind effects. Accelerometers and an anemometer were installed in 2005 and in 2006 a GPS unit was added (placed on the rooftop) to the monitoring system. Data from three reference stations were analyzed together with data from the GPS rover on the tower, forming baselines of 1.1km, 5km and 21km in length. Large wind events were captured on September 7 and November 15, 2006. The monitoring system was intended to measure sway and torsional response. The resonant response obtained from both GPS (sampling at 10Hz) and accelerometers agreed well with each other. The first detected natural frequencies were 0.25Hz for the N-S direction and 0.29Hz for the EW direction, with a first torsional frequency of 0.41Hz. It was very significant that the researcher showed that the GPS reference station 21km away from the rover also captured the 0.25Hz resonant signal very clearly. To split the static and dynamic motions and to suppress the multipath effect, a low-pass filter was designed to extract the very low frequency component from the GPS time series. The quasi-static motion was extracted by a band-pass filter with cut-off frequencies of 0.01Hz and 0.2Hz, just below the statistically defined multipath frequency range from 0.0008 to 0.01Hz (see Kijewski-Correa and Kochly, 2007; Tamura et al., 2002; Li et al., 2006). The amplitude of the static extracted component was less than ± 4 mm. Post-processing with the precise ephemeris was used to produce the GPS displacement time series.

Table 2.2 summarizes the above mentioned reference cases.

Table 2.2. State of the art of GPS applications for tall buildings

| Frequency range | Around 0.17Hz | Around 0.3Hz | Around 0.2Hz | From 0.5Hz to 2Hz |
|-------------------------------|----------------------------|--|---------------------------------------|--|
| Displacements range | Around ± 5 mm | From -1.0cm to +1.0cm | From 2.5cm to 4cm | More than 2cm |
| Type of excitation | Wind events (typhoons) | Earthquakes Wind events | Ambient vibrations Weak wind loads | Wind action Seismic action |
| GPS technique (sampling rate) | Real Time Kinematic (20Hz) | DGPS (10Hz) | DGPS | Real Time Kinematic (10Hz) |
| Number of sensors | One reference One rover | One reference Two rovers | One reference One rover | One reference One rover |
| Type of structure | Diwang Tower (China) | 44-stories building in Los Angeles | Stuttgart TV tower | Steel tower in Tokyo |
| Authors | Guo and Ge, 1997 | Celebi, 2000 Celebi and Sanli, 2002 | Breuer et al., 2002 | Tamura et al., 2002 Li et al., 2005 |

| | | | |
|--------------------------------------|---|------------------------------------|---------------------------------|
| From 0.1Hz to 0.2Hz | Around 0.2Hz | Around 0.3Hz | From 0.25Hz to 0.4Hz |
| Up to ± 2 cm | From -10mm to +30mm | Between ± 5 mm and ± 15 mm | Around 40mm |
| Wind events | Wind s loading Earthquakes | Wind loading | Wind event: Damrey typhoon |
| DGPS (10Hz) | Real Time Kinematic (10Hz – 8Hz) | Real Time Kinematic (10Hz) | DGPS (20Hz) |
| One reference One rover | One reference Two rovers | One reference Two rovers | Post-processing GPS (10Hz) |
| One reference One rover | One reference Two rovers | One reference One rover | Three reference One rover |
| Tall building in Chicago | Republic Plaza Building (Singapore) | Calgary Tower | High-rise building in Hong Kong |
| Kijewski-Correa et al., 2003a, 2003b | Ogaja et al., 2003 Hristopulos et al., 2007 | Lovse et al., 2005 | Campbell et al., 2005 |
| | | | Rizos et al., 2008 |
| | | | Latitude Tower (Sidney) |

2.4 Conclusions

Chapter 2 presents an overview of the more significant GPS applications and solutions. In particular different GPS-based systems are described with the aim to underline the different solutions proposed in the field of the dynamic structural monitoring of long period structures such as tall buildings and long span bridges.

The state of the art, that is provided along this chapter, tries to answer some questions of common interest among the scientific community, in particular:

- (i) which can be the achievable GPS resolution;
- (ii) which combination of displacements and frequencies can be detected;
- (iii) how much the GPS accuracy is dependent on the sampling rate;
- (iv) how much the GPS accuracy is dependent on the sensors orientation along the North or the East directions;
- (v) how significant can be the influence of the satellite constellation;
- (vi) in which way the GPS accuracy can be increased using integrated solutions.

Chapter 3

GPS PRECISION IN STATIC AND DYNAMIC TESTS

Introduction

The reliability and the accuracy of the measurements of dual frequency GPS receivers are investigated in this chapter for both static and dynamic tests. The accuracy of GPS measures is assessed by testing a GPS system made by a fixed reference receiver and a rover. The latest one moves along rails driven by a linear electromagnetic motor. The aim is to simulate harmonic displacements with the rover GPS receiver moving in the horizontal plane. By comparing the recorded coordinates of the receiver with the known parameters of the motor movements, one checks the accuracy of the whole acquisition system. The comparison is based on sufficiently long records.

3.1 The experimental mock-up

The system architecture is made of two parts: an outdoor part constituted by the GPS antennas (6.2cm height, 17.0cm of diameter, 0.4Kg weight) and an indoor part assembling the receivers and a computer running two Leica software products.

The devices installed are (Leica 2005):

- a dual frequency high precision Leica GMX902 GPS receiver, working as reference, with a maximum sampling rate of 20Hz;
- a dual frequency high precision Leica GMX902 GPS receiver, working as rover, with a maximum sampling rate of 20Hz;
- two dual frequency Leica AX1202 antennas, recording signal with a sampling rate up to 20Hz.

The GPS signals are recorded by the Leica GPS Spider software (Leica, 2004), that provides information on the satellites configuration and allows corrections of data for a real time positioning. The recorded displacements signals are then analyzed using a system identification toolbox (Matlab 2004).

The two GPS antennas were anchored on a stiff concrete surface in an open field location and in a position that guarantees to track a minimum of 6 satellites during the day.

Two scenarios were conceived. First the two antennas were placed on a concrete block at the height of around 3m near an industrial steel building in Pavia (Casciati et al. 2007). In a second experimental campaign, the antennas were located on the roof of this industrial building at the height of about 11m and at the distance of 13m.

The first case, with the GPS antennas placed at the height of 3m and besides the steel building, was used to calibrate the resolution of the GPS system in acquiring known and fixed longitudinal displacements. Many tests were conducted and the results showed an interesting and promising agreement with the imposed displacements. In this case the moving antenna was mounted on a LinMot linear motor (LinMot, 2008) as depicted in Figure 3.1.

The linear motor moves, following assigned displacement time histories, of different amplitudes and periods, driven by a software program. The antenna fixed on the moving part of the motor is forced to move to a known position, along the direction of the linear motor, working in the horizontal plane. The coordinates of the point where the antenna is fixed are recorded by the rover

receiver. They can be compared with the change of position imposed by the linear motor.

The main conclusion achieved by the first GPS network set-up can be summarized as follows (Casciati and Fuggini, 2007):

(i) the tests carried out were influenced by the bad localization of the GPS antennas;

(ii) the position of the antennas, besides the steel building, does not completely satisfy the requirement of a clear view of the sky above the antennas (i.e., “cut-off angle” $>15^\circ$) and this led sometimes to an instantaneous and unexpected loss of signal;

(iii) when data were recorded, the achieved results were very good in terms of precision;

(iv) when the building was obstructing the view of overhead satellites, a lack of satellites signal happened and consequently no data were recorded.

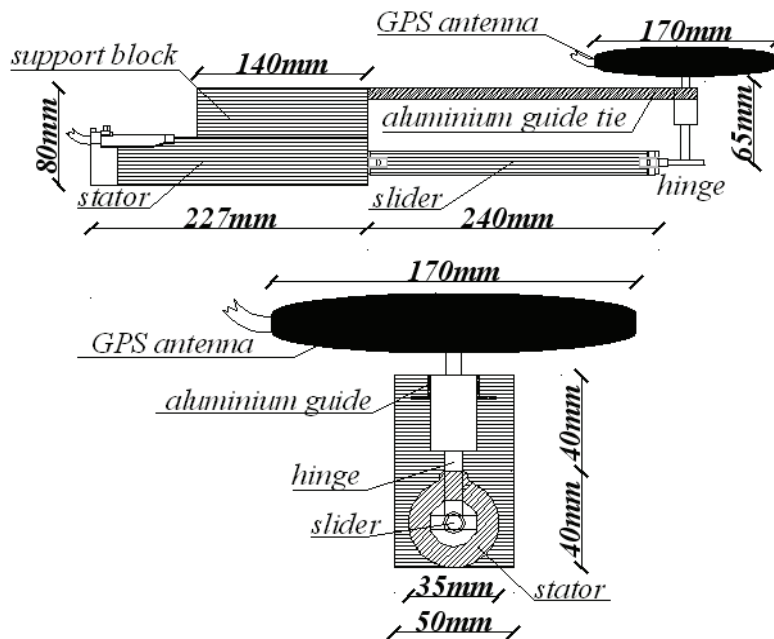


Figure 3.1. Lateral (top) and frontal (bottom) view of the linear motor with the rover antenna

These remarks suggested to identify a different location of the sensors, able to provide open sky conditions above the sensors and a continuous receiving of the satellites signal.

In the new arrangement the antennas are placed on the roof of an industrial steel building in an open field environment, free from sources of multi-paths errors and from buildings that may obstruct the view of the low elevation satellites (i.e., “cut-off angle” of around 15-20°). The antennas are linked to their receivers by wires connections, and others wires connect the receivers to a computer for the acquisition of the GPS signals.

Even if single frequency L1 GPS receiver are improving their performance (Brown et al., 2006; Saeky and Hori, 2006), dual frequency L1/L2 GPS receivers are adopted to guarantee the maximum achievable accuracy. The rover and the reference receivers communicate each to the other to allow the correction of position errors. For this purpose the GPS Differential Point Positioning (DGPS) is used (Dana 1997). The correct position of the reference is sent towards a wire connection to an acquisition software, that in real time acquires the coordinates and the information from the reference position, computes new coordinates and transmits the correction of position to the rover.

This positioning allows one to remove the rover errors of position and to obtain the correct position, with a resolution of sub-centimetres.

3.2 Experimental results

Two kind of tests were carried out in order to collect any possible information in view of assessing the achievable accuracy of the GPS units for long-term precise monitoring applications (Casciati and Fuggini, 2009a, b):

- Static tests;
- Dynamic tests;

The first kind of tests were carried out to quantify the background noise in the GPS configuration, and to investigate, the influence of the “geometric dilution of precision” (GDOP) on the recorded signal. They provided answers to two main questions: a) repeatability of long-period oscillations in both the longitudinal and transversal directions for two consecutive satellite

configurations at rest (i.e., repetition of the same longitudinal and transversal signal amplitude for two equal and consecutive satellites constellation configurations); b) evaluation of the best resolution possible when adopting dual frequencies GPS receivers.

The second set of tests was designed to quantify the range of frequencies and amplitudes that can be successfully tracked by GPS sensors in Civil Engineering applications.

3.2.1 Static tests

Some static calibration tests were carried out in order to assess the performance and the stability of the Differential Global Positioning System (DGPS) system when no motion is imposed to the movable antenna. This phase allows one to quantify the background noise in the GPS configuration and, with 48 hours of acquisition available, to also elaborate the influence of the GDOP on the recorded signal. The experiments were conducted using the two GPS antennas staying in a known position for about two consecutive days. The GPS sampling rate was chosen to be 10Hz.

The baseline connecting the reference and the rover GPS antennas is chosen to be mainly along the East direction. These tests were conducted in January 2009 and in the following will be indicated as #Jan09.

As the purpose is to assess if the baseline direction connecting the rover and the reference receivers influence the GPS accuracy in detecting movements during a whole day, a new GPS sensors configuration was conceived for static tests being now the line connecting the two antennas along the North direction.

Also in this second tests (conducted in February 2009, in the following indicated as #Feb09) the GPS sampling rate was chosen to be 10Hz.

Since the full 24 hours sidereal day registration is too long to be depicted, extracts of twelve hours in the E-W direction, in the N-S direction and in the vertical direction are plotted in Figures 3.2 and 3.3 for the two days and for the two sensors configurations. Note that relative motions along the N-S axis are marked as ΔN , while those along the E-w axis as ΔE and those along the vertical axis are marked as ΔH .

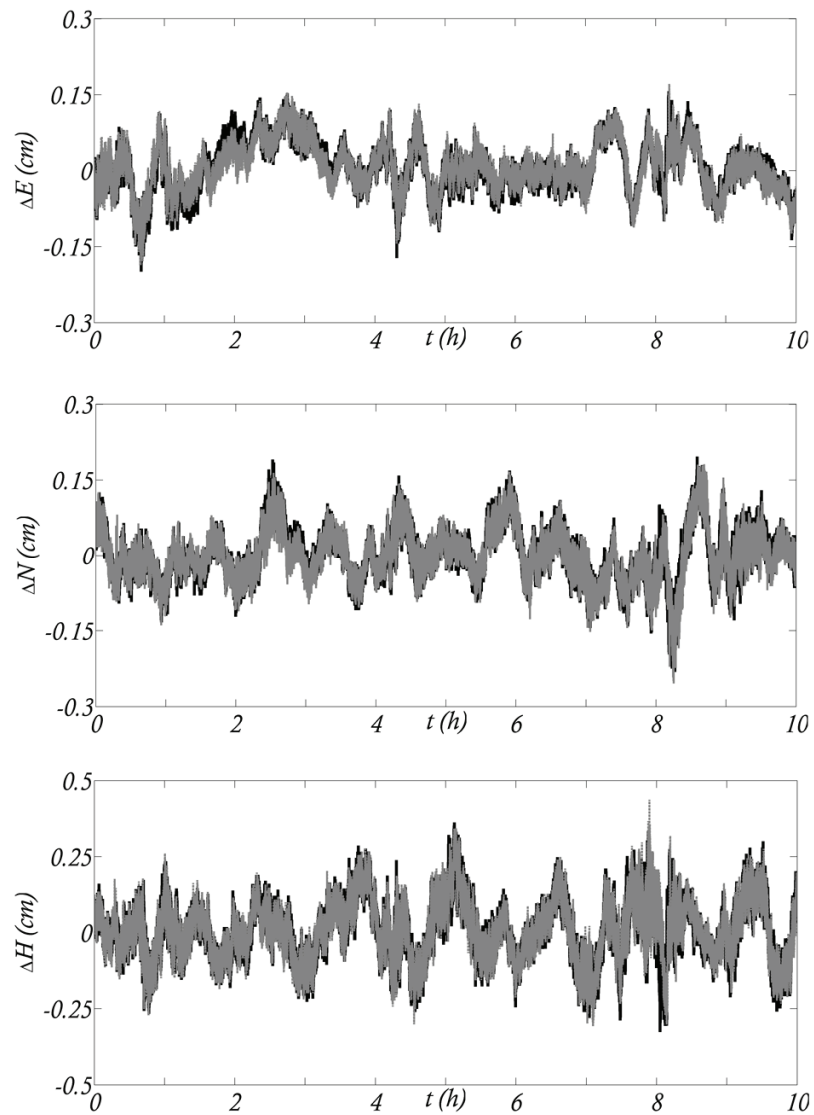


Figure 3.2. Correlation between two consecutive days (day 1 in black and day 2 in grey) for #Jan09 tests: East component time history (top); North component time history (middle);vertical component time history(bottom)

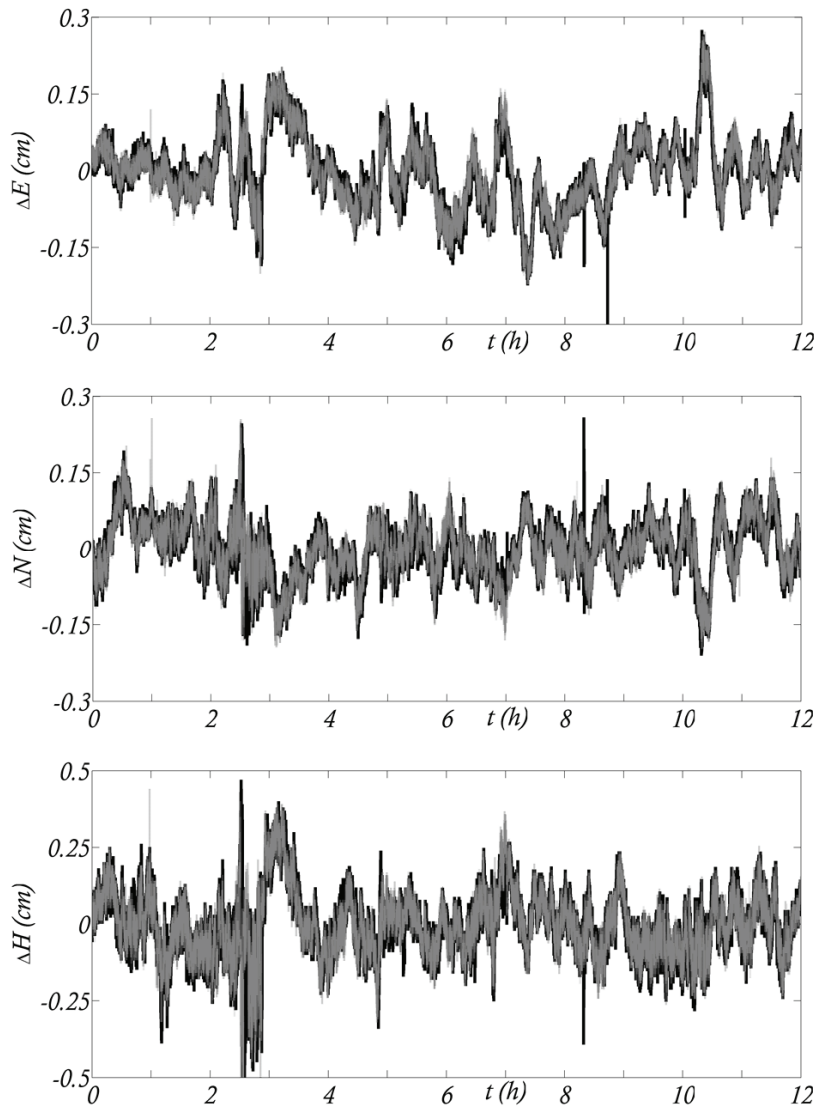


Figure 3.3. Correlation between two consecutive days (day 1 in black and day 2 in grey) for #Feb09 tests: East component time history (top); North component time history (middle); vertical component time history (bottom)

The correlation between the values recorded at instants shifted of 24 hours can be studied. For all the three components (East-North-vertical) a strong correlation between the two days peaks is made evident.

Figures 3.4 and 3.5 show the correlation, for #Jan09 and #Feb09 tests respectively, between the two days in the East, North and vertical directions.

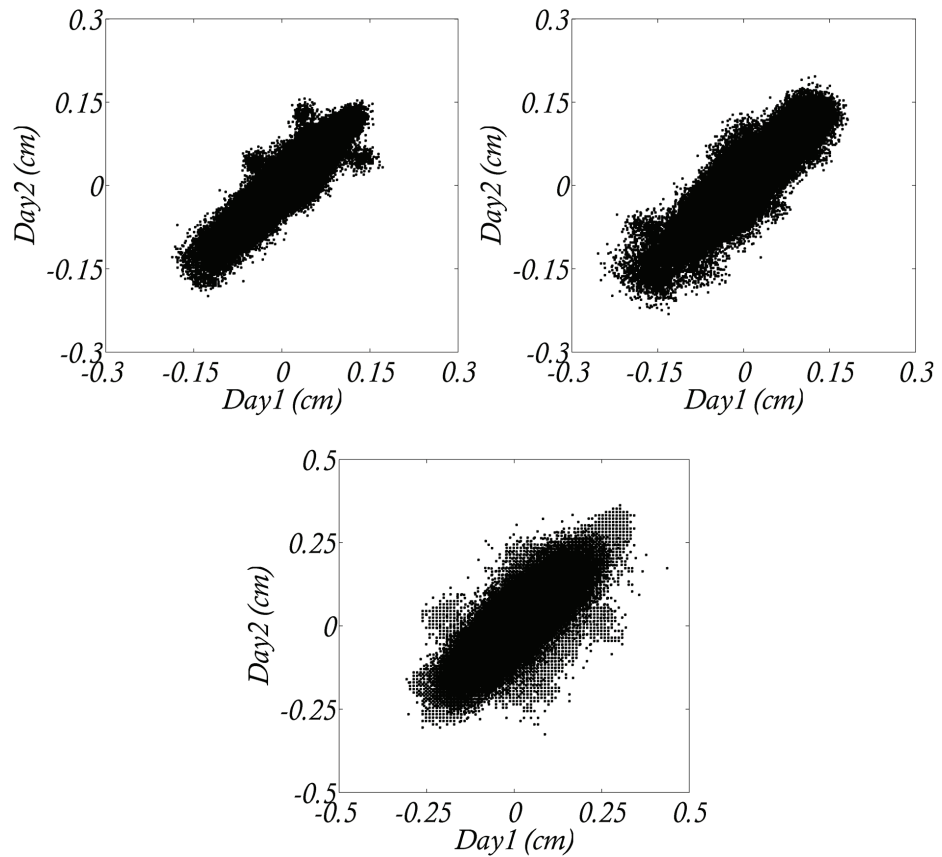


Figure 3.4. Correlation between days for #Jan09 tests: East component response (left top); North component response (right top); Vertical component response (bottom)

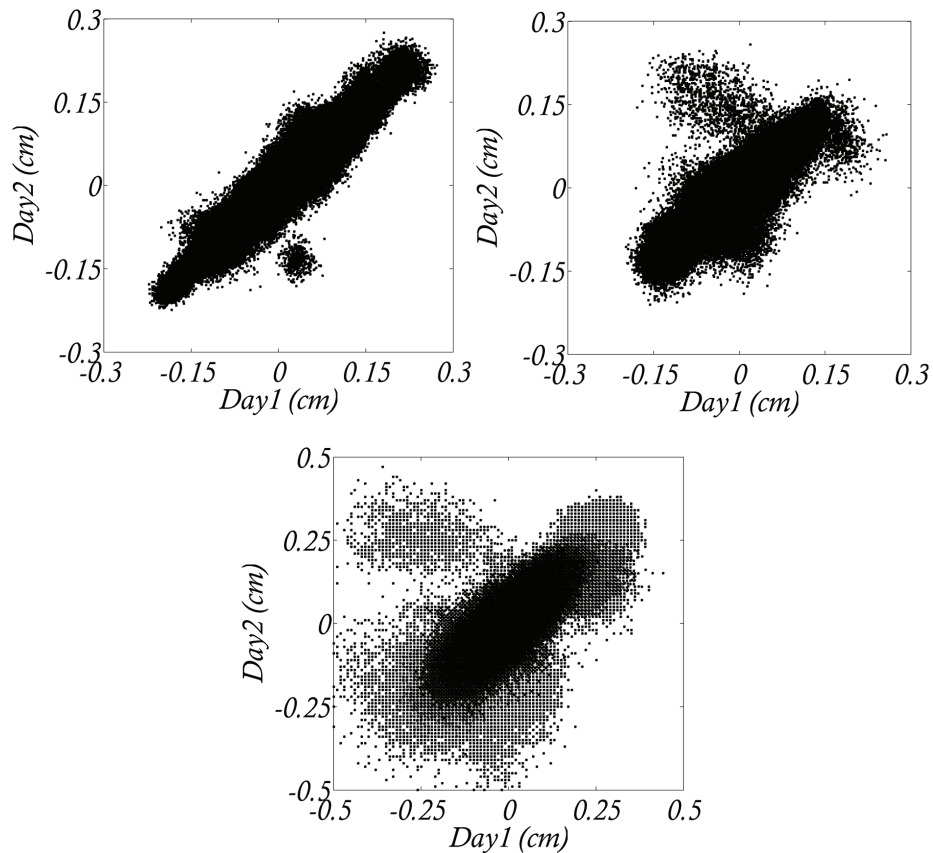


Figure 3.5. Correlation between days for #Feb09 tests: East component response (left top); North component response (right top); Vertical component response (bottom)

From the previous Figures 3.4 and 3.5, it is clear that having a baseline connection along East direction provides a better accuracy. For the vertical component on the contrary the main difference which arises is not an accuracy decrement but a more significant dispersion of data when the baseline connection is along the East. This effect is probably the consequence, for this sensors orientation, of the low accuracy which whom the antenna initialize its

height. However, these data dispersion does not have a significant influence on the fluctuation of the vertical displacement accuracy in the two test campaign.

The three root mean square (rms) couple of values corresponding to the East, North and vertical components of displacements, respectively, for the two days were also calculated.

Tables 3.1 and 3.2 summarize these values that can be considered as the radii of rms ellipses, for #Jan09 and #Feb09 tests, respectively. Table 3.3 reports a comparison of rsm variations between components for the two different tests campaign.

Table 3.1. Rms values of the North, East and vertical components for two consecutive days for #Jan09 tests

| | <i>Day 1 rms</i> | <i>Day 2 rms</i> | <i>Difference rms</i> |
|---------------|------------------|------------------|-----------------------|
| <i>East</i> | <i>0,0465cm</i> | <i>0,048cm</i> | <i>4,2%</i> |
| <i>Nord</i> | <i>0,0494cm</i> | <i>0,0506cm</i> | <i>2,5%</i> |
| <i>Height</i> | <i>0,0927cm</i> | <i>0,0935cm</i> | <i>0,9%</i> |

Table 3.2. Rms values of the North, East and vertical components for two consecutive days for #Feb09 tests

| | <i>Day 1 rms</i> | <i>Day 2 rms</i> | <i>Difference rms</i> |
|---------------|------------------|------------------|-----------------------|
| <i>East</i> | <i>0,0681cm</i> | <i>0,0672cm</i> | <i>1,3%</i> |
| <i>Nord</i> | <i>0,0552cm</i> | <i>0,0539cm</i> | <i>2,4%</i> |
| <i>Height</i> | <i>0,1008cm</i> | <i>0,1012cm</i> | <i>0,4%</i> |

Table 3.3. Rms values comparison of the North, East and vertical components between #Jan09 tests and #Feb09 tests

| | <i>#Jan09 tests</i> | <i>#Feb09 tests</i> | <i>Difference rms</i> |
|---------------|---------------------|---------------------|-----------------------|
| <i>East</i> | <i>0,04725cm</i> | <i>0,06765cm</i> | <i>30,15%</i> |
| <i>Nord</i> | <i>0,050cm</i> | <i>0,05455cm</i> | <i>1,92%</i> |
| <i>Height</i> | <i>0,0931cm</i> | <i>0,10064cm</i> | <i>1,93%</i> |

Looking at the “difference rms” column of table 3.3 the following one consideration derives: the East measurements (which can be the more accurate if the baseline reference-rover is oriented along the East, as in #Jan09 tests) is very sensitive to baseline direction changes. On the contrary the North and the Vertical components are extremely stable to baseline changes from the East to the Nord direction.

To check the in-plane accuracy (East-North), the simultaneous couple (ΔN , ΔE) are collected in the diagram on Figure 3.6 , where the ellipses having as radius the two root means square (rms) values are also drawn.

The ellipse of Figure 3.6 (left) denotes a lightly lower level of accuracy in the North direction than along the East direction. It depends on the direction of the baseline connecting the reference and the rover that for #Jan09 tests is oriented along the East direction.

On the contrary the ellipse of Figure 3.6 (right) denotes a significant lower level of accuracy in the East direction than along the North direction. In fact during #Feb09 tests the baseline connecting the reference and the rover was oriented along the North direction.

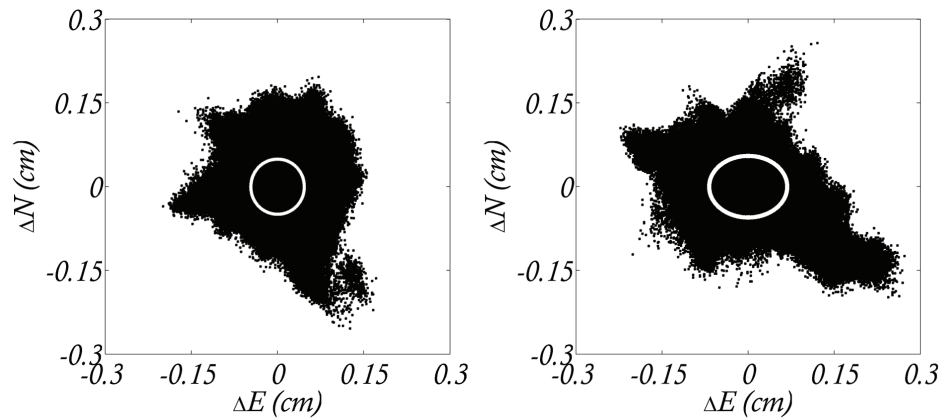


Figure 3.6. Correlation between E-N components during two consecutive days with the calculated E-N rms in white, for #Jan09 tests (left) and for #Feb09 tests (right)

The previous considerations suggest to carry out a more accurate analysis of the rms measurements variations with time for the East, North and vertical component. As it is clear when looking at the graphs of Figures 3.2 and 3.3, the GPS signals show a fluctuation during the day. This aspect is not so evident if compared to the rms values of a whole day records, but starts to be significant if considering its variation hour by hour during the day. The rms values are so calculated for each hour for each two days records of the #Jan09 and #Feb09 tests campaign. A comparison is made between components (East, North and Vertical) and between their variation during the two consecutive days for the same time interval.

Tables 3.4 and 3.6 summarize the rms values as calculated hour by hour, for #Jan09 and #Feb09. An extract of the maximum and the minimum rms values is presented in Tables 3.5 and 3.7. It is showed a significant variation between components, above all for the East one. This difference, which is evident when looking at Figures 3.7, 3.9, 3.11 and 3.13 for #Jan09 tests and Figures 3.15, 3.17, 3.19 and 3.21 for #Feb09 tests, is a consequence of the signal GDOP already mentioned in chapter 1.

In addition the ellipses, having as radius the two root means square (rms) values, are drawn for each hours, referring to the data of Table 3.4 and 3.6. Each

ellipses figures is placed below the corresponding variation with time of the rms values in Figures 3.8, 3.10, 3.12 and 3.14 for #Jan09 tests and Figures 3.16, 3.18, 3.20 and 3.22 for #Feb09 tests.

Table 3.4. Hour by hour rms values of North, East and vertical components for #Jan09 tests

| <i>Day time</i> | <i>RMS-East day1</i> | <i>RMS-East day2</i> | <i>RMS-North day1</i> | <i>RMS-North day2</i> | <i>RMS-Height day1</i> | <i>RMS-Height day2</i> |
|-----------------|----------------------|----------------------|-----------------------|-----------------------|------------------------|------------------------|
| 12-13 | 0,0521 | 0,0521 | 0,0414 | 0,0422 | 0,0682 | 0,0670 |
| 13-14 | 0,0342 | 0,0481 | 0,0285 | 0,0285 | 0,0667 | 0,0681 |
| 14-15 | 0,031 | 0,0255 | 0,0482 | 0,0547 | 0,0725 | 0,0745 |
| 15-16 | 0,0328 | 0,0334 | 0,0381 | 0,0394 | 0,0934 | 0,0937 |
| 16-17 | 0,0504 | 0,0500 | 0,0403 | 0,0400 | 0,0870 | 0,0843 |
| 17-18 | 0,024 | 0,0247 | 0,0473 | 0,0495 | 0,1057 | 0,1073 |
| 18-19 | 0,0166 | 0,0158 | 0,0357 | 0,0349 | 0,0913 | 0,0896 |
| 19-20 | 0,0530 | 0,0522 | 0,0329 | 0,0333 | 0,1087 | 0,1079 |
| 20-21 | 0,0517 | 0,0515 | 0,0842 | 0,0808 | 0,0813 | 0,0845 |
| 21-22 | 0,0329 | 0,0312 | 0,0288 | 0,0311 | 0,1108 | 0,1144 |

Table 3.5. Extract of the maximum and minimum rms values of Table 3.4

| | <i>RMS-East day1</i> | <i>RMS-East day2</i> | <i>RMS-North day1</i> | <i>RMS-North day2</i> | <i>RMS-Height day1</i> | <i>RMS-Height day2</i> |
|-------------------------|----------------------|----------------------|-----------------------|-----------------------|------------------------|------------------------|
| <i>Minimum Day time</i> | 0,0166 18-19 | 0,0158 18-19 | 0,0285 13-14 | 0,0285 13-14 | 0,0667 13-14 | 0,0670 12-13 |
| <i>Maximum Day time</i> | 0,0530 19-20 | 0,0522 19-20 | 0,0842 20-21 | 0,0808 20-21 | 0,1108 21-22 | 0,1144 21-22 |
| <i>Variation (%)</i> | 68,6 | 69,6 | 66,2 | 64,7 | 39,8 | 41,4 |

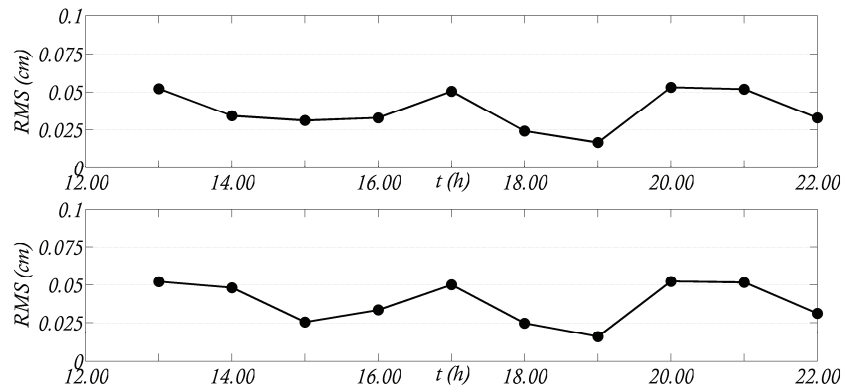


Figure 3.7. Rms values variation with time for East measurements during #Jan09 tests: day1 (top), day2 (bottom)

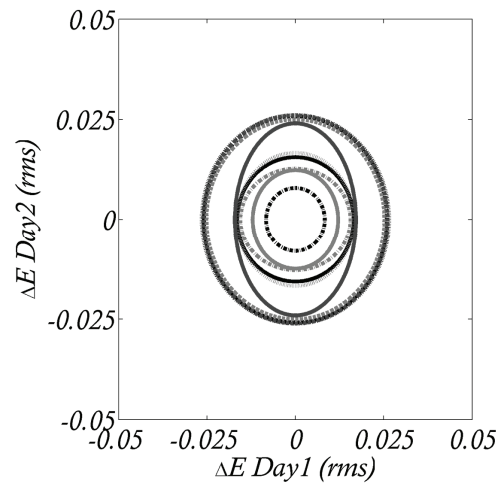


Figure 3.8. Rms ellipses for East measurements during #Jan09 tests: day1 vs day2

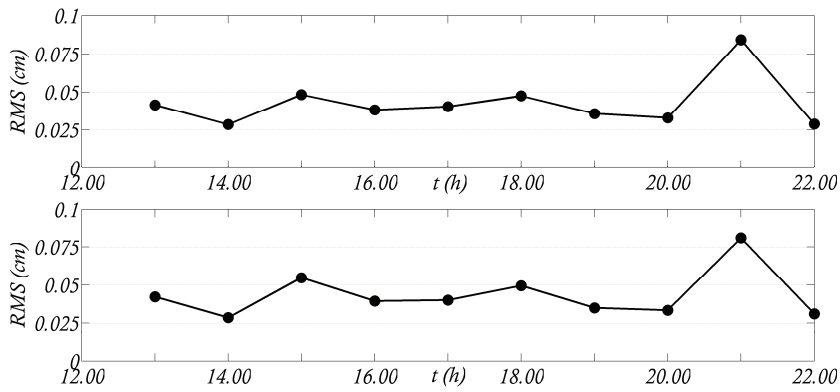


Figure 3.9. Rms values variation with time for North measurements during #Jan09 tests: day1 (top), day2 (bottom)

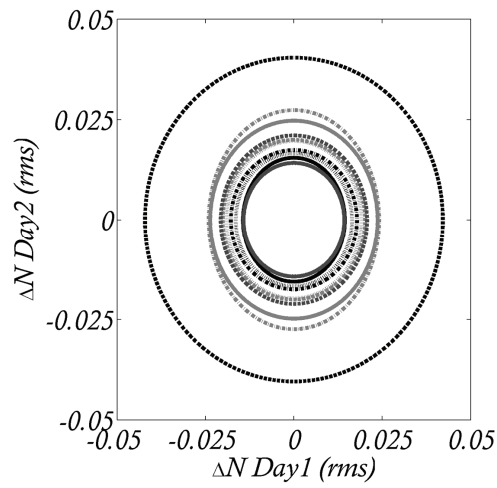


Figure 3.10. Rms ellipses for North measurements during #Jan09 tests: day1 vs day2

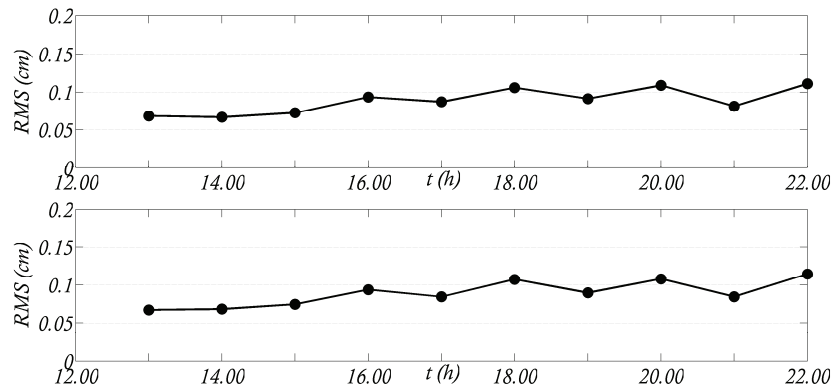


Figure 3.11. Rms values variation with time for vertical measurements during #Jan09 tests: day1 (top), day2 (bottom)

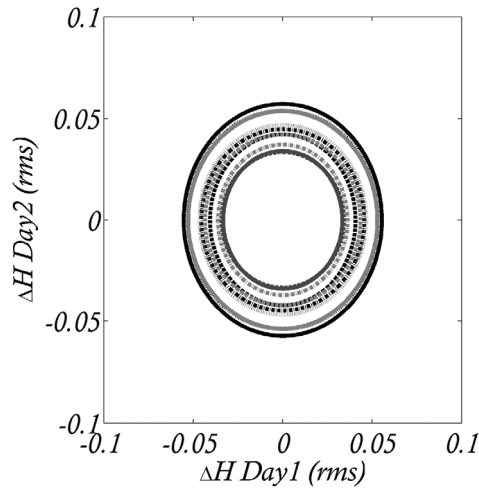


Figure 3.12. Rms ellipses for vertical measurements during #Jan09 tests: day1 vs day2

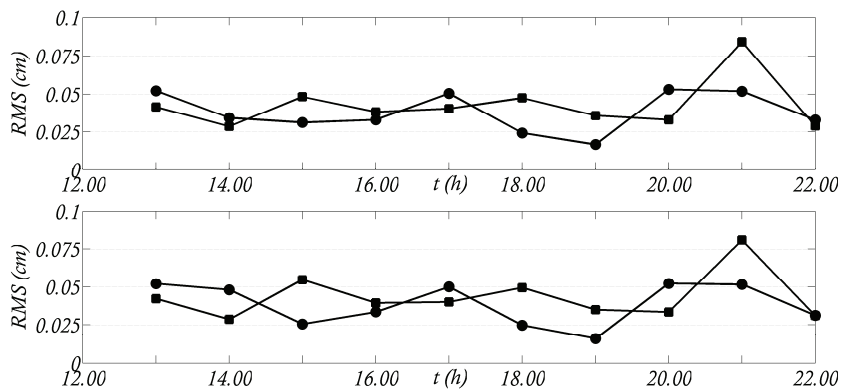


Figure 3.13. Rms values variation with time for North (square dot) and East (round dot) measurements during #Jan09 tests: day1 (top), day2 (bottom)

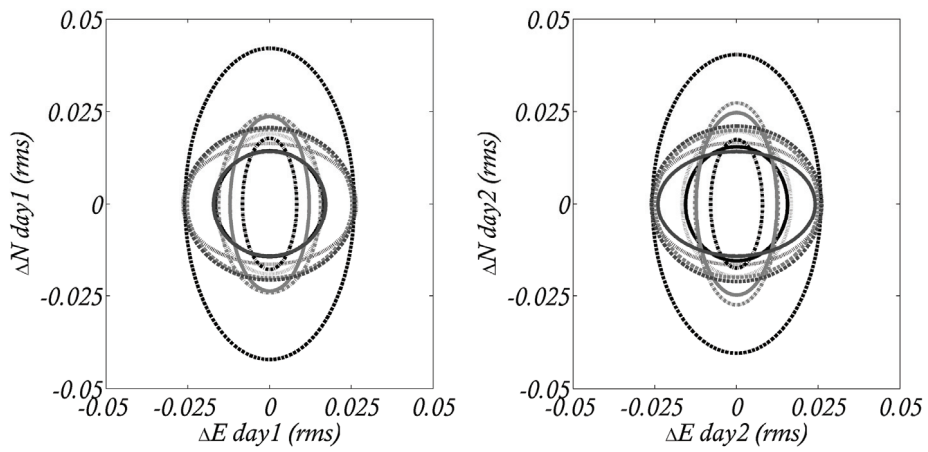


Figure 3.14. Rms ellipses for North and East measurements during #Jan09 tests: day1 (left), day2 (right)

Table 3.6. Hour by hour rms values of North, East and vertical components for #Feb09 tests

| <i>Day time</i> | <i>RMS-East day1</i> | <i>RMS-East day2</i> | <i>RMS-North day1</i> | <i>RMS-North day2</i> | <i>RMS-Height day1</i> | <i>RMS-Height day2</i> |
|-----------------|----------------------|----------------------|-----------------------|-----------------------|------------------------|------------------------|
| 07-08 | 0,0213 | 0,0224 | 0,0569 | 0,0562 | 0,0695 | 0,0693 |
| 08-09 | 0,0217 | 0,0218 | 0,0337 | 0,0339 | 0,0688 | 0,0724 |
| 09-10 | 0,0725 | 0,0721 | 0,0538 | 0,0597 | 0,1434 | 0,1498 |
| 10-11 | 0,0632 | 0,0620 | 0,0523 | 0,0507 | 0,1490 | 0,1474 |
| 11-12 | 0,0479 | 0,0481 | 0,0458 | 0,0449 | 0,0791 | 0,0824 |
| 12-13 | 0,0523 | 0,0527 | 0,0402 | 0,037 | 0,0614 | 0,0597 |
| 13-14 | 0,0711 | 0,0660 | 0,0503 | 0,0404 | 0,0971 | 0,0777 |
| 14-15 | 0,0646 | 0,0605 | 0,0428 | 0,0403 | 0,0795 | 0,0751 |
| 15-16 | 0,0433 | 0,0429 | 0,0384 | 0,0378 | 0,0841 | 0,0822 |
| 16-17 | 0,0292 | 0,0286 | 0,0328 | 0,0321 | 0,0506 | 0,0512 |
| 17-18 | 0,0818 | 0,0816 | 0,0686 | 0,0694 | 0,0767 | 0,0778 |
| 18-19 | 0,0381 | 0,0400 | 0,0513 | 0,0511 | 0,0775 | 0,0774 |

Table 3.7. Extract of the maximum and minimum rms values of Table 3.6

| | <i>RMS-East day1</i> | <i>RMS-East day2</i> | <i>RMS-North day1</i> | <i>RMS-North day2</i> | <i>RMS-Height day1</i> | <i>RMS-Height day2</i> |
|-------------------------|----------------------|----------------------|-----------------------|-----------------------|------------------------|------------------------|
| <i>Minimum Day time</i> | 0,0213 07-08 | 0,0218 08-09 | 0,0328 16-17 | 0,0321 16-17 | 0,0506 16-17 | 0,0512 16-17 |
| <i>Maximum Day time</i> | 0,0818 17-18 | 0,0816 17-18 | 0,0686 17-18 | 0,0694 17-18 | 0,1490 10-11 | 0,1498 09-10 |
| <i>Variation (%)</i> | 73,9 | 73,2 | 52,1 | 53,7 | 66,0 | 65,8 |

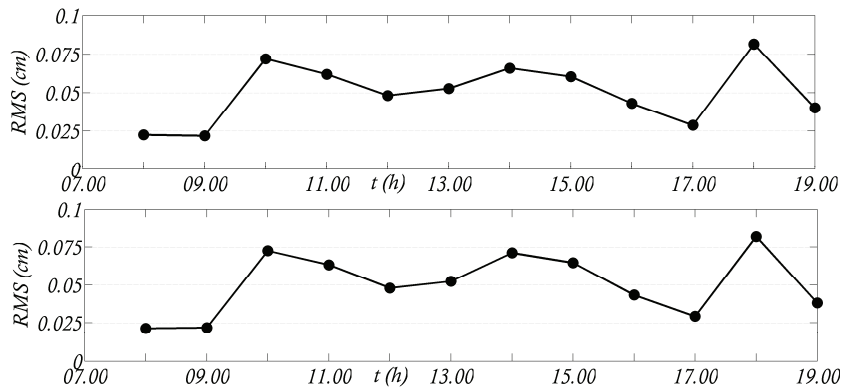


Figure 3.15. Rms values variation with time for East measurements during #Feb09 tests: day1 (top), day2 (bottom)

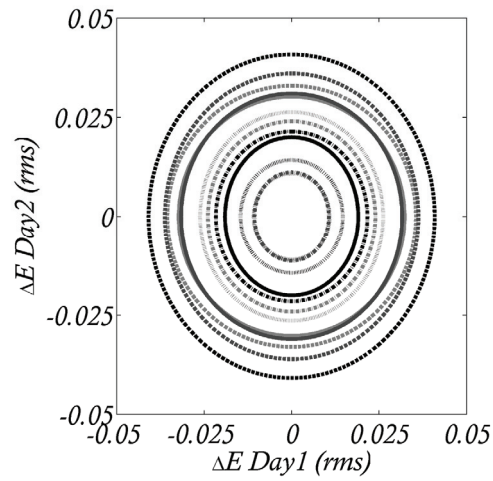


Figure 3.16. Rms ellipses for East measurements during #Feb09 tests: day1 vs day2

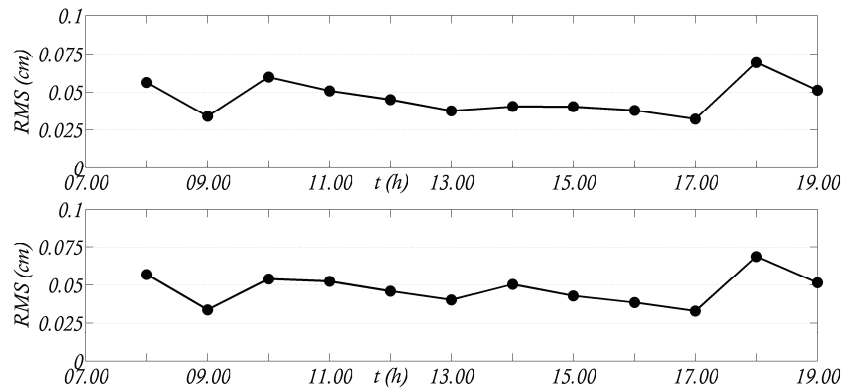


Figure 3.17. Rms values variation with time for North measurements during #Feb09 tests: day1 (top), day2 (bottom)

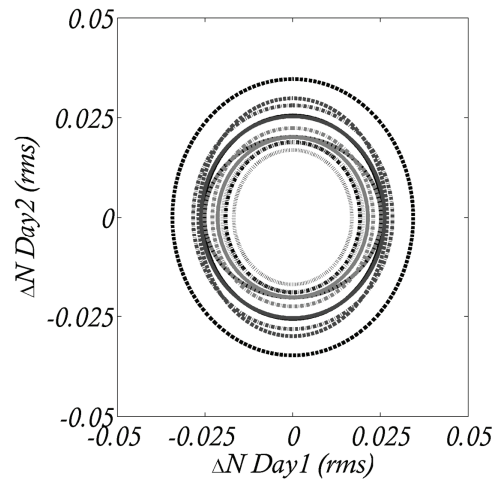


Figure 3.18. Rms ellipses for North measurements during #Feb09 tests: day1 vs day2

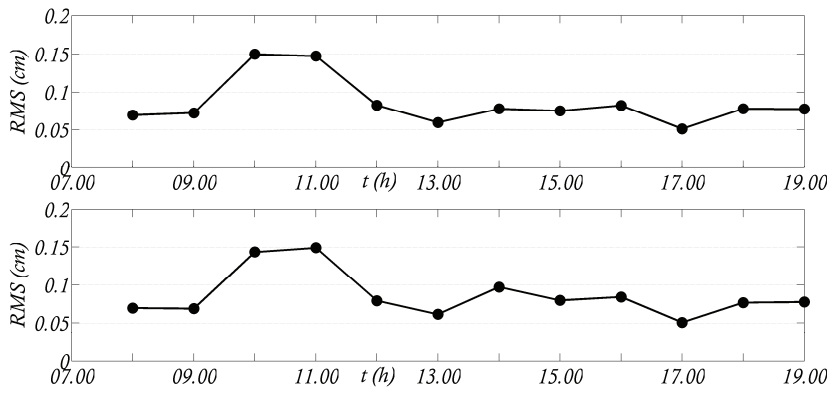


Figure 3.19. Rms values variation with time for vertical measurements during #Feb09 tests: day1 (top), day2 (bottom)

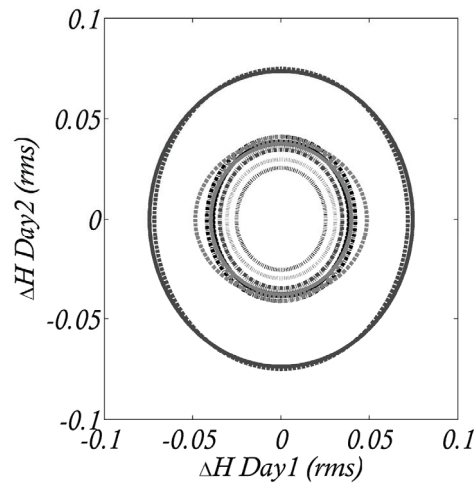


Figure 3.20. Rms ellipses for vertical measurements during #Feb09 tests: day1 vs day2

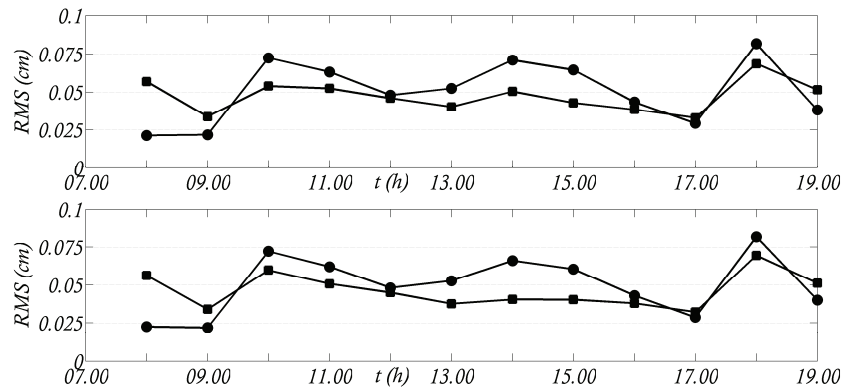


Figure 3.21. Rms values variation with time for North (square dot) and East (round dot) measurements during #Feb09 tests: day1 (top), day2 (bottom)

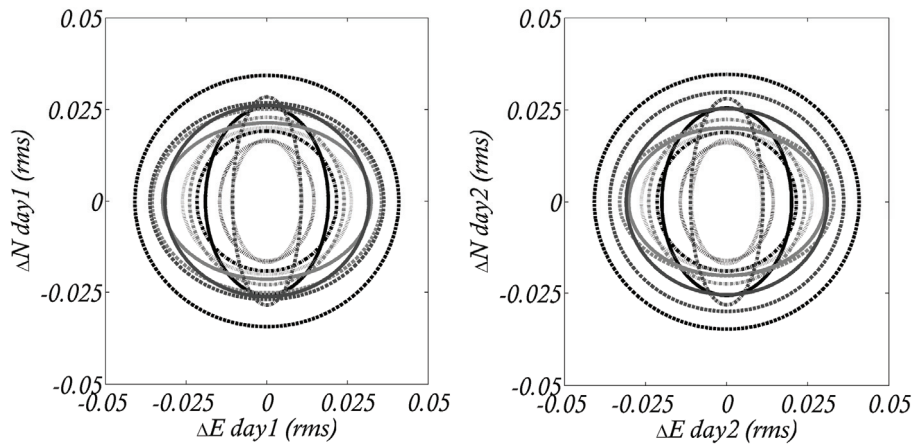


Figure 3.22. Rms ellipses for North and East measurements during #Feb09 tests: day1 (left), day2(right)

The previous two sets of figures, clearly show a trend in the rms variation with time. This happens for both in plane East and North components, while is not so significant for the vertical component.

Based on this assumption, two main considerations arise:

(i) the GPS signal is not completely stable during a day record and its stability depends on the location, along East or North direction, chosen for the fixed and the moving receivers;

(ii) according to the place of the Earth one is using the GPS sensors the influence of the GDOP on the three-dimensional measurements has to be analyzed, modeling the GDOP as a standard deviation (rms) of the recorded data.

A further analysis was then conducted also in the frequency domain.

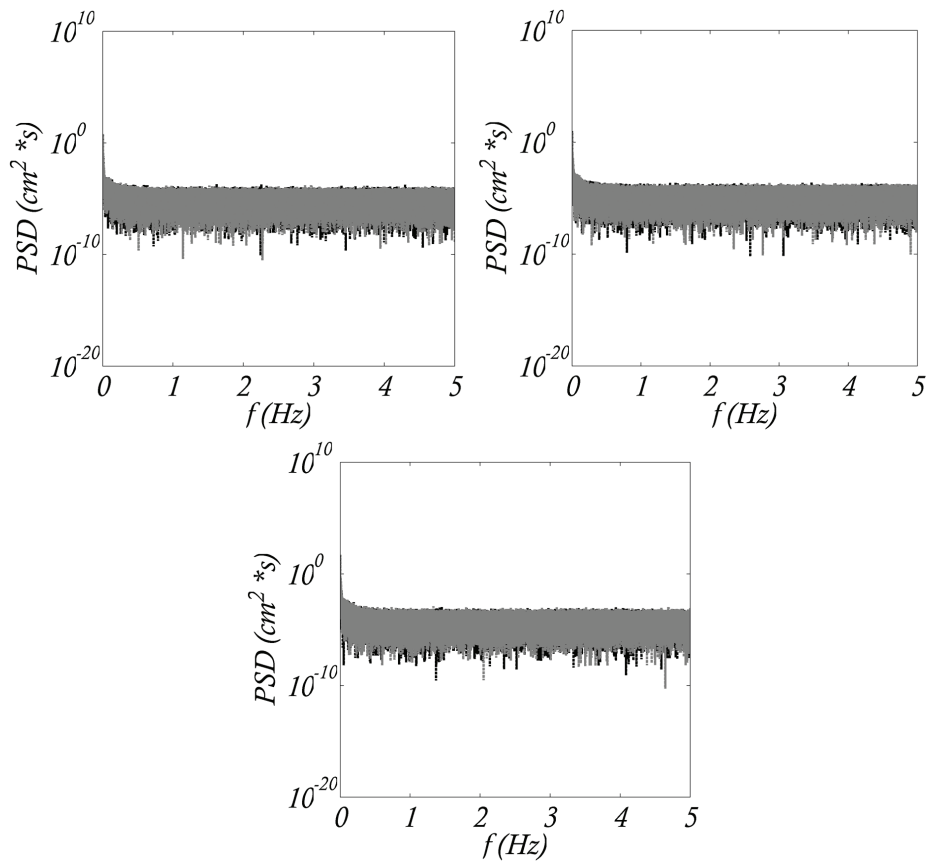


Figure 3.23. #Jan09 tests Power Spectral Density function: East component (top left), North component (top right) and vertical component (bottom)

A power spectral analysis of the recorded time histories was carried out in order to compare the frequency content in the two consecutive days for the East, North and vertical components. In Figures 3.23 and 3.24 (for the #Jan09 and #Feb09 tests, respectively) the Power Spectral Densities (PSD) for the three directions are plotted.

It is worth noting that for the three components and for the two days, the PSD of the recorded displacements show, as expected, a nearly white noise spectrum.

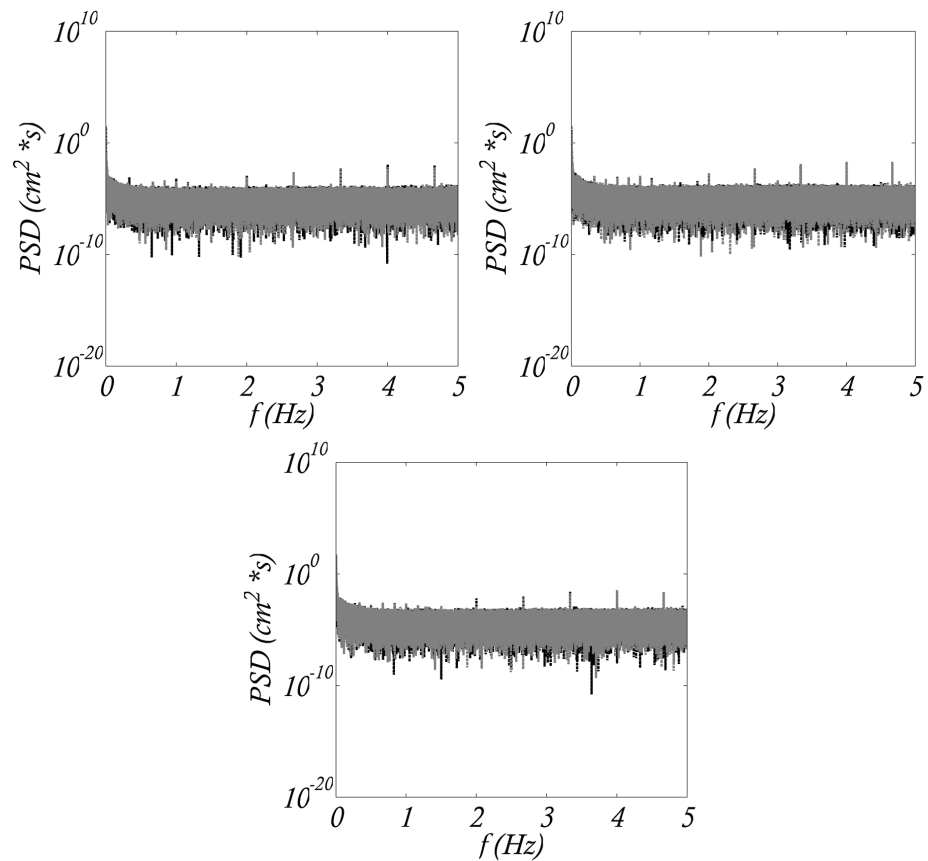


Figure 3.24. #Feb09 tests Power Spectral Density function: East component (top left), North component (top right) and vertical component (bottom)

3.2.2 Dynamic tests

Some dynamic calibration tests were designed to quantify the range of frequencies and amplitudes that can be successfully tracked by dual frequency GPS receivers. The dynamic tests were carried out for different combinations of frequency and amplitude by imposing sinusoidal time histories to the linear motor. In particular attention is focused on a frequency range of oscillations lower than 4Hz, which is typical of the main modal frequencies of large engineering structures (i.e., high-rise building, suspension bridge, etc.).

The recorded coordinates of the moving receiver are processed and then compared with the real values of the linear motor movement. The GPS raw data are recorded in real time by the Leica GPS software and then processed into the Matlab environment.

Preliminary to the two main tests campaign (#Nov08 and #Mar09) introduced below, some dynamic tests (indicated as #PD) were carried out by simply imposing to the linear motor sudden variations of movements in amplitudes and frequencies. In these #PD tests the sampling rate was chosen to be 20 Hz and the baseline connecting the rover and the reference was along the East direction.

In Figures 3.25 and 3.26 two displacement time history records of the uniaxial AL motion are plotted, showing the behaviour of the rover GPS for this sudden variations in the linear motor displacements.

In particular in Figure 3.25 both the frequency (with values of 0.2, 0.5 and 1Hz) and the amplitude (from 1 to 12.5 cm) were varied, while in Figure 3.26 only the amplitude was changed in a range from 1 to 10cm, maintaining a fixed frequency of 0.5Hz.

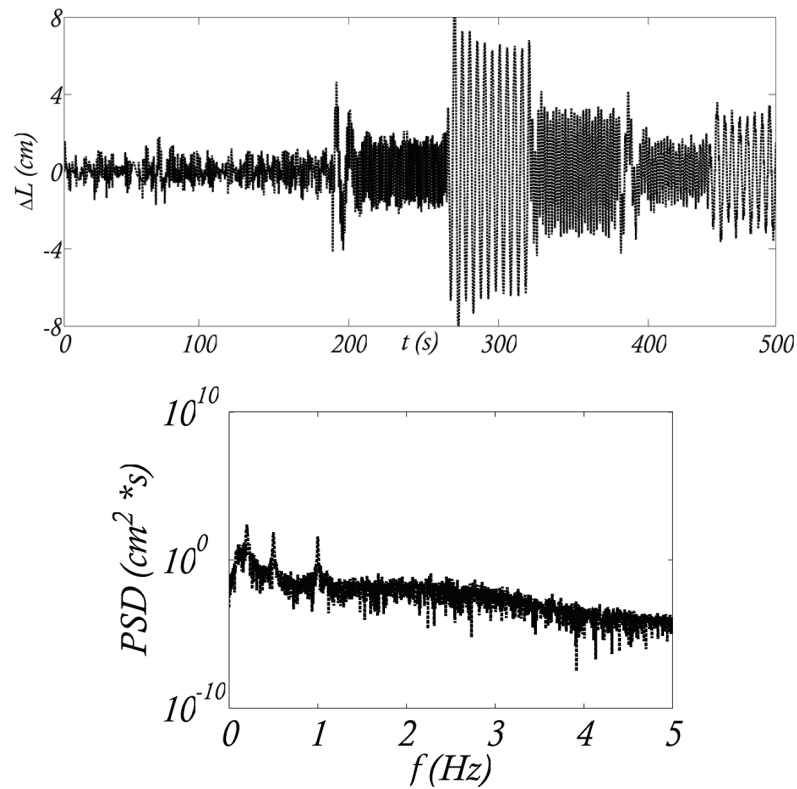


Figure 3.25. GPS longitudinal displacement time history with frequencies 0.2, 0.5 and 1Hz and amplitudes 1-12.5cm (top); corresponding PSD (bottom)

The two Power Spectral Density diagrams are plotted at the bottom of Figures 3.25 and 3.26. In figure 3.25 the frequencies of 0.2, 0.5 and 1Hz are clearly detected, while in Figure 3.26 the PSD only shows the frequency of 0.5Hz, as expected.

Two main considerations arise from the diagrams built on the results of the #PD tests:

- (i) the GPS can follow suddenly changes of the displacements amplitude;
- (ii) the GPS is able to detect the changes of frequencies occurring in a short time period.

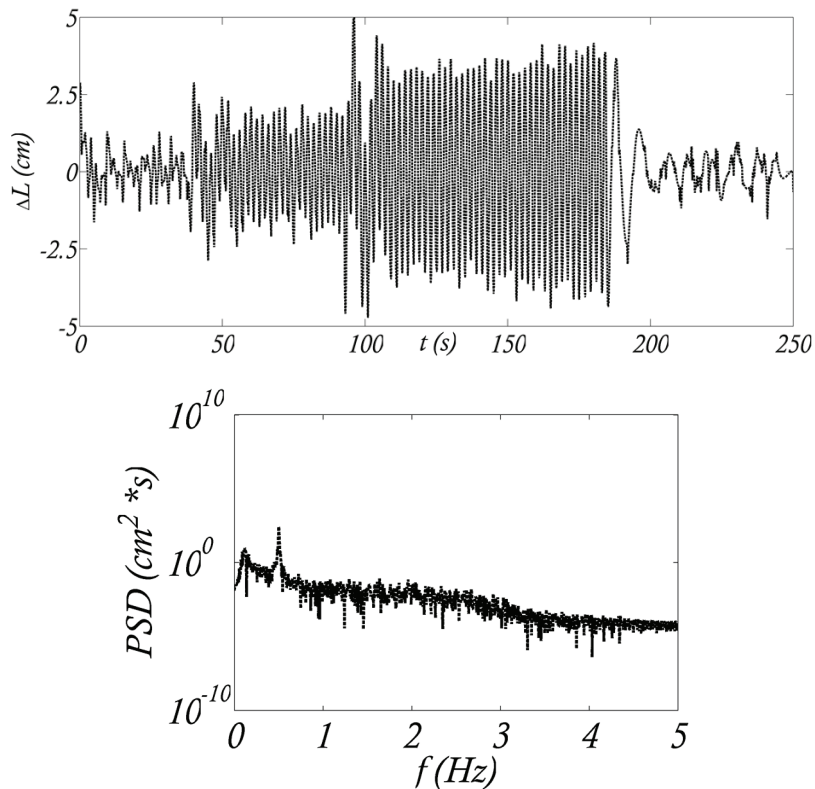


Figure 3.26. GPS longitudinal displacement time history with frequency 0.5Hz and amplitudes 1-10cm (top); corresponding PSD (bottom)

After the #PD tests, two further dynamic test campaigns were carried out by varying the amplitudes and the frequencies of the motion. The sampling rate was chosen to be 10Hz.

The first campaign was done in November 2008 (indicated as #Nov08 in the following) and the second in March 2009 (#Mar09 in the following). It is worth noting that in both the campaign the position of the fixed GPS receiver was not changed.

In the first test campaign the amplitudes of the oscillations imposed to the moving GPS antenna vary in the range from ± 0.5 cm up to ± 5 cm with frequencies of 0.1; 0.2; 0.5; 1; 2Hz.

In the #Mar09 tests campaign the number of amplitudes variation was reduced to $\pm 0.75\text{cm}$ and $\pm 1.25\text{cm}$ (as representative values of the ones in #Nov08 tests). The frequency of oscillation was 0.5; 1; 2 and 4Hz for each of the two amplitudes. This second test campaign was planned mainly to focus on the frequency variation of the results up to 4 Hz (which was not considered in the #Nov08 tests campaign).

The time history for any combination of amplitudes and frequency has the duration of 300s, assumed it as long enough to assess the stability of the measurements. It is worth noting that the data comparison is made with the real recorded linear motor longitudinal movements as the actual imposed displacements are not always those one assigns, due to inherent linear motor errors.

As the whole tests are too long to be reported in a single diagram, a synthesis is presented in term of (a) displacements time series; (b) root mean square variations in time; (c) Power Spectral Density changes in time.

The three plots in each of the Figures from 3.27 to 3.30 show, for the #Nov08 tests, the time history (a), the variation in time of the rms (b) and of the associated Power Spectral Density (PSD) function (c), respectively.

In detail: the comparison between the displacement estimates recorded by the GPS moving receiver and the displacements recorded by the linear motor is showed in the first graph. The rms values of the second plot are calculated as the rms of the ratio between the GPS estimate and the motor displacement at each instant, for subsequent 60 seconds segments of the recorded time history. The PSD shown in the third plot is computed for each separate segments of 60 seconds for the recorded GPS and linear motor movements.

Figure 3.27 refers to a test with displacements amplitude of $\pm 0.75\text{cm}$ and frequency of 0.2Hz; while in Figure 3.28 the frequency is chosen to be the same but the amplitude is set to $\pm 1.75\text{cm}$. Figure 3.29 shows the result for a test with the displacement amplitude of $\pm 1.25\text{cm}$ and the frequency of 1Hz, while Figure 3.30 reports the result of a test with the same amplitude but frequency of 2Hz.

For all these figures, the middle plots, which report the variation in time of the rms of the ratio between GPS estimate and motor displacement, show an

interesting trend of convergence in time. The bottom plots show a perfect agreement in the frequency domain, and this is the reason why the GPS grey line and the linear motor black line are overlapped.

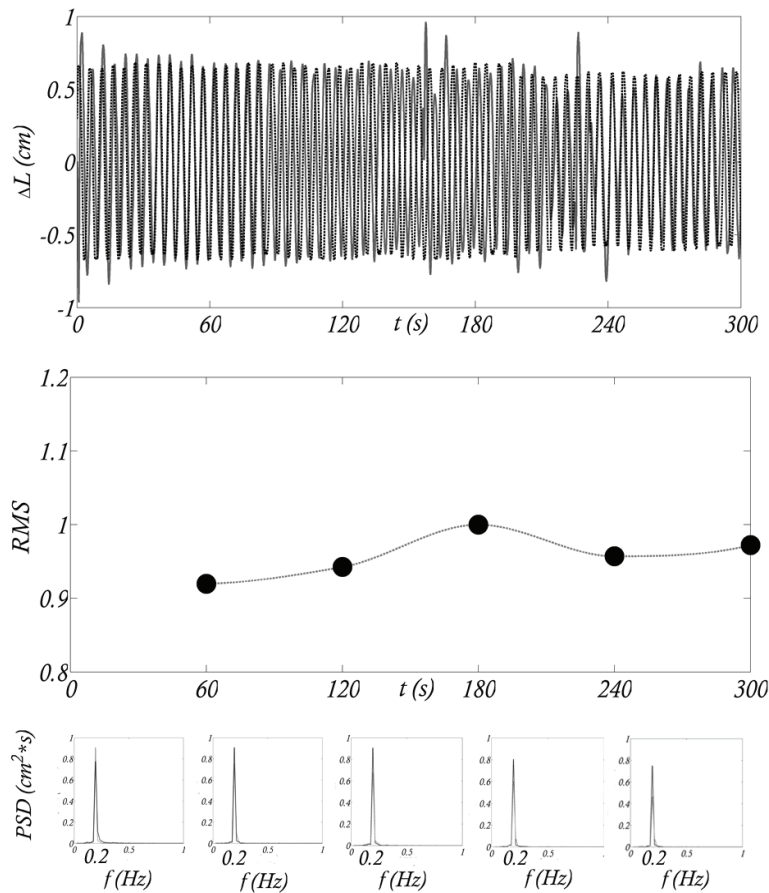


Figure 3.27. Result for the #Nov08 dynamic test (amplitude= ± 0.75 cm, frequency=0.2Hz). GPS (grey) and linear motor (black) displacements time history (top); variation in time of the rms of the ratio between GPS estimate and linear motor amplitude (middle); corresponding GPS (grey) and linear motor (black) power spectral densities (PSD) (bottom)

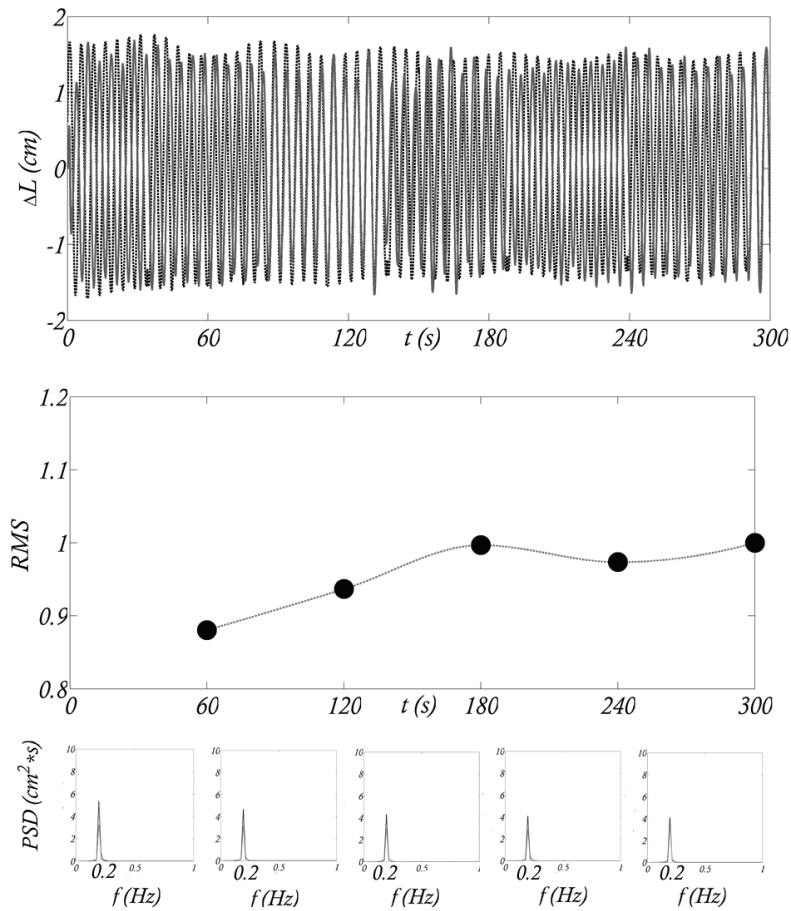


Figure 3.28. Result for the #Nov08 dynamic test (amplitude= ± 1.75 cm, frequency=0.2Hz). GPS (grey) and linear motor (black) displacements time history (top); variation in time of the rms of the ratio between GPS estimate and linear motor amplitude (middle); corresponding GPS (grey) and linear motor (black) power spectral densities (PSD) (bottom)

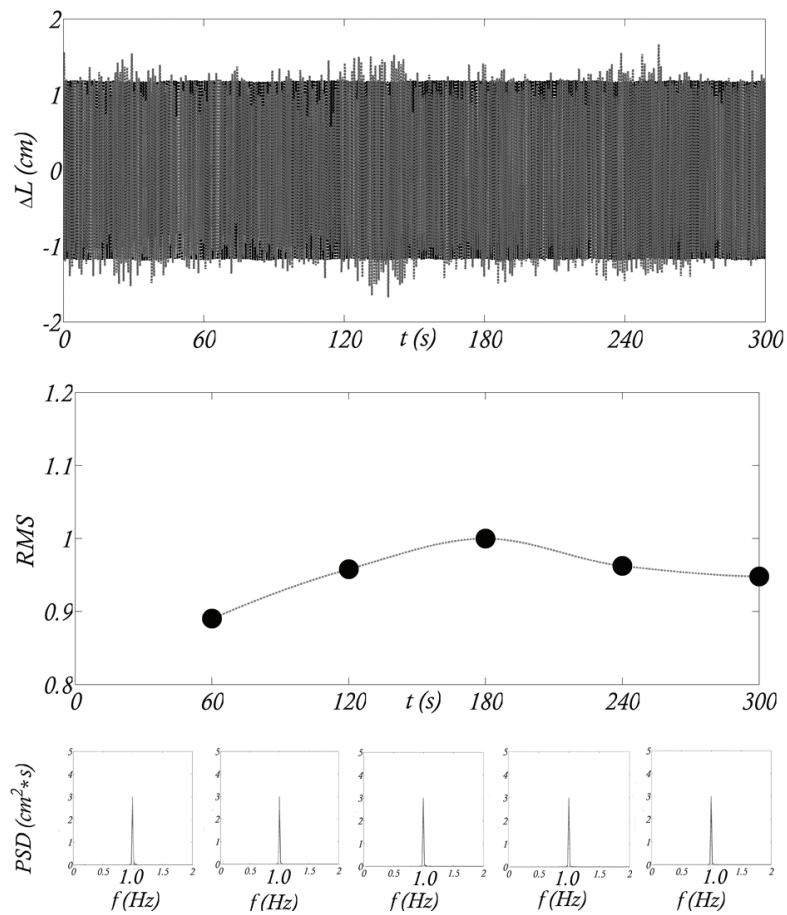


Figure 3.29. Result for the #Nov08 dynamic test (amplitude= $\pm 1.25\text{cm}$, frequency= 1.0Hz). GPS (grey) and linear motor (black) displacements time history (top); variation in time of the rms of the ratio between GPS estimate and linear motor amplitude (middle); corresponding GPS (grey) and linear motor (black) power spectral densities (PSD) (bottom)

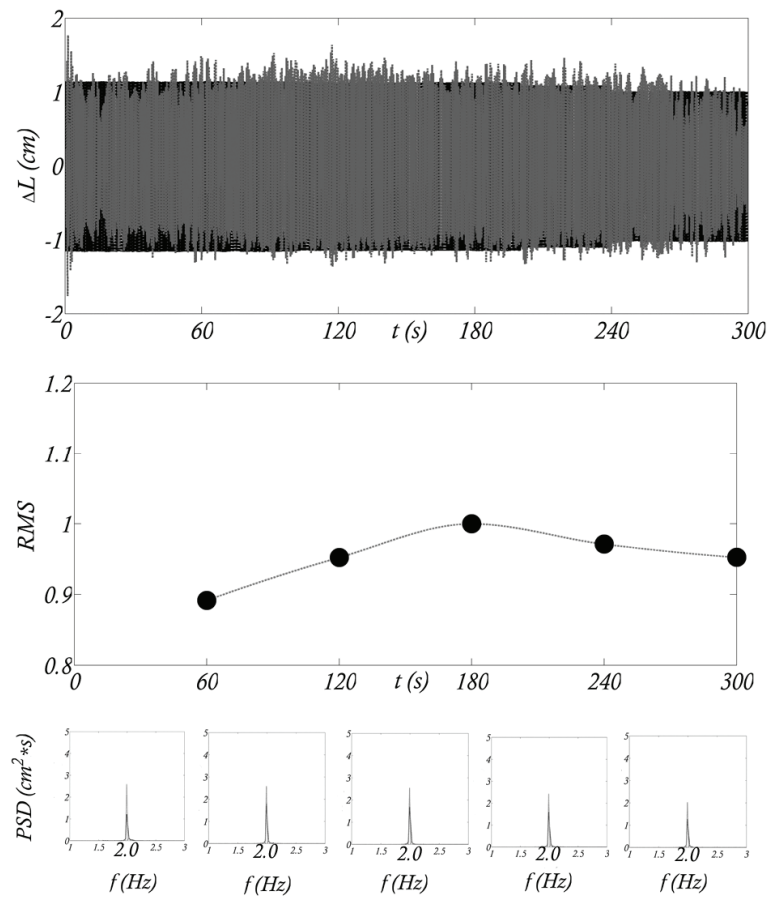


Figure 3.30. Result for the #Nov08 dynamic test (amplitude= ± 1.25 cm, frequency=2.0Hz). GPS (grey) and linear motor (black) displacements time history (top); variation in time of the rms of the ratio between GPS estimate and linear motor amplitude (middle); corresponding GPS (grey) and linear motor (black) power spectral densities (PSD) (bottom)

A synthesis of the results can be found in the plots in Figures 3.31 and 3.32, where the rms ratio between the GPS estimate and the motor displacement (for each 300s test) is plotted versus the frequency and versus the amplitude, respectively.

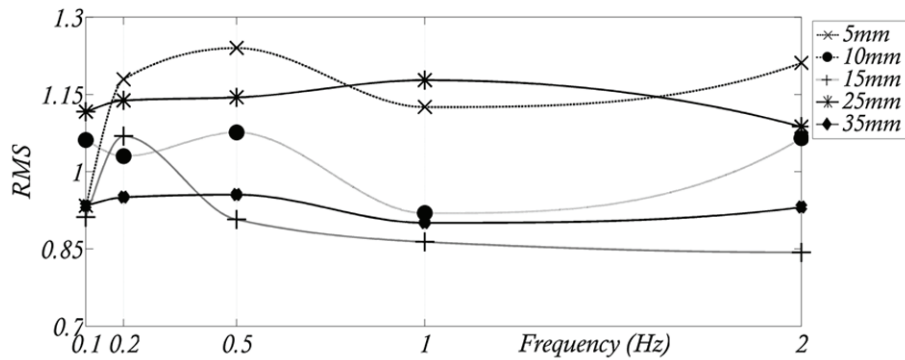


Figure 3.31. Ratio between the rms values computed along the whole record for the GPS estimate and the motor movement versus frequency of oscillations referring to the #Nov08 tests campaign

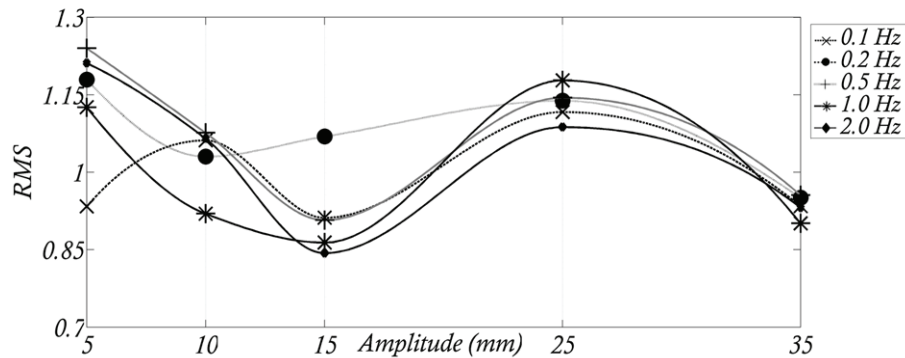


Figure 3.32. Ratio between the rms values computed along the whole record for the GPS estimate and the motor movements versus amplitudes of oscillations referring to the #Nov08 tests campaign

It is difficult to comment the previous results in absolute terms. Therefore, equivalent plots of measurements were collected by a non-contact laser sensor of good precision and plotted in Figure 3.33 and 3.34. The comparison confirms the better quality of the GPS measurements with respect to the laser sensor and gives a range of the GPS effectiveness.

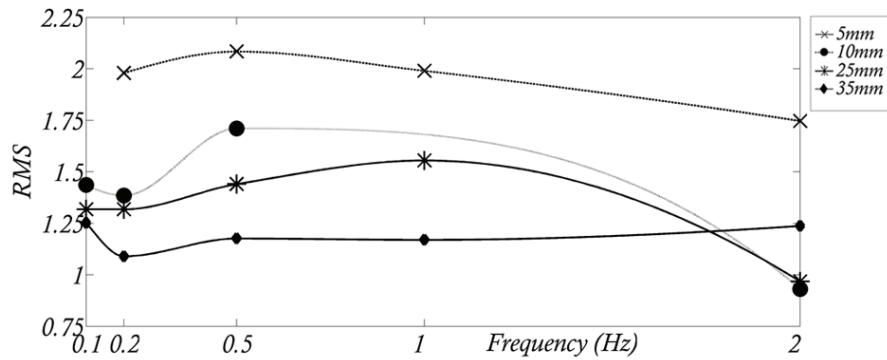


Figure 3.33. Plot equivalent to Figures 3.31 but achieved by measuring the displacement with a non-contact laser sensor

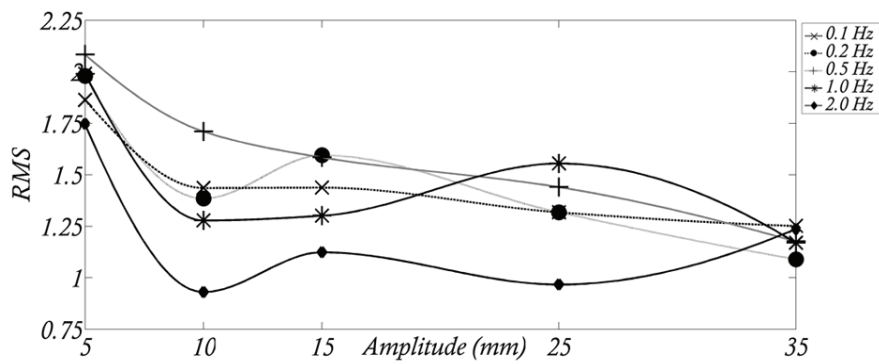


Figure 3.34. Plot equivalent to Figures 3.32 but achieved by measuring the displacement with a non-contact laser sensor

To have a comparison with the results of the #Nov08 tests, similar plots have been elaborated for the #Mar09 tests. In particular, the time history (a), the variation in time of the rms measure (b) and of the associated power spectral density (PSD) function (c) are plotted in Figure from 3.35 to 3.39, respectively.

Figure 3.35 refers to a test with displacements amplitude of $\pm 0.75\text{cm}$ and frequency of 0.5Hz ; while in Figure 3.36 the frequency is 1Hz and the amplitude is set to $\pm 1.25\text{cm}$, and Figure 3.37 shows the result for a test with the displacement amplitude of $\pm 0.75\text{cm}$ and the frequency of 2Hz . Figures 3.38 and

3.39, finally, report the result of two test with the same frequency of 4Hz but amplitudes of $\pm 0.75\text{cm}$ and $\pm 1.25\text{cm}$, respectively.

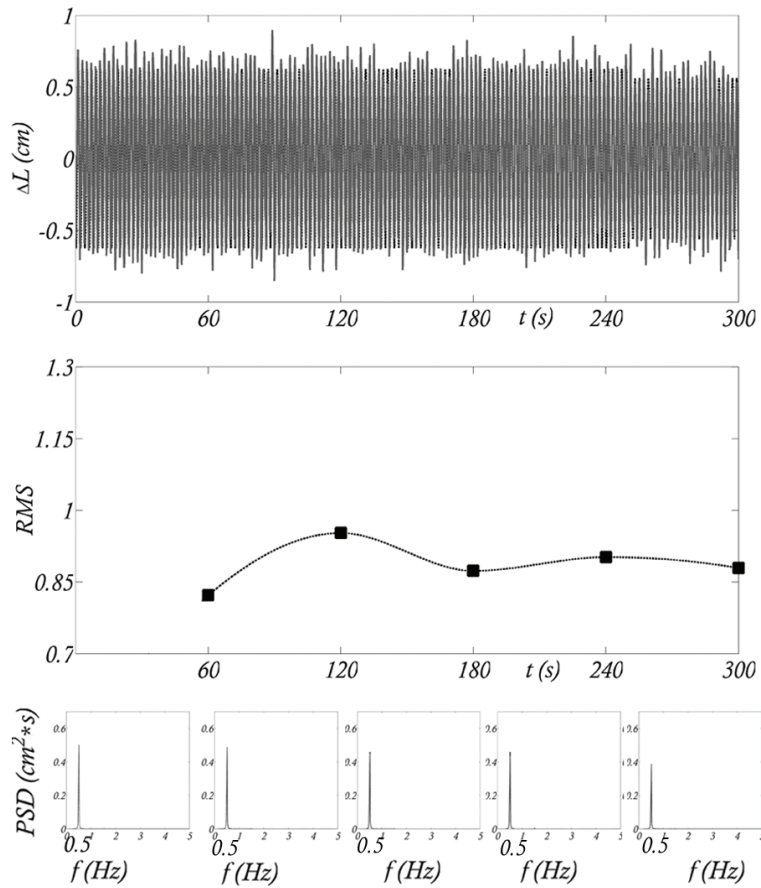


Figure 3.35. Result for the #Mar09 dynamic test (amplitude= $\pm 0.75\text{cm}$, frequency= 0.5Hz). GPS (grey) and linear motor (black) displacements time history (top); variation in time of the rms of the ratio between GPS estimate and linear motor amplitude (middle); corresponding GPS (grey) and linear motor (black) power spectral densities (PSD) (bottom)

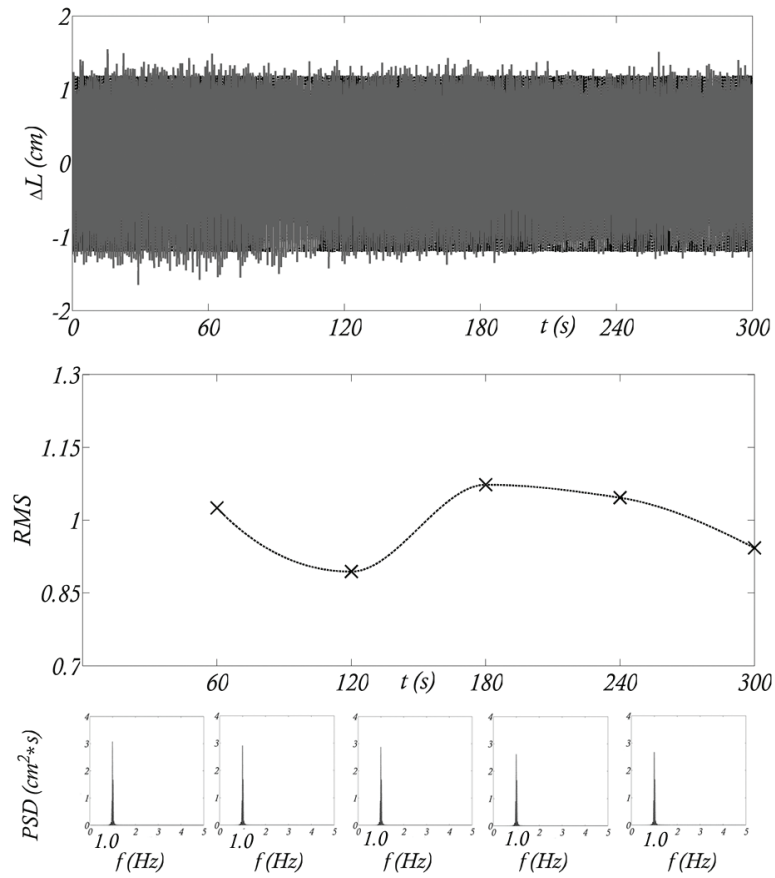


Figure 3.36. Result for the #Mar09 dynamic test (amplitude= ± 1.25 cm, frequency=1.0Hz). GPS (grey) and linear motor (black) displacements time history (top); variation in time of the rms of the ratio between GPS estimate and linear motor amplitude (middle); corresponding GPS (grey) and linear motor (black) power spectral densities (PSD) (bottom)

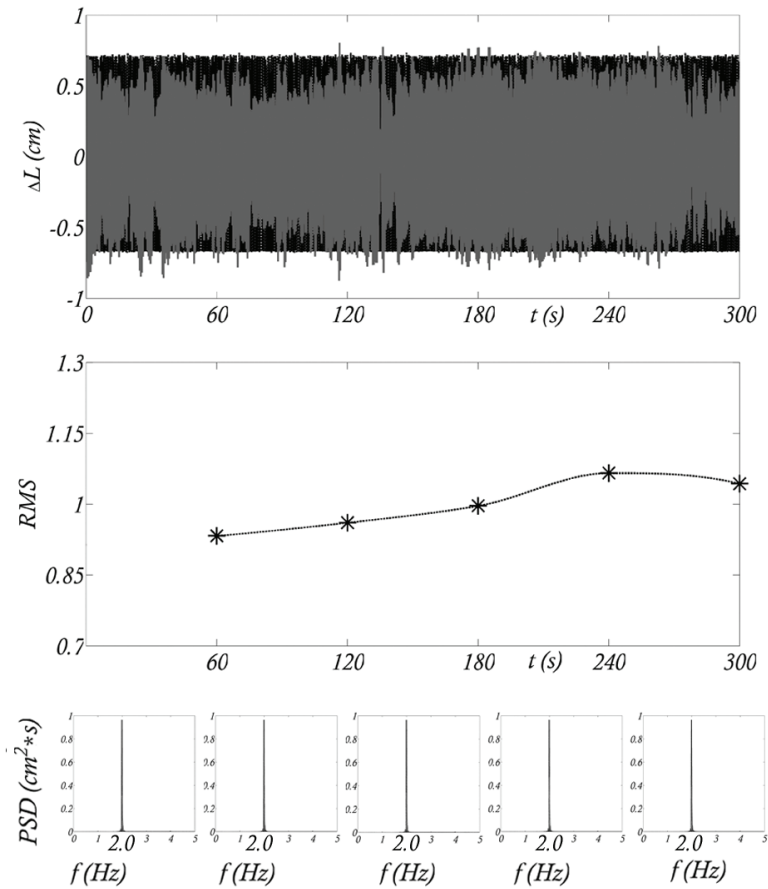


Figure 3.37. Result for the #Mar09 dynamic test (amplitude= ± 0.75 cm, frequency=2.0Hz). GPS (grey) and linear motor (black) displacements time history (top); variation in time of the rms of the ratio between GPS estimate and linear motor amplitude (middle); corresponding GPS (grey) and linear motor (black) power spectral densities (PSD) (bottom)

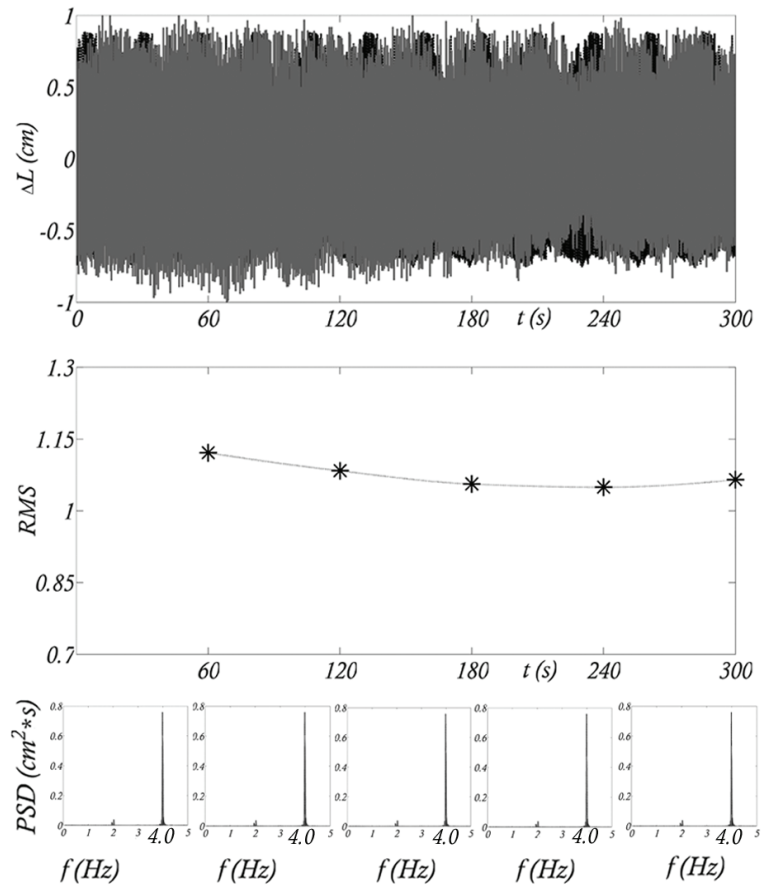


Figure 3.38. Result for the #Mar09 dynamic test (amplitude= ± 0.75 cm, frequency=4.0Hz). GPS (grey) and linear motor (black) displacements time history (top); variation in time of the rms of the ratio between GPS estimate and linear motor amplitude (middle); corresponding GPS (grey) and linear motor (black) power spectral densities (PSD) (bottom)

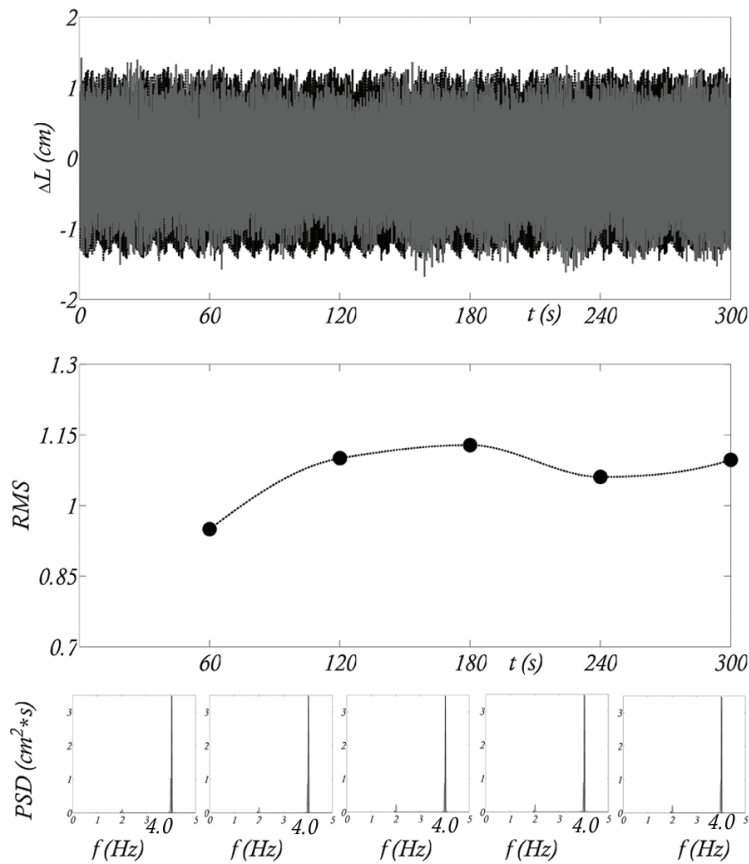


Figure 3.39. Result for the #Mar09 dynamic test (amplitude= ± 1.25 cm, frequency=4.0Hz). GPS (grey) and linear motor (black) displacements time history (top); variation in time of the rms of the ratio between GPS estimate and linear motor amplitude (middle); corresponding GPS (grey) and linear motor (black) power spectral densities (PSD) (bottom)

For all the reported figures, the middle plots, which report the variation in the time of the rms of the ratio between GPS estimate and motor displacement, show different trends of convergence in time. The trend is in particular interesting for Figure 3.38, representing the results for a 4Hz oscillation with an amplitude of ± 0.75 cm, which is a typical and signifying movement difficult to

be detected by a GPS sensor. In fact, as previously mentioned, one of the main GPS limitation is that the accuracy decay when increasing the frequency of oscillations. The convergence in time of the middle plot of Figure 3.38 (to a value of 1) suggests that after a very short period of adjustment such kinds of movements can be tracked by GPS.

When looking to the bottom plots of all the previous figures, a perfect agreement can be noted in the frequency domain.

A synthesis of the results can be found in the plots in Figures 3.40 and 3.41, where the rms ratio between the GPS estimate and the motor displacement is plotted versus the frequency and versus the amplitude, respectively.

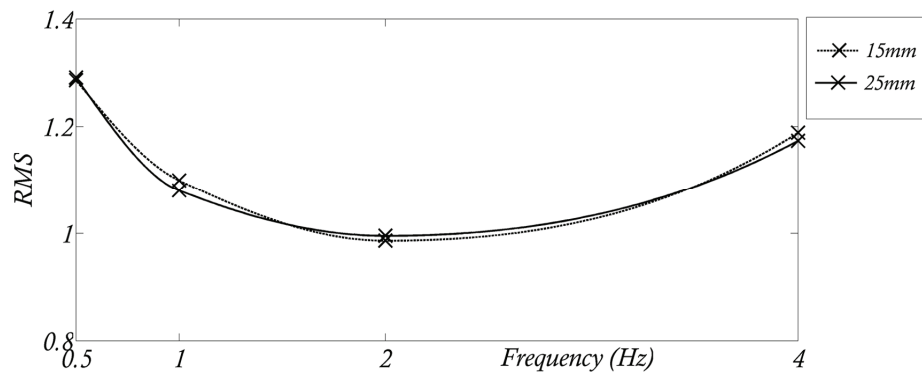


Figure 3.40. Ratio between the rms values computed along the whole record for the GPS estimate and the motor movements versus frequency of oscillations referring to the #Mar09 tests campaign

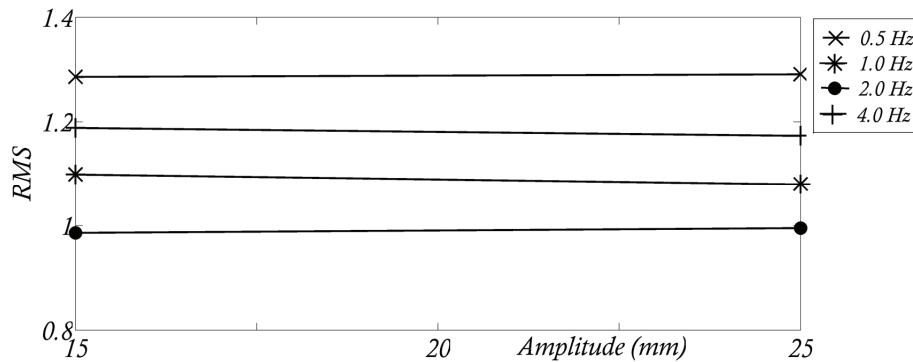


Figure 3.41. Ratio between the rms values computed along the whole record for the GPS estimate and the motor movements versus amplitudes of oscillations referring to the #Mar09 tests campaign

From Figures 3.31-3.32 and 3.40-3.41 one can observe some interesting trends and can formulate some deductions:

(i) in Figure 3.32 the accuracy increases when increasing the displacements amplitude;

(ii) in Figure 3.31 the rms values do not change, for the same amplitude of oscillations, when increasing the frequency of oscillations from 0.5 to 2Hz;

(iii) in Figure 3.40 a decreasing slope can be noted when increasing the frequency from 0.5 to 2Hz, where a value of 1 in the rms ratio is reached. Increasing the frequency up to 4Hz, corresponds to decrease the accuracy of the measurement but with a rms ratio which is not so far from the one calculated at 1Hz.

Based on the results presented above, the next step was to investigate how and in which measure the GPS sampling rate can affect the precision in detecting the dynamic movements of the linear motor. For convenience the tests were all carried out for a single value of displacement amplitude and frequency ($\pm 1.25\text{cm}$ and 1Hz) varying the sampling rate from 2 (#test1), to 5Hz (#test2) and from 10 (#test3) to 20Hz (#test4).

The time history of duration 300s of the displacements recorded by the GPS receiver for each of the four tests is plotted in Figure 3.42, where the dashed black line refers to the threshold of the imposed linear motor displacements.

The Power Spectral Density functions for the four tests data are also calculated and plotted in Figure 3.43, with the aim of showing the frequency detection and the energy content. Of course the PSD of #test1 is limited at 1Hz as the sampling rate was of 2Hz.

The root mean square (rms) values of the recorded data are calculated for the four tests and plotted in Figures 3.44 and 3.45, in terms of the rms ratio between the GPS estimate and the motor displacements.

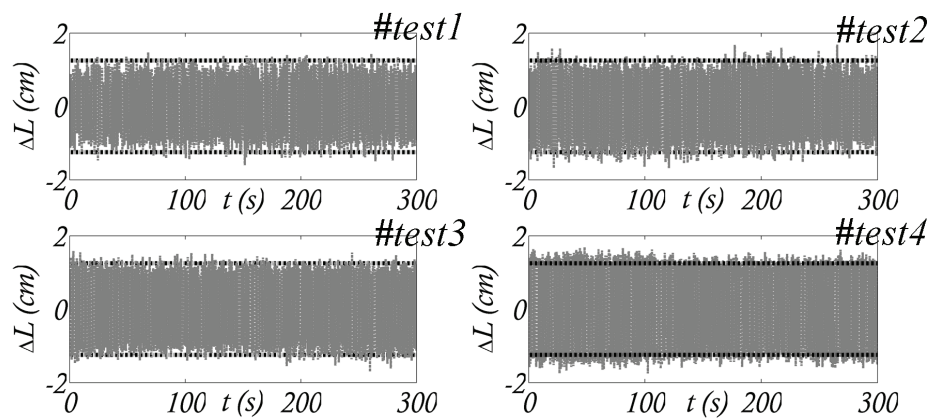


Figure 3.42. Time history of the GPS recorded displacements in tests 1-4, with the linear motor imposed displacements in dashed black line

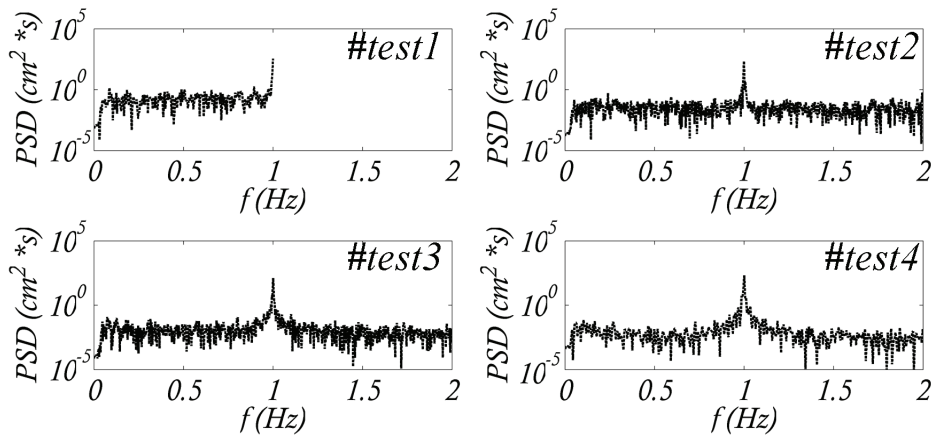


Figure 3.43. Power Spectral Density function of the GPS recorded displacements from #tests 1 to 4

Figure 3.44 shows the trend in the rms variation of the GPS longitudinal displacements from #test1 (2Hz) to #test4 (20Hz). In #test2 (5Hz), #test3 (10Hz) and #test4 a stabilization in the rms can be noted.

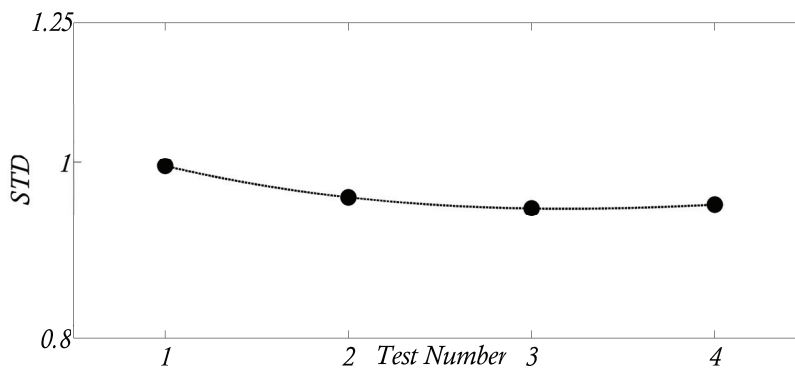


Figure 3.44. Ratio between the rms values computed along the 300s record for the GPS estimate and the motor movements versus amplitudes of oscillations

Based on the results depicted in Figures 3.42 and 3.44, one can conclude that for the GPS an increasing in the sampling rate does not correspond to an actual better accuracy. This probably derives from the limitation of the GPS in the

sampling rate and suggests to reflect on the possibility of using high sampling frequency (i.e., 20Hz or even more) when monitoring a structure.

3.3 Conclusions

This chapter focuses on some aspects related to the reliability and the accuracy of the measurements of dual frequency GPS receivers. The investigation is conceived for both static and dynamic tests. The accuracy of GPS measurements is assessed by testing a GPS system made by a fixed reference receiver and a rover, which moves along rails driven by a linear electromagnetic motor. By simulating harmonic displacements in the longitudinal horizontal direction, information is acquired from the GPS data records concerning the signal stability and repeatability and the accuracy in terms of both displacements detection and frequencies acquisition. Sufficiently long records enable to assume the effectiveness of the GPS techniques for dynamic movements in the range of low frequencies (from 0 to 4Hz) and small displacements (up to 5mm). How this accuracy is influenced by the GPS sampling rate is also analyzed.

Chapter 4

FULL SCALE GBS-BASED SHM OF AN INDUSTRIAL STEEL BUILDING

Introduction

The steel building which hosts the authors laboratory is the case-study within this chapter. Natural (i.e., wind actions) and man made (i.e., internal bridge crane movements) dynamic actions are considered. The natural actions are considered as long duration actions exciting mainly low frequencies, while the man made actions are considered as short duration actions, which induce significant displacements amplitude at relatively (for the structure) high frequencies.

A comparison of the data collected by GPS units with those recorded by tri-axial accelerometers is also presented within this chapter. Different GPS units locations on the roof of the building , conceived to detect any signal dilution of precision (DOP), are also analyzed.

Finally a comparison of the results of a numerical simulation, achieved by a finite element FE model of the building, with the elaborations from the GPS position readings is arranged.

4.1 Overview of the full scale tests

Full scale tests were carried out by installing two or three GPS on the roof of the industrial steel building in Pavia (see Figure 4.1), which hosts the author's laboratory, at the height of about 11m (i.e., on the top of the lower building in Figure 4.1) (Casciati and Fuggini, 2008a, b, c, 2009a).

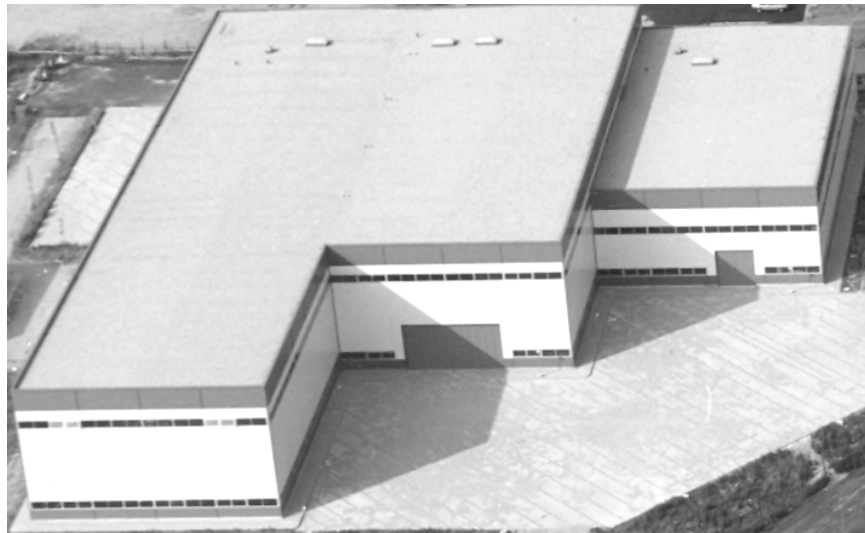


Figure 4.1. Birds eye view of the industrial steel building

When only two antennas were placed, the baseline connecting them, was a line oriented towards the East or the North. When three sensors were placed they formed a triangle with the three antennas in the three vertices. In each sensors placement, one antenna is fixed, and the others (one or two) are movable. The fixed unit, (at the height of 13m), marked in the following as “*a*”, corrects the position of the movable unit “*b*” by sending it a new position purified by the errors. The same scheme is applied when two movable units are considered: in this case unit “*a*” simultaneously makes the position correction for both the receivers “*b*” and “*c*”.

Two experimental scenarios were conceived:

- (i) excitations during the wind actions (i.e., long duration records), exciting the building and producing oscillations tracked by the GPS sensors;
- (ii) bridge-crane movements (i.e., short duration records), producing vibrations detected by the GPS sensors.

The case (i), in the following indicated as long duration records (*LDR*), allows the author to study the effectiveness of GPS for events which produce a long time response of the structure, exciting very low frequencies.

The case (ii), in the following indicated as short duration records (*SDR*), enables to analyze the GPS ability to detect sudden and different actions which produce very fast effects on the structure, exciting relatively high frequencies.

The estimation of GPS precision is so discussed for oscillations caused by winds events (*LDR*) and by movements of the internal bridge-crane (*SDR*). The duration of the recorded time histories was of some hours for the wind events and of some seconds for the bridge-crane impact force.

The *LDR* obliges one to account for the variations in the GPS accuracy during one sidereal day, as due to changes in the satellites constellation configuration during the day. On the other side, the problem related to the *SDR* is mainly the GPS ability to detect sudden changes in the behavior of the structures due to an impact force. The elaborations from the GPS records for the impact force are also compared with the measurements obtained by standard tri-axial accelerometers. The same elaborations from the GPS position readings are compared with the results obtained by a finite-element numerical simulation (Casciati et al., 2009)

As previously mentioned, both the tests campaigns were carried out by placing the sensors on the roof of the industrial building.

It is a steel structure made of three block; 81m long in the longitudinal direction and 64.5m in the transverse one. The weight-bearing element is a 2D Pratt truss, which connects, along the longitudinal direction, the columns.

Transverse links along the transverse direction are repeated every 5.4m. Perimeter wind-braces are also present (see Figures 4.2 and 4.3).

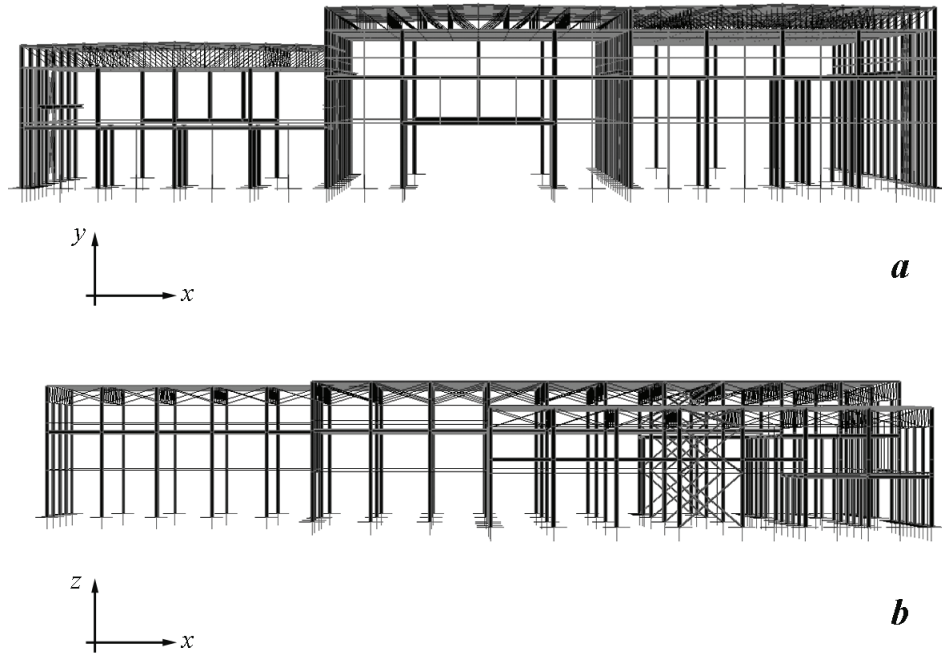


Figure 4.2. Internal rendering view of the industrial steel building: frontal side (a), lateral side (b)



Figure 4.3. Internal 2D Pratt truss (left) and wind-braces (right)

4.2 Long duration record results

Three different GPS sensors locations were adopted for three wind events which occurred in Pavia in:

- (i) November 9, 2007 (in the following indicated as #Nov07);
- (ii) January 22, 2008 (in the following #Jan08);
- (iii) October 30, 2008 (in the following #Oct08).

During these events the wind approached mainly from the North-West direction.

For each event, the wind speed and the wind direction were recorded by a permanent wind station (Cascina Pelizza) near the equipped industrial steel building and at about the same height as the roof of the building. Therefore it was assumed that the wind velocity on the case study structure was that recorded at the permanent station of Cascina Pelizza.

The mean wind speed for the three events was quite similar, while the most significant wind peak intensity was that of November 2007, when the wind, approaching from North, produced ten minutes of significant peaks up to 20.7m/s.

Figure 4.4 shows the three plan views of the GPS locations on the roof of the industrial building. Looking at Figure 4.4, note that for the January and October events, the baseline connecting the reference unit "a" with the movable units "b" and "c", respectively, approximately corresponds to the East component of the GPS reference system.

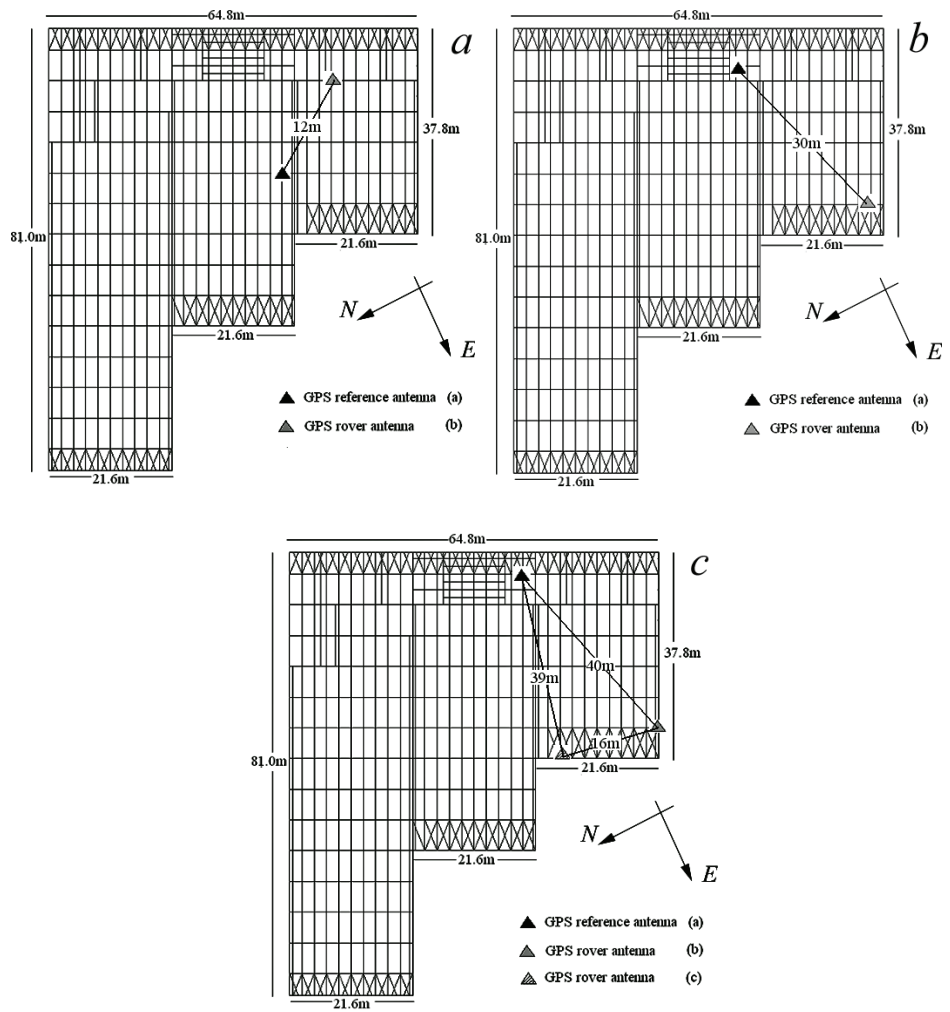


Figure 4.4. Plan view of GPS sensor location during the three recorded wind events: #Nov07 (a); #Jan08 (b); #Oct08 (c)

A zoom of the baseline connection for the #Oct08 event configuration is plotted in Figure 4.5.

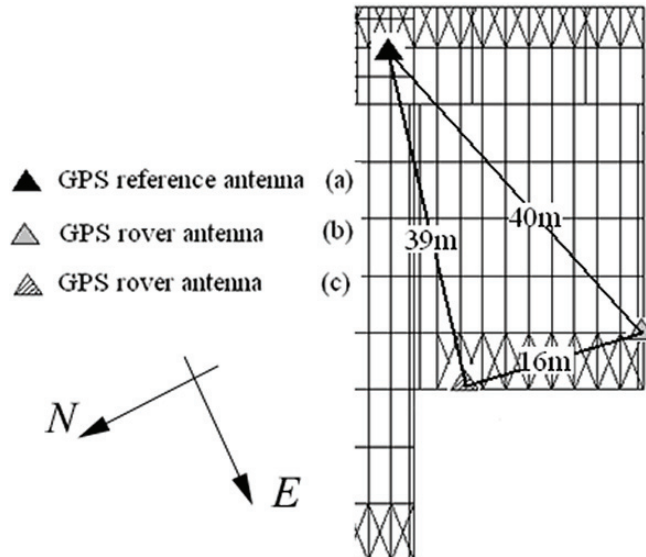


Figure 4.5. Zoom of GPS sensor placement during #Oct08 wind events

4.2.1 Data processing of GPS records

The GPS rover sensors mounted on the roof of the industrial building recorded the oscillations of the building due to the three specific wind events mentioned above. For the #Nov07 event in particular the main amplitude of the recorded GPS movements was in the North direction, corresponding to the along wind approach, while in the East direction the amplitude was rather low. For this first event a comparison is made between:

- a) the peak interval in the displacement time history recorded by the GPS in the North direction;
- b) the corresponding results derived by a simulation, in a finite element environment (see section 4.3.3), adopting as input wind excitation the one recorded at Cascina Pelizza. The wind action is applied as a pressure on the structure.

The comparison shows good agreement in detecting the peak amplitude (see Figure 4.6). It is worth noting that the Cascina Pelizza record is sampled at 1 point every 5 minutes, the asserted structural analysis is conducted with an integration step of 0.05 sec. and the GPS signal is recorded at 1 point per second. The content of the excitation between 0.2 and 1Hz is just added as noise to the Cascina Pelizza record.

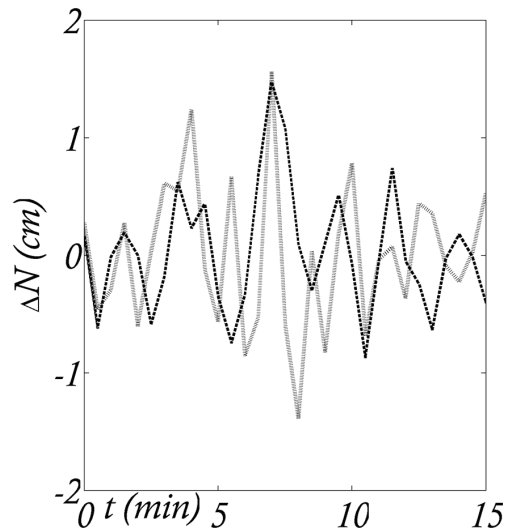


Figure 4.6. Peak displacements time history of #Nov07 wind event: numerical results (black); experimental GPS recorded data (grey)

The pure recorded signal is then filtered by applying a filtering scheme, having two main purposes: i) to remove distortions in the estimated displacement response and consequently ii) to decompose the signal in a background (signal noise) and in a resonant components.

Once the recorded signal (i.e., the wind response displacement time history) is converted in the frequencies domain, the filter is applied to remove a range of low frequency components from the frequency spectrum, with a cut-off frequency f_c of 0.05Hz. The re-conversion into the time domain is then obtained by the inverse Fourier Transform of the modified spectrum.

The value of the cut-off frequencies is chosen accounting for two sources of uncertainties: multipath (Kijewsji-Correa and Kochly, 2007) and GPS residual noises. The frequencies associated to these effects are in fact, in most of the cases, in the range between 0 and 0.05Hz, as also depicted in Figures 3.23 and 3.24.

For the three considered wind events, the recorded displacement time histories for both North and East components, are plotted in Figures from 4.7 to 4.10, respectively.

Figures 4.7 and 4.8 are relevant to test the GPS ability to track the induced displacements when only one rover was active. On the contrary figures 4.9 and 4.10, which refer to the #Oct08 event, gives the signal of the two active rovers "b" and "c", respectively.

For each group of figures, the top subplot gives the signal as recorded, the central sub-plot the filtered part of the signal using the above described filter and the bottom sub-plot is the mere difference of the previous two time-histories.

Each couple of records (i. e., North and East components) has a different duration, as reported in the figures. Moreover the sampling frequencies were also different in the three recording days: on #Nov07 events, it was 1Hz; on #Jan08 event, 10Hz and on #Oct08 event 20Hz.

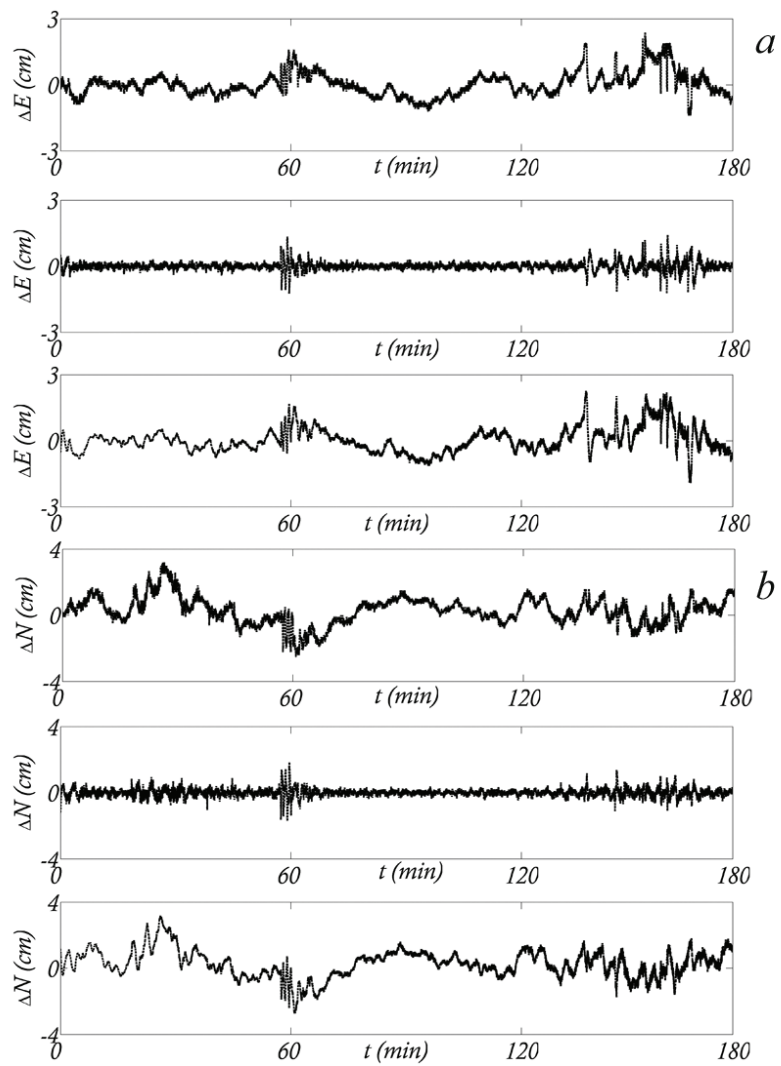


Figure 4.7. Response time histories during the #Nov07 wind event: GPS signal as recorded in the top plot; filtered GPS displacement signal (middle plot); difference of the two previous signals (bottom): a) East component; b) North component

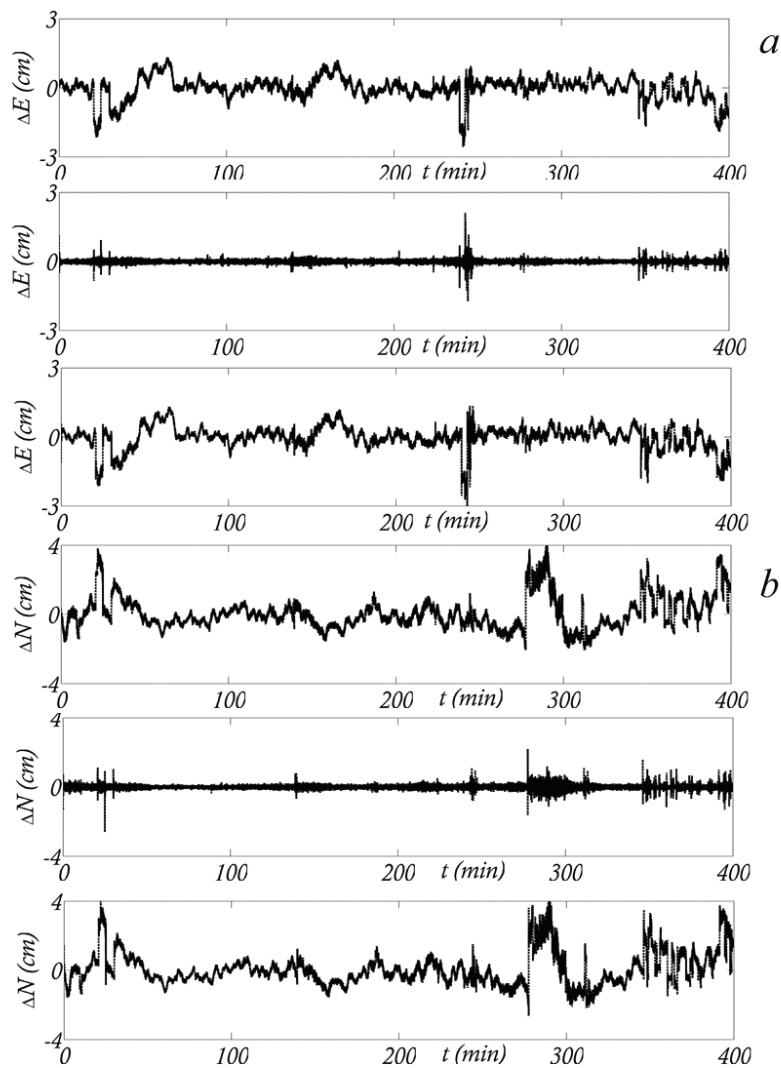


Figure 4.8. Response time histories during the #Jan08 wind event: GPS signal as recorded in the top plot; filtered part of the GPS displacement signal (middle plot); difference of the two previous signals (bottom): a) East component; b) North component

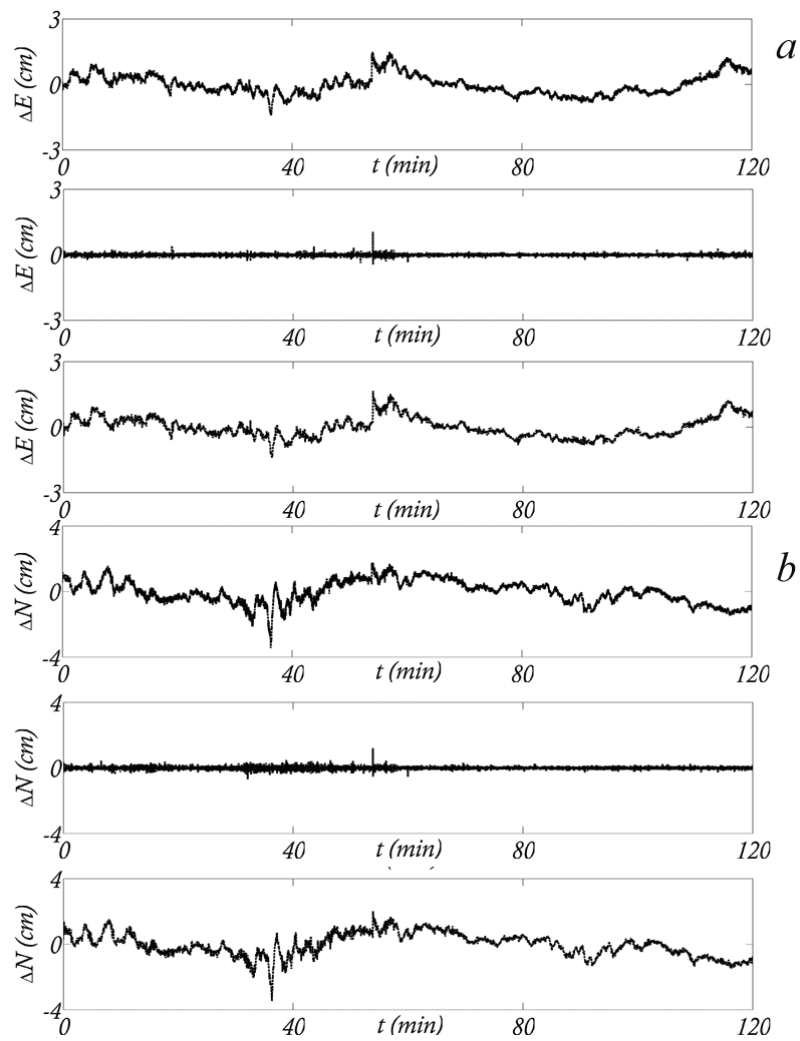


Figure 4.9. Response time histories during the #Oct08 wind event: GPS “b” signal as recorded in the top plot; filtered part of the GPS displacement signal (middle plot); difference of the two previous signals (bottom): a) East component; b) North component

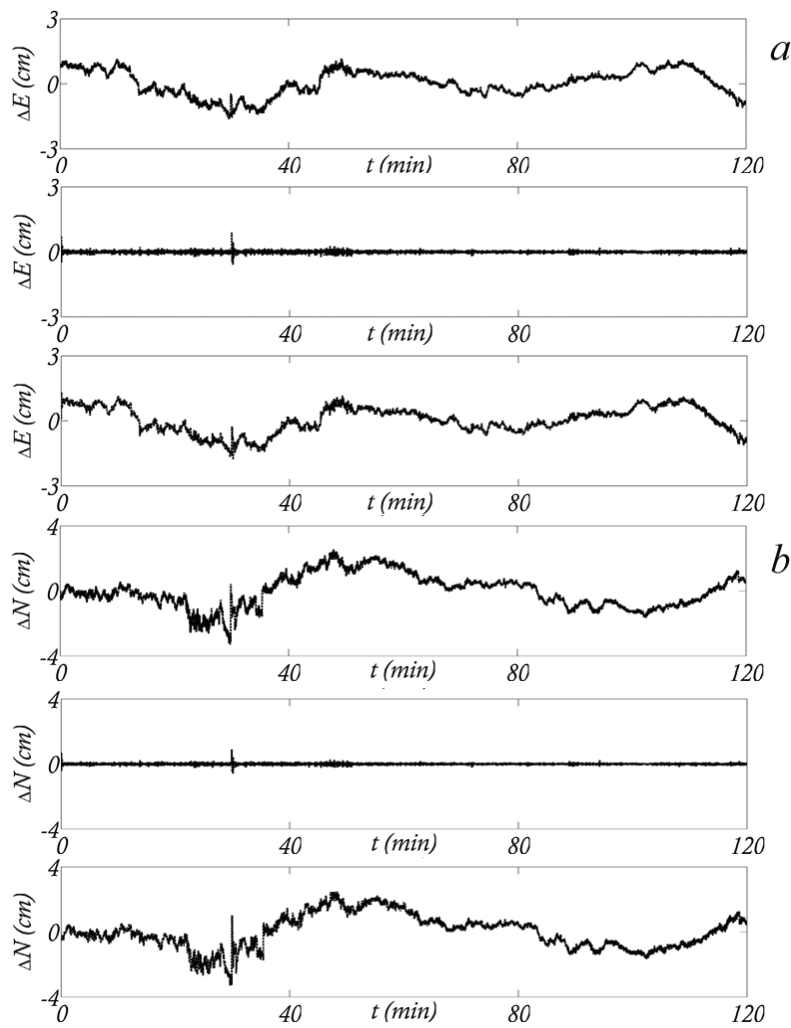


Figure 4.10. Response time histories during the #Oct08 wind event: GPS “c” signal as recorded in the top plot; filtered part of the GPS displacement signal (middle plot); difference of the two previous signals (bottom): a) East component; b) North component

A sampling frequency of 1Hz should be sufficient to detect the main frequency content of the wind induced oscillations. But the purpose of

increasing sampling rate was just to investigate the dependence of the accuracy on it, if any.

The information summarized in Figures from 4.6 to 4.10 is re-arranged to show how the receiver move in the plane according to the signals as recorded and the filtered part of the signals. The plots are in Figures 4.11 and 4.12, for the signals of receiver “b” only.

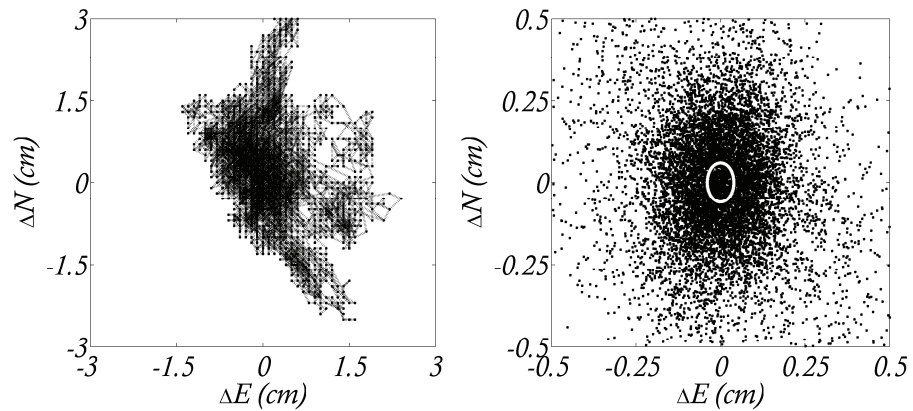


Figure 4.11. 2D plot of East-North GPS displacements during #Nov07 wind event: unfiltered data (left); filtered part of the recorded data (right)

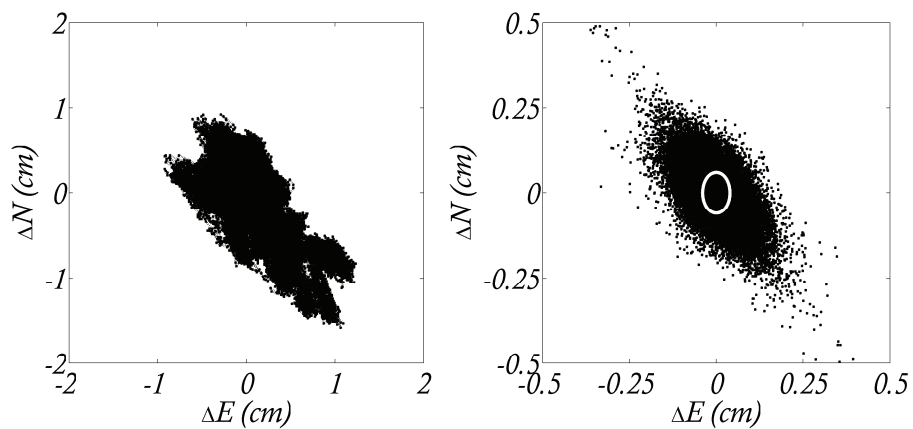


Figure 4.12. 2D plot of East-North GPS displacements during #Jan08 wind event: unfiltered data (left); filtered part of the recorded data (right)

Figures 4.13 and 4.14 then show the signal recorded by receivers “b” and “c”, to give the influence of the relative position between rover and reference.

The ellipses depicted in the right plots of Figures 4.11, 4.12, 4.13 and 4.14 have as radii the rms values calculated for the East and the North components.

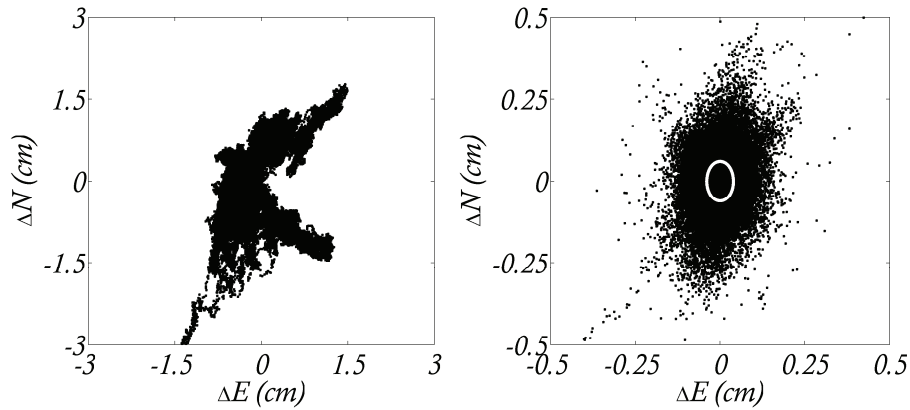


Figure 4.13. 2D plot of East-North GPS “b” displacements during #Oct08 wind event: unfiltered data (left); filtered part of the recorded data (right)

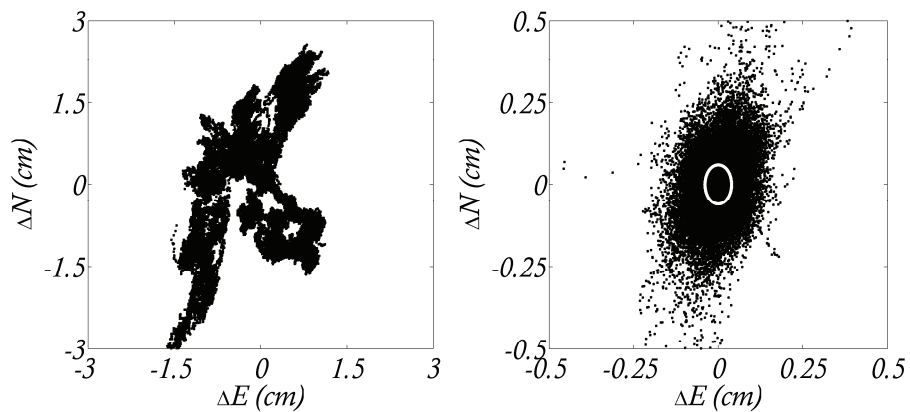


Figure 4.14. 2D plot of East-North GPS “c” displacements during #Oct08 wind event: unfiltered data (left); filtered part of the recorded data (right)

4.2.2 Resolution

The previous time histories refer not only to different days of acquisition (i.e., the three wind events) but also to different hours along the day. This represents an interesting aspect as the GPS precision can be affected by changes in the configuration of the satellites constellation (as previously reported and analyzed in Chapter 3) during a day. These changes are functions of the positions of the tracked overhead satellites and can produce significant signal distortions (the geometric dilution of precision GDOP as mentioned in chapter 1), in term of standard deviation variations. In particular when the tracked satellites are arranged toward the North, this automatically produces a small degradation of the signal.

The long duration GPS records (which vary from 120 to 400min) of wind induced displacements cover different satellites configurations, as the registrations are carried out at different hours along the day. The hours by hours variation of the GPS measurements in terms of GDOP has to be considered and how this behavior affects the wind measurements is worth being investigated.

Figure 4.15 shows the root mean squares (rms) of the East (black lines) and the North (grey lines) GPS displacements recorded at rest on different days and at different hours along the day, covering the range hours of the three wind events measurements.

What is presented here follows what is reproduced in Chapter 3. In that section, in fact, it was investigated how the baseline direction connecting one reference and one rover receiver could affect the acquired precision. In this section the same procedure is discussed with the only difference of comparing the GPS GDOP at rest with that during wind events records, considering the same baseline direction, the same sampling rate and the same hours of a day (Casciati and Fuggini, 2009a, c).

Looking at Figure 4.15a and b, it is observed an equivalent trend (but a different rms value) of the GPS unit “*b*” and “*c*” for East and North component. It is worth noting that the baseline “*a*”-“*c*” is mainly in the along East direction more than the baseline “*a*”-“*b*”.

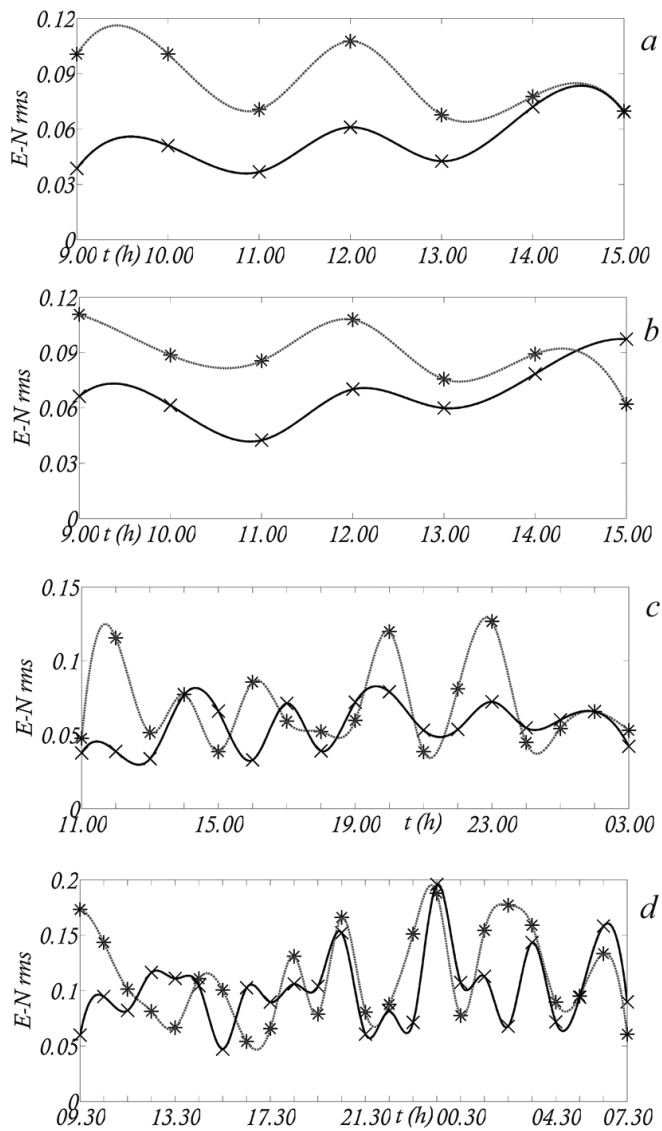


Figure 4.15. GPS rms of GPS pure recorded displacements at rest for the East component (black lines) and the North component (grey lines):
a) sampling rate of 20 Hz (receiver “b”); b) sampling rate of 20Hz (receiver “c”); c) sampling rate of 1Hz for record of a duration of 16 hours; d) sampling rate of 1 Hz for record of a duration of 22 hours

In the North-East plan one can also see the rms values as the radii of an ellipse which evolves hour by hour (Figure 4.16).

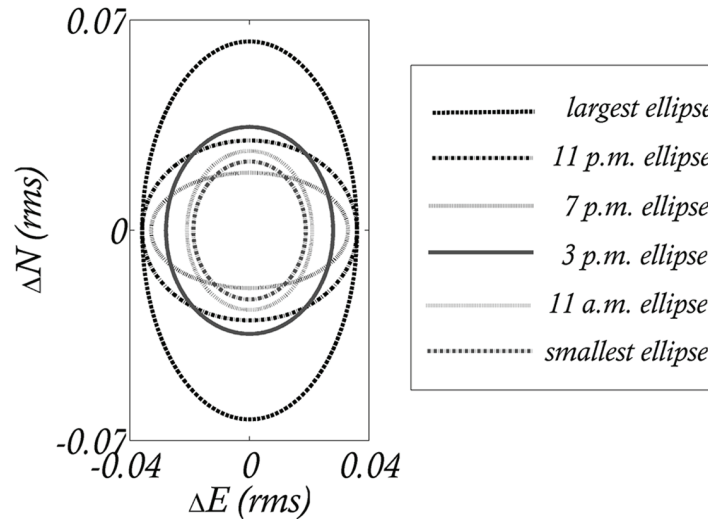


Figure 4.16. The rms ellipses computed at different hours during the day

In Figure 4.16 the ellipses between the smallest and the largest one were recorded at 11 a.m., 3 p.m., 7 p.m. and 11 p.m., respectively. Their E-N rms values are derived from those of the plot c) in Figure 4.15. Note that the largest ellipse is also drawn in the plots on the right side of the Figures from 4.11 to 4.14.

4.3 Results from short duration records

In the *SDR* the GPS ability to detect the response of the structure due to movements of an internal bridge-crane is considered.

The bridge-crane is mounted on rails running inside the steel building at the height of 8m and covering a span of around 20m (Figure 4.17).

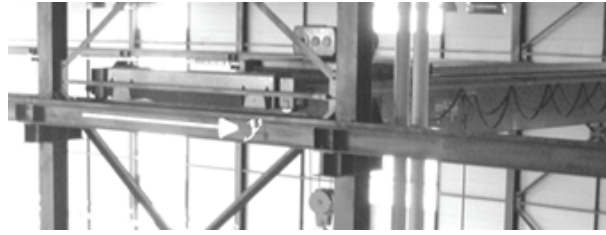


Figure 4.17. The bridge-crane inside the building

It allows three types of movements (Figure 4.18):

- (i) vertical movements of the load, inducing a vertical reaction P ;
- (ii) longitudinal horizontal movements (i.e., along its way beam), inducing a longitudinal reaction R ;
- (iii) transversal displacements for horizontal movements of the load, inducing a transversal reaction Q .

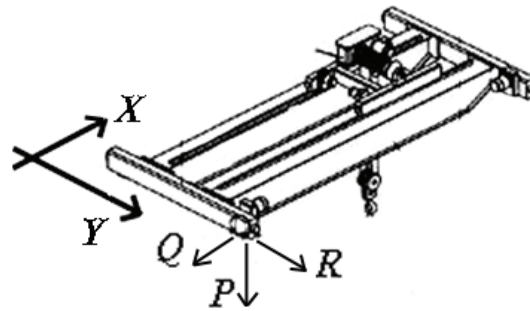


Figure 4.18. Bridge-crane reaction forces in the X-Y plane

The longitudinal backward and forward bridge-crane movements induce significant vibrations on the steel structure. The bridge-crane can be moved at the speed of 0.7m/s. While the bridge-crane is moving along the longitudinal direction (Y), the GPS devices placed on the roof record these oscillations. When the bridge-crane stops, at the end of his ride a peak force (opposite to the R reaction) of 10.93kN is introduced, according to the producer declaration.

To detect the different types of movements that the bridge-crane can follow, the GPS antennas position, on the roof of the industrial steel building, shown in

Figure 4.4c (see the #Oct08 event), was also adopted to record the structural vibration of the building induced by movements of the internal bridge-crane.

In this case a further Cartesian system is chosen to display the results of the GPS records, with X and Y axis, corresponding to the transversal and longitudinal direction of motion for the bridge-crane, as showed in Figure 4.19.

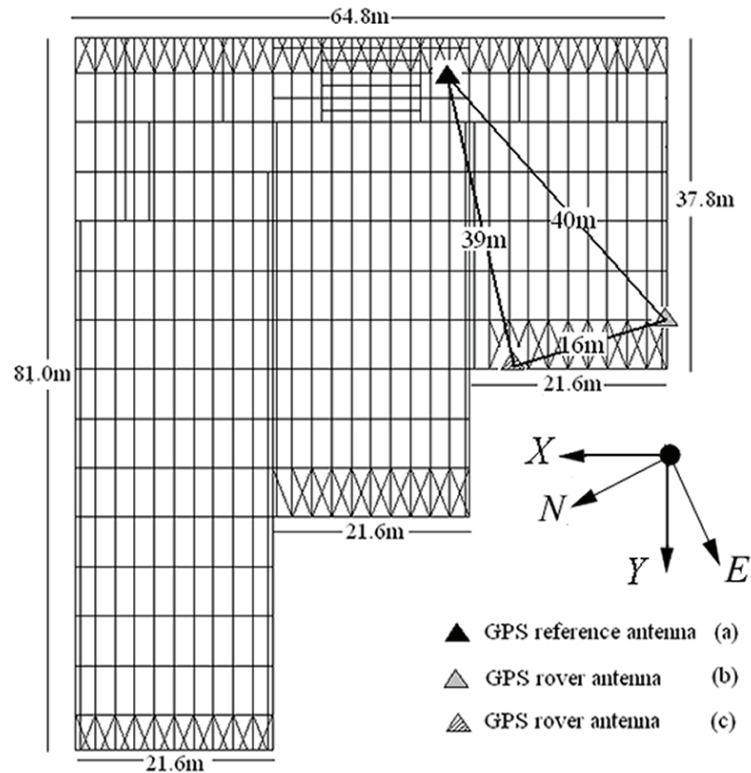


Figure 4.19. The GPS configuration in the N-E and X-Y plane for the short duration test

Looking at Figure 4.19, the sensors placement was chosen such as the baseline connecting the rover “c” (movable) with the reference “a” (fixed) is mainly oriented along the East direction. Indeed, the East-North GPS reference system does not coincide with the X and Y axis of the Cartesian System chosen

to indicate the direction of the bridge-crane movements along its rails (Figure 4.17).

A coordinate system transformation is introduced to calculate, from the East and North GPS recorded data, the displacements component along the X and Y axis, which denote the transversal and the longitudinal direction of the building, respectively. The coordinates transformation from the N-E Cartesian System to the X-Y one is made by adopting a suitable rotational matrix Γ such as presented in Equation (4.1):

$$\begin{pmatrix} n \\ e \end{pmatrix} = \begin{bmatrix} \cos \alpha & \text{sen} \alpha \\ -\text{sen} \alpha & \cos \alpha \end{bmatrix} \begin{pmatrix} x \\ y \end{pmatrix} \quad (4.1)$$

which can be inverted to obtain the x and y coordinates:

$$\begin{pmatrix} x \\ y \end{pmatrix} = \begin{bmatrix} \cos \alpha & -\text{sen} \alpha \\ \text{sen} \alpha & \cos \alpha \end{bmatrix} \begin{pmatrix} n \\ e \end{pmatrix} \quad (4.2)$$

where α ($=18,9^\circ$) represents the angle of rotation from the X-Y to the N-E Cartesian Systems.

4.3.1 Short duration records data processing

The *SDR* data, as derived by the bridge-crane movements, have been processed focusing on two different aspects:

(a) the comparison of the GPS derived accelerations with those recorded by tri-axial accelerometers placed nearby the GPS antennas;

(b) the structural identification of the standard industrial building from the results of GPS experimental tests. For this purpose a FE model of the structure is realized and man made actions (i.e., the bridge-crane movements, by which the real structure is excited) are simulated.

Both the aspect have been partially treated in (Casciati and Fuggini, 2008b, 2009a). In that follows a new set of tests is also reported.

4.3.2 GPS vs Accelerometers results comparison

Two GPS tests were carried out, with a different number of sensors involved and different sampling rate: the first campaign was held on March 15, 2008 (in the following #Mar08) and the second on May 10, 2009 (in the following #May09).

In #Mar08 tests the GPS topology was exactly the one reported in Figure 4.19, with three GPS sensors sampling at 20Hz. In #May09 tests, on the contrary, only two of the three sensors where used, the reference one “*a*” and as rover the one marked as “*c*” in Figure 4.19. In the #May09 tests also the sampling rate was varied, reducing it to 10Hz.

In both the tests campaign, three or two tri-axial Kinematics accelerometers were placed near the GPS antennas (Figure 4.20).

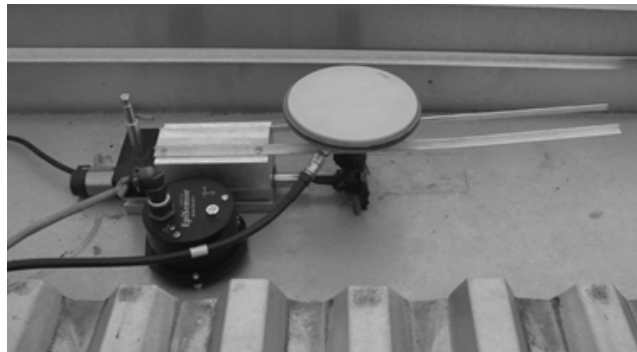


Figure 4.20. View of the short duration records experimental setup

The accelerometers record, at a sampling rate of 100Hz, the accelerations in the *X* and *Y* directions when the bridge-crane is moving inside the building. The along *X* signal corresponds to the calculated GPS *X* component, while the along *Y* accelerometers record corresponds to the calculated GPS *Y* component.

For the purpose of a direct comparison, a double differentiation procedure is applied to the GPS measured displacement data, in order to convert them into accelerations and to compare with the accelerometer measured accelerations. A band stop filter with a cut-off frequency f_c is 0.05Hz is also applied to the pure GPS recorded displacements.

Figures from 4.21 to 4.24 show the results for #Mar08 tests, for both X and Y directions. In each figure, the upper plot gives the GPS displacement record as filtered, the bottom plot provides the comparison between the acceleration measures estimated from the GPS records (continuous black) and the accelerations measured by the accelerometer (dashed grey). The first two figures refer to the GPS rover receiver "b", while the last two refer to the GPS rover receiver "c".

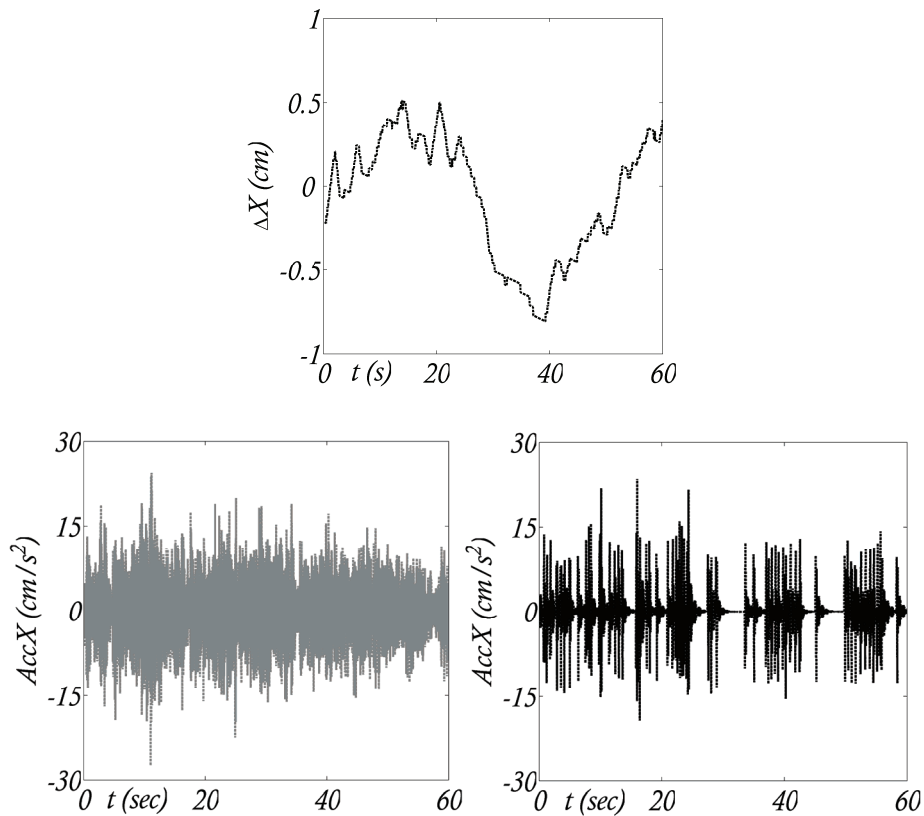


Figure 4.21. X direction time histories for #Mar08 tests. Top: GPS "b" displacements; Bottom: tri-axial accelerometer accelerations (left), GPS "b" derived accelerations (right)

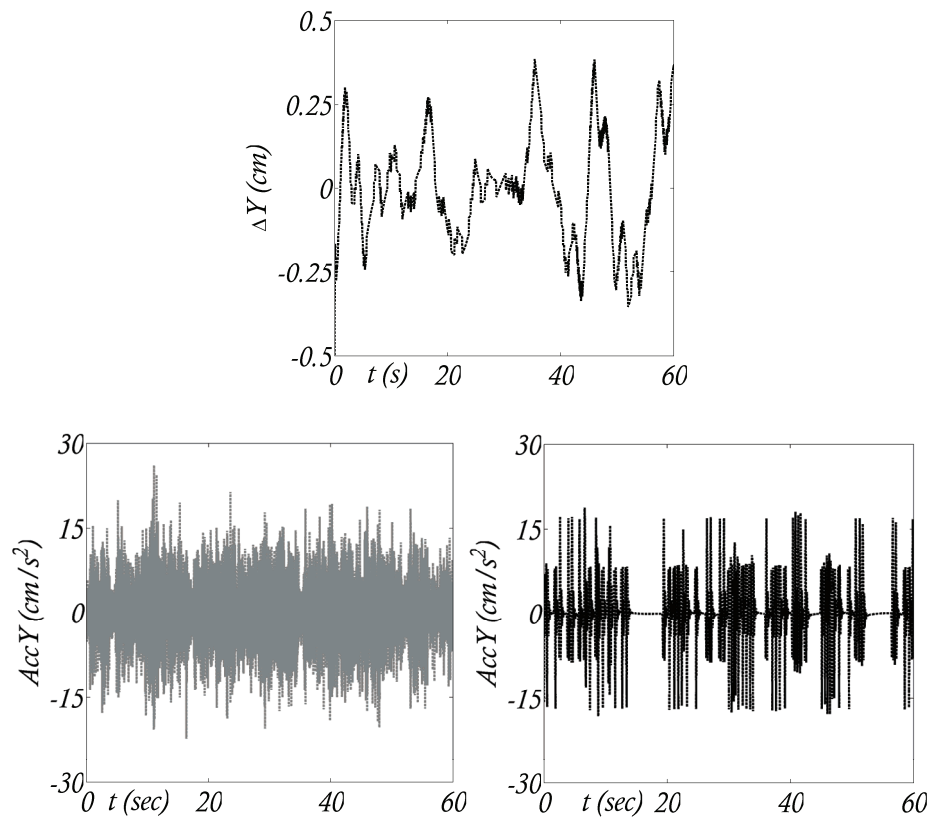


Figure 4.22. Y direction time histories for #Mar08 tests. Top: GPS “b” displacements; Bottom: tri-axial accelerometer accelerations (left), GPS “b” derived accelerations (right)

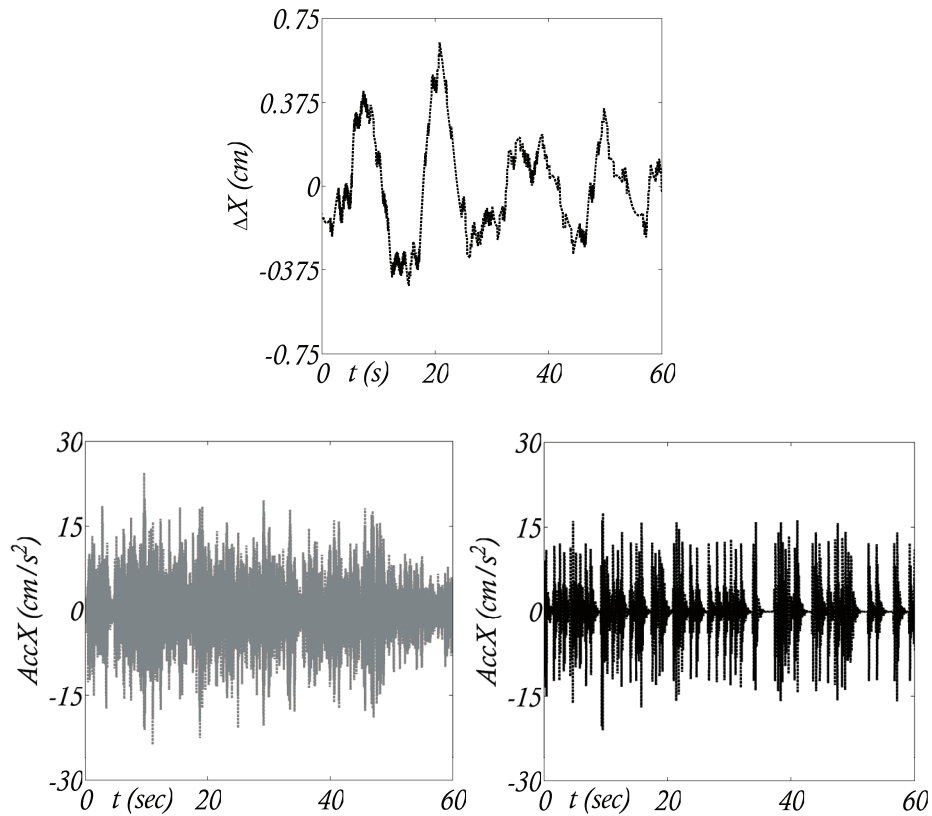


Figure 4.23. X direction time histories for #Mar08 tests. Top: GPS “c” displacements; Bottom: tri-axial accelerometer accelerations (left), GPS “c” derived accelerations (right)

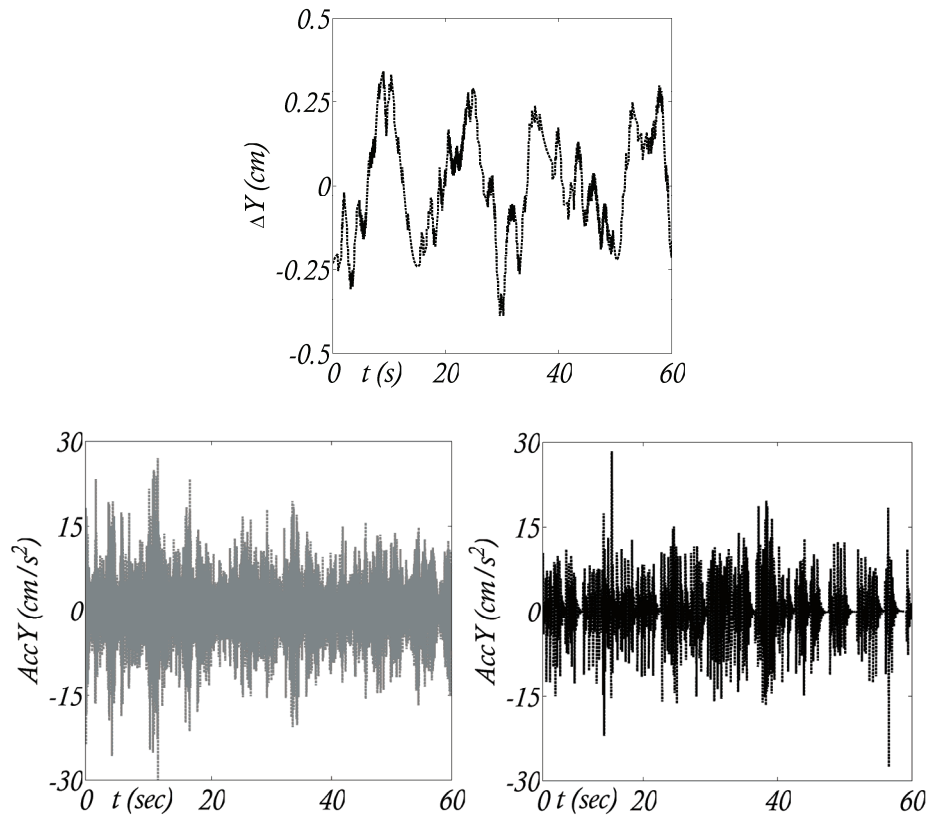


Figure 4.24. Y direction time histories for #Mar08 tests. Top: GPS “c” displacements; Bottom: tri-axial accelerometer accelerations (left), GPS “c” derived accelerations (right)

Comparing the time series in the bottom plots (of Figures 4.21-4.24), it can be seen that they agree with each other, although the GPS seems to reveal a certain level of noise, as indicated from the Power Spectral Density (PSD) analysis in Figures 4.25 and 4.26.

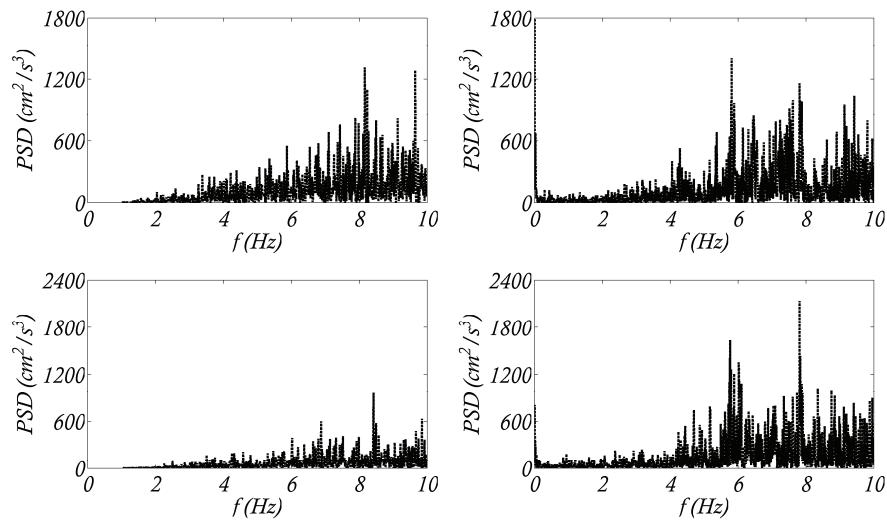


Figure 4.25. PSD functions from the measurements of #Mar08 tests along the X (top) and the Y axes (bottom). GPS “b” estimated acceleration (left), accelerometer measured accelerations (right)

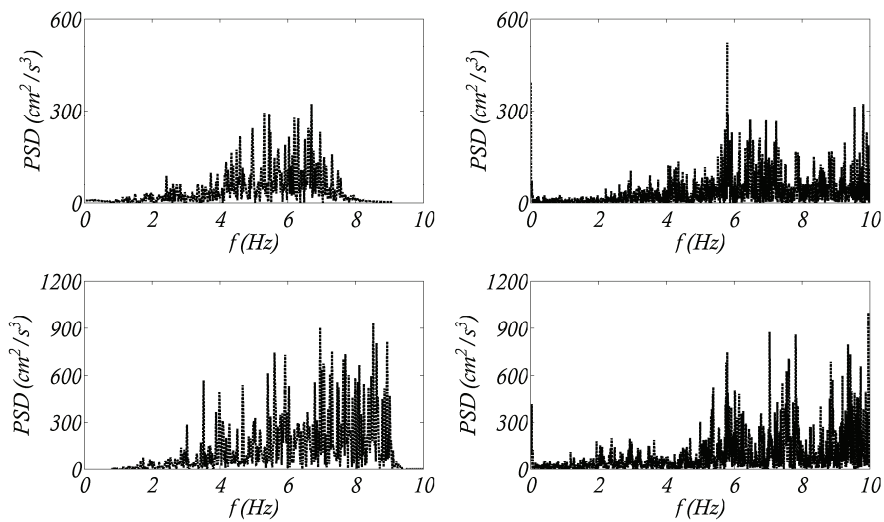


Figure 4.26. PSD functions from the measurements of #Mar08 tests along the X (top) and the Y axes (bottom). GPS “c” estimated acceleration (left), accelerometer measured accelerations (right)

On the other side, Figures 4.27 and 4.28 show the results for #May09 tests. In this case, in each figure, the upper plot gives the GPS displacement record, while the bottom plots provide the comparison between the acceleration measures estimated from the GPS records (black) and the accelerations measured by the accelerometer (grey). As previously introduced, the two figures refer to the GPS rover receiver “c”.

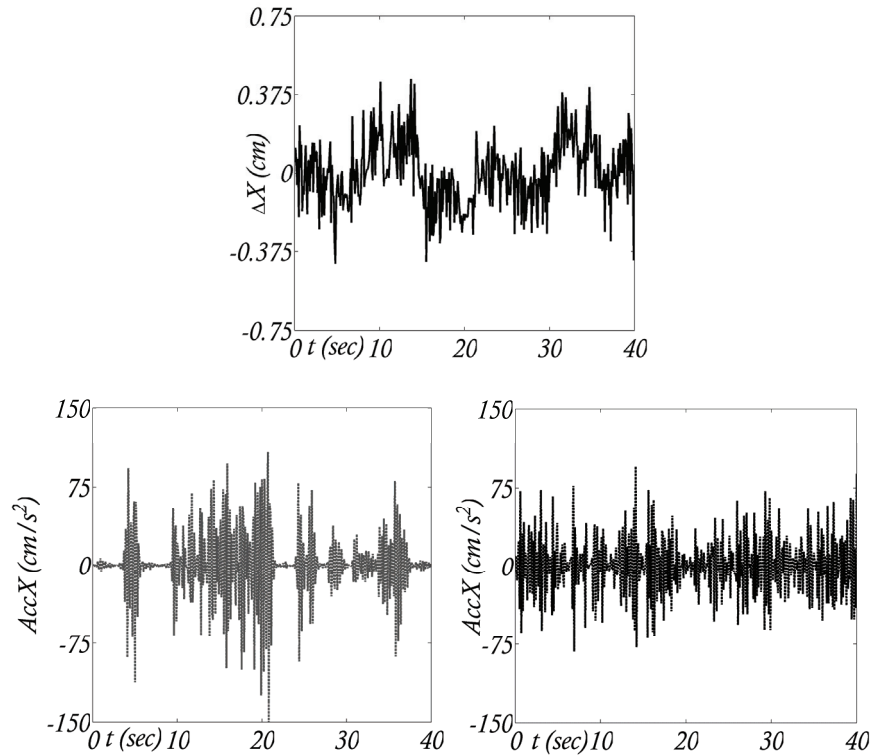


Figure 4.27. X direction time histories for #May09 tests. Top: GPS “c” displacements. Bottom: tri-axial accelerometer accelerations (left), GPS “c” derived accelerations (right)

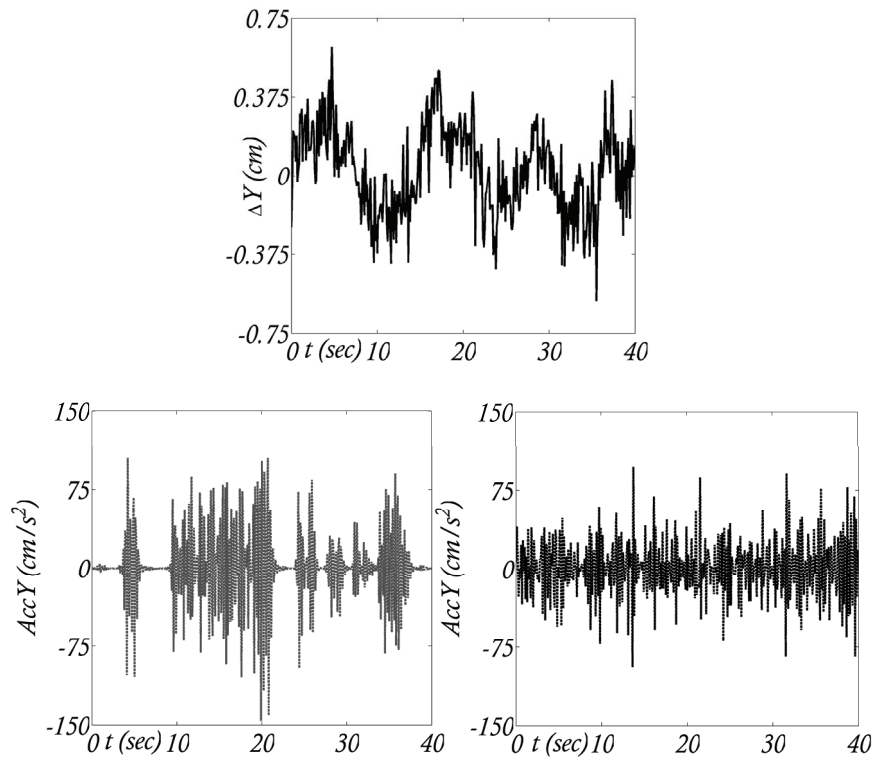


Figure 4.28. Y direction time histories for #May09 tests. Top: GPS “c” displacements. Bottom: tri-axial accelerometer accelerations (left), GPS “c” derived accelerations (right)

Comparing the time series of the above plots, it can be seen that they agree each with the other, revealing that the GPS a small level of noise than two one showed in Figures 4.25 and 4.26, as indicated from the Power Spectral Density (PSD) analysis in Figure 4.29. The noise reduction can be a consequence of the reduction on the sampling rate that was 10Hz in #May09 tests, while it was 20Hz in #Mar08 tests.

Due to the different sampling rate the frequencies at 6 and 8Hz of the #Mar08 tests PSD cannot be detected in the #May09 tests PSD, where a clearer 4Hz peak frequency is shown (see Figure 4.29).

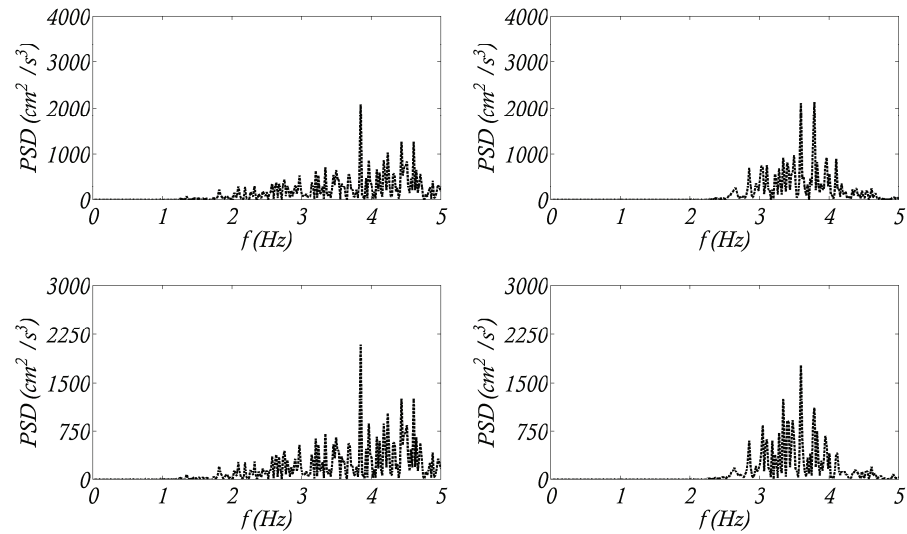


Figure 4.29. PSD functions from the measurements along axes X (top) and Y (bottom). GPS “c” estimated acceleration (left), accelerometer measured accelerations (right)

Furthermore, some other explanations need to be added due to the significant differences evidenced when comparing the plots of #Mar08 and #May09 in terms of displacements and accelerations amplitude.

These differences can be explained by taking into account the environmental condition during the two tests campaigns and their purposes. The #Mar08 tests were conceived to compare GPS and accelerometers records for repetitive impact movements of the bridge crane near the two GPS rover receivers “b” and “c”. In #May09 the purpose was to verify if decreasing the sampling rate a clearer peak in the frequency domain can be identified. During #May09 tests the impact bridge crane movements were realized on the opposite side of the rover receiver. This could explain the reduction of the displacements amplitude with respect to #Mar08 tests, while the increasing in the acceleration values could be imputed to continuous vibrations imposed by the bridge-crane to the structure just before starting to record the data.

4.3.3 Structural identification for impact and deceleration force

In this section the structural identification process via parameters calibration and its validation procedure are explained.

The purpose is to identify the structure and to analyze the way the GPS data have to be processed in the identification scheme.

Attention is mainly paid to the longitudinal movements of the bridge-crane which induce significant vibrations in the steel structure.

Two main operations are considered:

(a) the bridge-crane moves at a constant speed of 0.7m/s and is stopped along its way introducing a constant deceleration force F_d of amplitude 10.93KN for a duration of 0.7sec;

(b) the bridge-crane impact at its end introducing an impact force F_i .

While the bridge-crane is moving along the longitudinal direction, the GPS devices on the roof record the consequent oscillations. The Y direction displacements, as calculated from the recorded by GPS unit “ c ” data, are then compared with the results achieved by the FE model numerical simulation.

The structural identification procedure pursues the model calibration by comparing the experimental response to the bridge-crane deceleration force with the results of numerical models with different base constraints.

When the experimental and the numerical results match each the other, the achieved structural model has to be validated for the internal impact force.

A 3D frame FE model of the steel building (Figure 4.30) is realized within the Ansys Software (Ansys, 2005) in order to meet two items:

- (i) to identify the mode shapes and the natural frequencies of the structure;
- (ii) to simulate the bridge-crane movements and to detect the nodal displacements to be compared with the GPS experimental data.

- The main FE types considered in the model are as follows (see Figure 4.31):
- the steel columns (European HEA 280), the perimeter horizontal beam (European IPE 100) and the purlin roof (European IPE 140) are modelled by BEAM44 element;
 - the upper chords, bottom chords, verticals and diagonals elements (European Double L sections) which constituted the 2D Pratt truss are modelled with TRUSS8 element;
 - the perimeter longitudinal wind-braces (European Double L section) and for roof horizontal wind-braces (European Double T section) are also modelled with TRUSS8 element;
 - the concrete first and second floor slabs are represented by SHELL43 element.

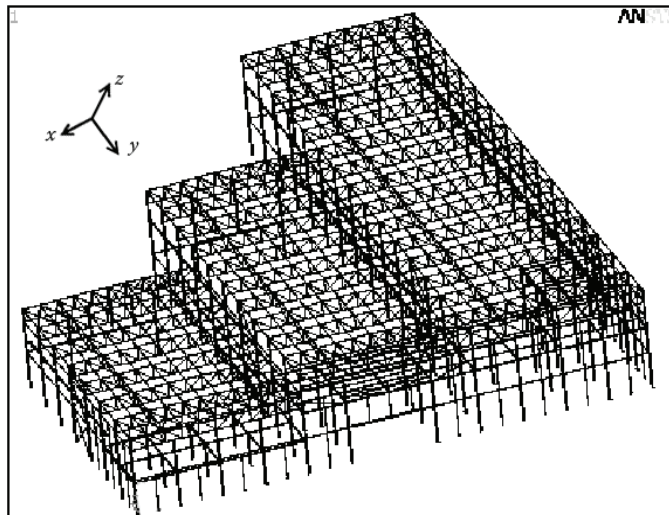


Figure 4.30. 3D view of the FE model

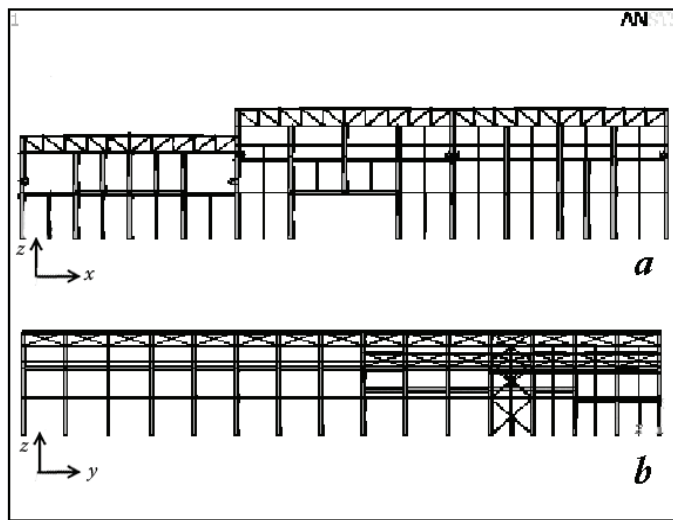


Figure 4.31. Frontal view (a) and lateral view (b) of the FE model

The model calibration is carried out by considering the case of the bridge-crane stopping along its rails. This case is represented in the FE environment by analyzing, through a dynamic analysis, the response of the structure subjected to a deceleration force F_d (of 10.93KN) induced by the bridge-crane, when the along beam motion is suddenly stopped. In the FE model the action is reproduced considering the bridge-crane as a mass M (sum of the crane trolley and crane bridge) of 10145 Kg, moving at a constant speed of 0.7m/s, stopped in 0.7s.

The main effort in the iterative numerical calibration process (to match the experimental results) is carried out by considering the base constrains as the uncertainty of the model to be reduced. By approaching in this way different base constrains conditions have been studied until an agreement with the experimental data is reached (see Figure 4.32).

In particular, looking at the columns sustaining the bridge-crane, starting from a condition of fixed support, the final solution was elaborated by considering free all the base rotational degrees of freedom and maintaining fixed the along X and along Z movements. This lead to consider the base nodes

of the sustaining bridge-crane columns free to move along the bridge-crane axis of motion (Y) and to rotate around the X, Y and Z axes.

Figure 4.32 reports the initial constrains model configuration (on the left) and the final calibrated one (on the right), with the arrows indicating the translational degrees of freedom.

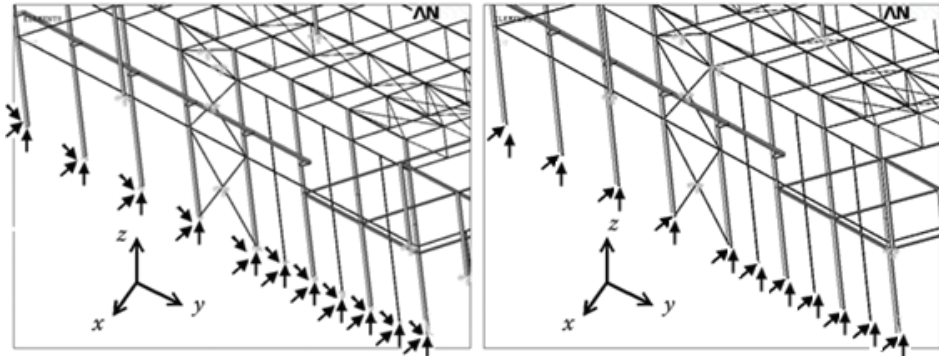


Figure 4.32. Particular of the constrains of the columns supporting the bridge-crane: fixed supports condition (left); calibrated model constraints condition (right)

What is graphically showed in Figure 4.32, can be also expressed in terms of the FE global equation formulation. The meaning is to show how the calibration procedure leads to introduce non zero terms into the column vector u representing all the nodes displacements.

Let's write the global FE system equation:

$$Ku = F \quad \text{with} \quad \begin{bmatrix} k_{11} & k_{12} & \dots & k_{1n} \\ k_{21} & k_{22} & \dots & k_{2n} \\ \dots & \dots & \dots & \dots \\ k_{n1} & k_{n2} & \dots & k_{nn} \end{bmatrix} \begin{bmatrix} u_1 \\ u_2 \\ \dots \\ u_n \end{bmatrix} = \begin{bmatrix} F_1 \\ F_2 \\ \dots \\ F_n \end{bmatrix} \quad (4.3)$$

the vector u , which corresponds to the vector of all the displacements at all the nodes, can be separated into two components: the really unknowns displacements u^* and the imposed (known) degrees of freedom u' :

$$u = u^* + u' \quad (4.4)$$

By this formulation the vector of the unknowns u^* is separated from the vector of the imposed nodes restraints u' , which is modified during the calibration process.

Supposing that the vector u' contains, among the others, the translational and the rotational degrees of freedom of the base nodes columns sustaining the bridge-crane and supposing to consider a single node, the part of the transposed vector u' related to this node degrees of freedom can be written as follow:

$$\left(u'_{node}\right)^T = \left[u_x \quad u_y \quad u_z \quad \theta_x \quad \theta_y \quad \theta_z \right] \quad (4.5)$$

By applying the boundary conditions, the global stiffness matrix K is reduced in size deleting rows and columns associated to the constrained nodes (which refers to the vector u').

Equation (4.6) reports the part of the transposed vector u' when the boundary condition applied to the base nodes is the one of fixed support:

$$\left(u'_{node}\right)^T = \left[u_x = 0 \quad u_y = 0 \quad u_z = 0 \quad \theta_x = 0 \quad \theta_y = 0 \quad \theta_z = 0 \right] \quad (4.6)$$

In Equation (4.6) the cells to of the K matrix associated to these zero values degrees of freedom are removed.

Equation (4.6) can be rearranging by applying as boundary condition that derived by the calibration of the FE model where the base nodes are, as previously mentioned, free to move along the Y axis and to rotate around the X, Y and Z axes.

$$\left(u'_{node}\right)^T = \left[u_x = 0 \quad u_y \quad u_z = 0 \quad \theta_x \quad \theta_y \quad \theta_z \right] \quad (4.7)$$

In Equation (4.7) only the cells of K associated to the $u_x = u_z = 0$ condition are deleted.

Once, iteratively, the calibration procedure reaches a condition where the experimental and the numerical results match one with the other, a modal analysis is then conceived to detect the mode shapes and the modal frequencies of the structure (see Figure 4.33).

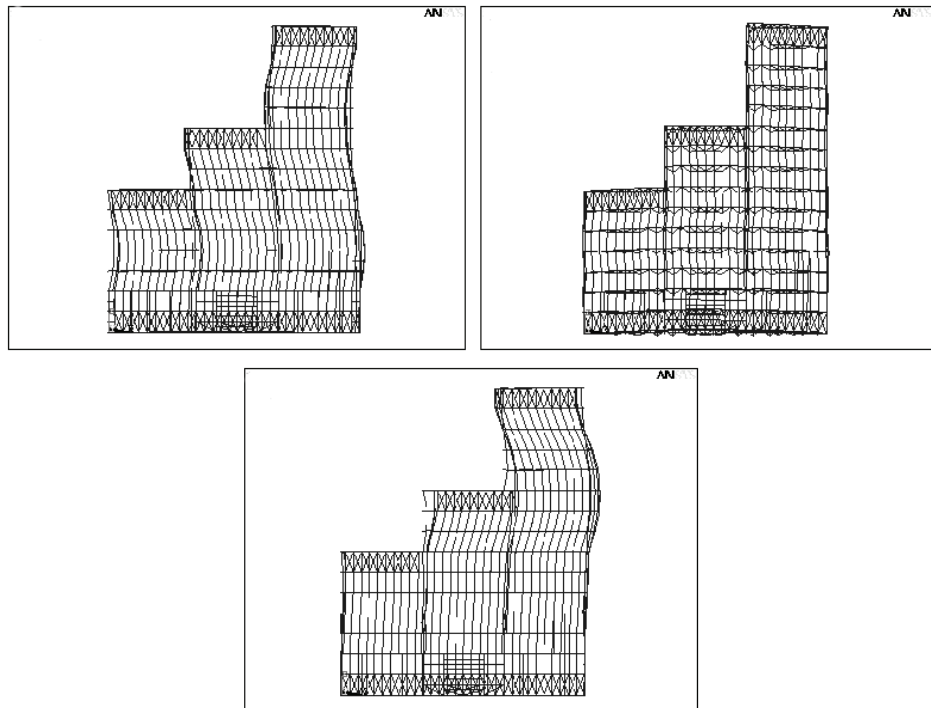


Figure 4.33. Top: 1st mode shape (left) and 2nd mode shape (right). Bottom: 3th mode shape

The purpose here is not to match the dynamic parameters (frequencies, damping and modes shapes) experimentally detected by the GPS, but to build a

FE model which can be accurate in a such a way to remove any uncertainties deriving from the numerical results.

This leads to understand, when comparing them with the experimental data, which could be the real GPS accuracy. The numerical results can in fact furnish a measurements of how the uncertainties of GPS data may influence the predictable response displacements of the building.

The numerical results are then used to in comparison with the experimental ones in assessing the structural response due to bridge-crane actions.

The comparison of the experimental and numerical displacements resulting from the response to the bridge-crane movements inducing a deceleration force F_d is depicted in Figure 4.34. It shows the experimental time history displacement recorded by the GPS receiver “c” and the numerically simulated displacement time history in the same position. The shape and the trend of the numerical results are similar to the experimental ones (also in peak value) and suggest that a good agreement has been reached for the calibration process for one single bridge-crane deceleration action.

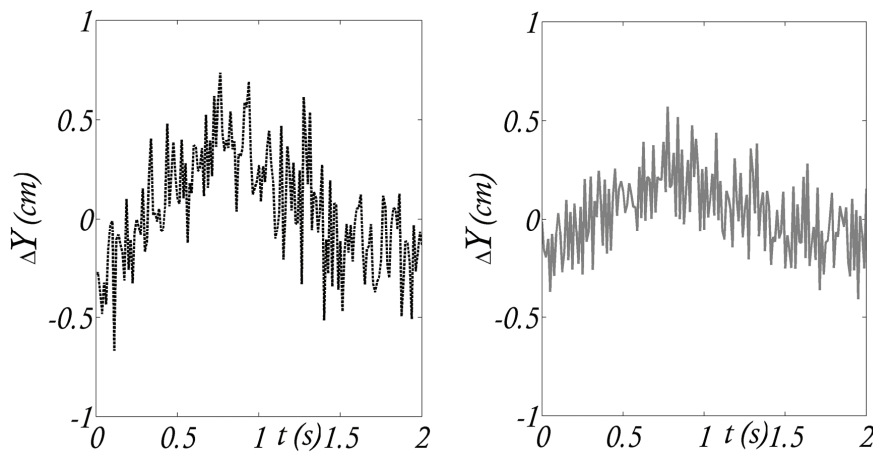


Figure 4.34. Deceleration force: experimental results from GPS receiver “c” data (left), numerical results (right)

In addition, a further dynamic analysis is carried out to study the behaviour of the structure subjected to repetitive decelerations of the bridge-crane. The numerical solution is calculated by reproducing the condition of the bridge-crane consecutively accelerated and decelerated, inducing each time an acceleration force F_a and a deceleration force F_d (Figure 4.35).

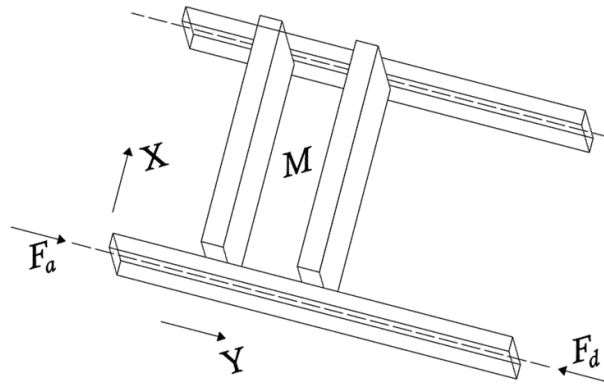


Figure 4.35. Scheme of bridge-crane forces during vibration tests

In the FE model these actions are reproduced considering the bridge-crane as a mass of 10145Kg, which accelerate with a constant acceleration of 0.49m/s^2 , moving at a constant speed of 0.7m/s and then stopping in 0.7s . In this way the acceleration-deceleration motions is reproduced.

Figure 4.36 shows the experimental time history displacement recorded by the GPS receiver “c” and the numerically simulated displacement time history in the same position.

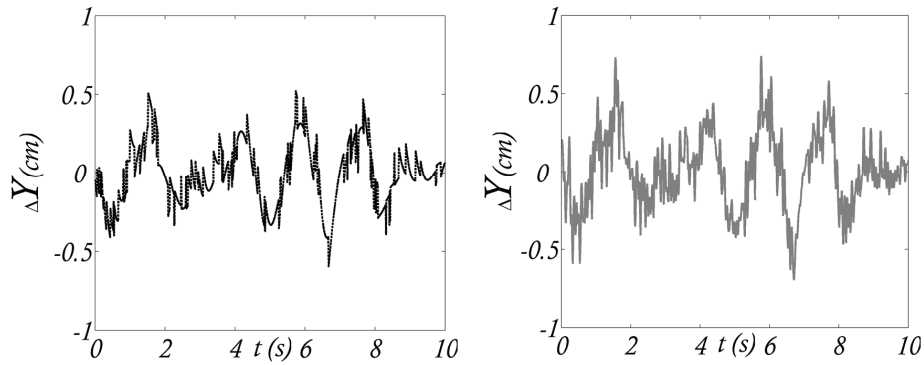


Figure 4.36. Deceleration-acceleration force: experimental results from GPS receiver “c” data (left), numerical results (right)

Also in this case a strong agreement is showed between numerical and experimental results, indicating that the way followed in the calibration of the model was correct.

Once the experimental and numerical results agree each with the other in the comparison of response displacements induced by the bridge-crane acceleration and deceleration force, the validation of the structural model is made by considering as input action the impact force F_i produced when the bridge-crane impacts at its end.

The force is simulated in the FE environment as an application of the impulse theorem as presented below:

$$I = mv_f - mv_i = \int_{t_i}^{t_f} F_i(t) dt \Rightarrow \begin{array}{l} \text{for a given} \\ \text{pulse shape} \end{array} \Rightarrow F_i(\max) \quad (4.8)$$

Iteratively, after different attempts the impact force is calculated as it is plotted in Figure 4.37.

Note that a white noise signal is added before and after the application of the impact force simulating the bridge-crane movements along its beam way.

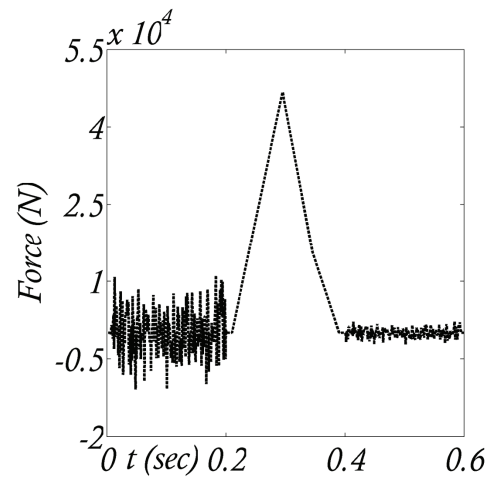


Figure 4.37. Fe model input impact force, as calculated

The resulting impact force produces displacements which are about three times greater than those induced by the deceleration force.

Figure 4.38 shows the experimental and numerical displacements time histories referred to the node where the GPS unit receiver “c” is placed.

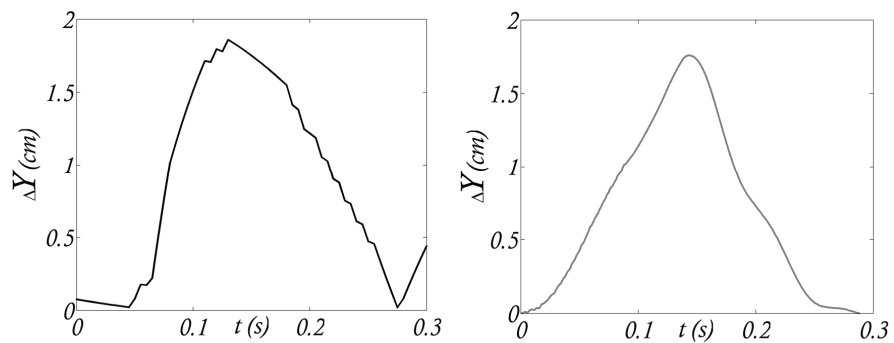


Figure 4.38. Impact force: experimental results from GPS receiver “c” (left), numerical results (right)

Looking at Figure 4.38 a good agreement is observed between experimental and numerical results, suggesting the goodness of how the input force is calibrated and applied. The shapes of the two graphs are similar even if the a more wide time interval seems to be covered by the experimental results at the moment of the impact (i.e., the peak area of the graphs from 0.1 to 0.2s) if compared with the numerical ones.

4.4 Conclusions

The results of a structural monitoring campaign have been presented in this chapter. The steel building which hosts the authors' laboratory is chosen as the case-study.

The effectiveness of the GPS solution is proved by relating to dynamic actions which induced structural response oscillation. Natural (i.e., wind actions) and man made (i.e., internal bridge crane movements) dynamic actions are considered.

They represents both (a) long duration actions (the wind events) and (b) short duration actions (the bridge crane impulse forces). The (a) type of actions is useful to excite mainly low frequencies (0-1Hz), while (b) forces mainly induce significant displacements amplitude (5-20mm) at relatively (for the structure) high frequencies (2-4Hz).

The data collected by GPS units when the bridge-crane is moving along its rail, inducing acceleration and deceleration force to the structure, are compared with those recorded by tri-axial accelerometers close to the GPS rover antenna.

The comparison is also made for different GPS units locations on the roof of the building, to detect the influence on the measurements accuracy of any geometric signal dilution of precision (GDOP) and of the baseline connection orientation.

In the last section of the chapter, a comparison of the results from a numerical simulation of the FE model of the building, with the elaborations of the GPS position readings is presented. The agreement reached between numerical and experimental data reflects the effectiveness and the feasibility of the GSP solution.

Chapter 5

FULL SCALE GPS-BASED SHM OF A SUPER TALL TOWER

Introduction

The use of GPS in the full-scale monitoring system of the Guangzhou New TV Tower (GNTVT) in China is discussed in this chapter. Attention is mainly focused on the ability of GPS to detect rotational movements of the tower induced by strong wind events, such as typhoons, which are very common in that area.

This chapter reports some measurements acquired by GPS receivers and accelerometers which are analyzed and processed aiming at proving their ability in detecting the response (i.e., in plane displacements, in-plane rotations) of tall flexible structures when subjected to wind actions. Tall buildings are in fact most likely to experience oscillations produced mainly by strong wind events.

Wind forces induce displacement responses in the structure in its both longitudinal and transversal directions, consequently, such two directional in plane forces induce also torsional responses, which are mostly more complex to be detected during full-scale experimental tests. Previous arrangement of

sensors topology (i.e., sensors combinations and locations) is quite important; they should be distributed on an upper level of the structure in such a way to provide measurements from which torsion could be calculated. A network of GPS receivers, installed on the top of a tall building is presented in this chapter, and its ability to provide sufficient accuracy in detecting the induced torsional effects is investigated.

The movements of the GNTVT were acquired by means of both GPS units and accelerometer sensors placed on the upper part of the construction. The way to process the displacement data, as recorded and elaborated from the acquired signals is reported.

Analyzed data were obtained considering the need to study the torsional behavior of the tower under different conditions; therefore two main scenarios are analyzed:

(i) processing of data recorded under two events of strong wind, namely the Nuri typhoon event in August 2008 (#Nur08) and the Hagupit typhoon event in September 2008 (#Hag08);

(ii) processing of data recorded in the absence of any significant wind events, as it occurred in March 2009 (#Mar09 tests).

In both cases, the contribution of both GPS and accelerometers acquired data is considered in quantifying the angle of rotation of the in-plane upper section, where the sensors are placed and, hence, to detect the torsional movements of the tower.

5.1 Experimental configuration of the GNTVT

The Guangzhou New TV Tower (GNTVT), which has been recently completed in Guangzhou- China, is a super-tall structure with the height of 610m (Ni et al., 2009). This tube-in-tube structure is made of a reinforced concrete inner tube and a steel outer tube constructed adopting concrete-filled-tube (CFT) columns style.

The outer tube consists of 24 CFT columns, uniformly spaced in an oval shape while inclined in the vertical direction. The oval section decreases with altitude from (50m by 80m) at ground level to the minimum dimensions of

(20.65m by 27.5m) at 280m height. Then it increases to (41m by 55m) at the top level of the tube (454m height). The columns are interconnected transversely by steel ring beams and bracings. The inner tube has an oval shape as well but of constant dimensions along the height (14m by 17m) as shown in Figure 5.1.

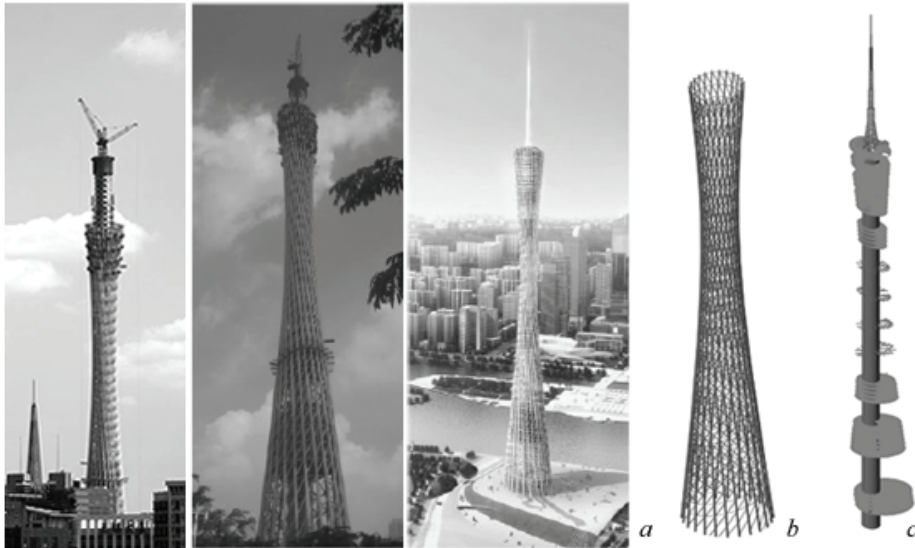


Figure 5.1. GNTVT: under construction and rendering view of the tower (a); external tube (b); interior tube, floors, connection girders and mast (c)

A Structural Health Monitoring (SHM) system consisting of over 600 sensors was designed and implemented by the Hong Kong Polytechnic University to GNTVT for both in-construction and in-service real-time monitoring.

For this purpose a SHM benchmark problem was conceived (Benchmark, 2008) by considering GNTVT as a test structure and using real measurement data. Within this context, cooperation with the Department of Civil Engineering at the Hong Kong Polytechnic University allowed the authors to get sets of data recorded by accelerometers and GPS units placed on the tower and to interact in the GPS sensors placement process. Attention is focused on the suitable topology (i.e., sensor combination and location) toward the characterization of

the torsional response of the structure when exposed to strong wind events, as typhoons, rather frequent in that geographic area (Alsaleh et al., 2009). The development of a methodology to process the acquired displacements is also addressed.

5.2 Data processing of records during Nuri and Hagupit typhoon events

During the Nuri typhoon on August 22, 2008, data were recorded on site by two GPS receivers and two accelerometers placed as shown in Figure 5.2.

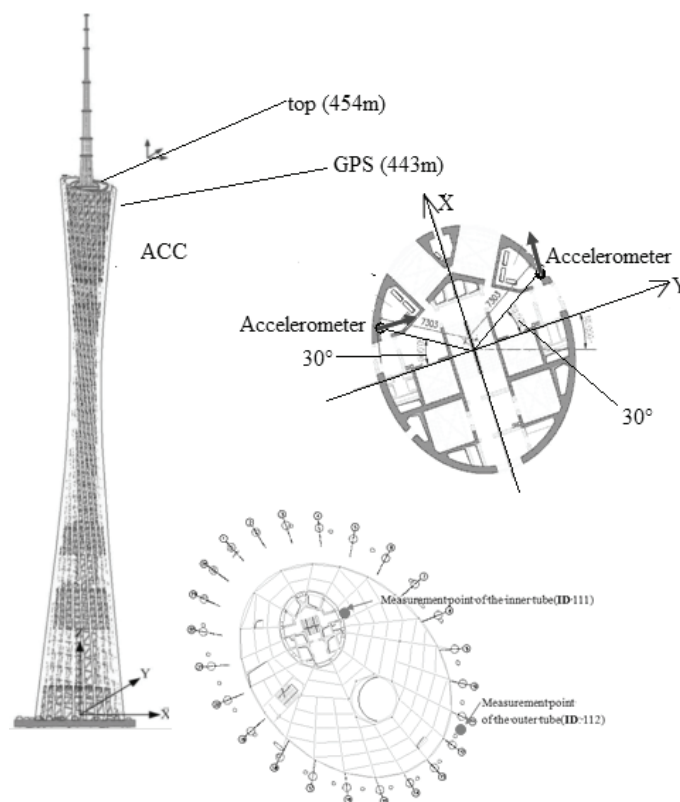


Figure 5.2 Location of the measurement points for both GPS and accelerometer sensors

The moving rover GPS unit was installed in the center of the oval concrete inner tube cross section, while the two accelerometers were placed at the edges of this section, one along the East-West direction and the second along the North-South direction; all were placed at 443m height level. The reference GPS receiver was placed at the ground level at a distance from the tower sufficient to prevent any multipath effects. This sensor was used to provide real time data correction within a Differential Global Positioning System (DGPS) to the moving receiver on the tower.

As plotted in Figure 5.2, the X and Y axes are respectively the directions along the long axis and the short axis of the inner tube oval cross section. Therefore the X -direction measurements obtained from the accelerometers correspond to the North coordinates of the GPS inner tube measuring point; while measurements in the Y -direction correspond to the East coordinates, as clarified in Figure 5.3.

Figure 5.3 shows how the outer tube steel section of the tower changes with altitude in both dimensions and orientation, while the inner tube concrete section (where the accelerometers and the rover GPS are installed) remains the same in both dimensions and orientation along the tower height.

Based on this geometry, the set of data obtained during the #Nur08 are used to assess the torsional angle of which the upper in-plane section of the tower is rotated.

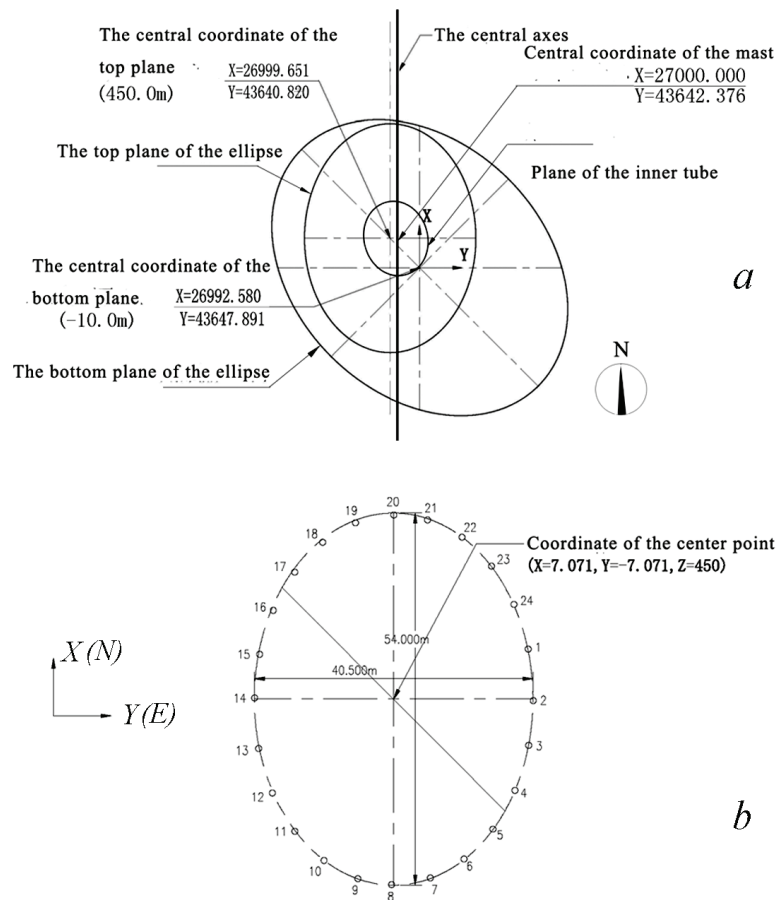


Figure 5.3. Geometrical representation of the oval shape changing in dimension and orientation of the GNTVT (a), zoomed view of the oval top section (b)

The GPS data for #Nur08 event have been recorded from 2 to 5 p.m. A segment of 40 minutes is extracted from this data and from those obtained by the accelerometers during the Nuri Typhoon, referring to the time interval from 2.10 and 2.50 p.m..

From the anemometer placed on the top of the structure, the measured maximum wind speed during the typhoon was 25.5m/s, while the wind direction was mostly North-Eastern (Ni et al., 2009).

The GPS sampling rate was 5 Hz, while the sampling rate of the two uniaxial accelerometers was 50 Hz.

The displacement records obtained by the GPS rover receiver are calculated with correspondence to the position of the receiver at the base of the tower, which is used as a fixed reference, in a differential global positioning mode (DGPS). This procedure enables to remove the measurement errors of the moving receiver, which may affect the precision of the torsional parameters calculation.

5.2.1 Data processing: torsional effects

As described in the previous section, the GNTVT consists of two oval section tubes. Therefore, in order to detect the torsional behavior of the tower using the in-situ experimental data, the governing relation of a cylindrical shaft with an oval cross-section must be preliminarily introduced.

For a given uniform torque M_t on a cylinder shaft (Figure 5.4), the twist angle γ can be calculated as a function of the angle of rotation φ through of the following equation:

$$\gamma = \frac{\varphi}{L} \times \sqrt{\frac{r_1^2 + r_2^2}{2}} \quad (5.1)$$

where r_1 and r_2 are the two radii of the oval cross section and L is the length of the cylinder.

In the considered case study the GPS receiver is placed at the center of the oval inner tube, and the two accelerometers are located at a distance r from the center, while the line drawn between these locations and the center is forming an angle θ , with the Y axis.

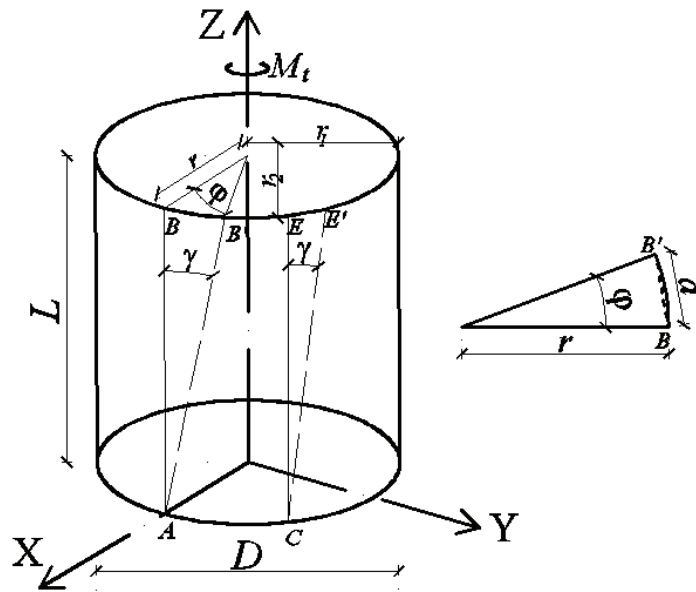


Figure 5.4. Torsion for shaft cylinder with elliptical section

The GPS receiver measures the displacements of the center of the cross-section in the two horizontal directions, with respect to its original position when the tower is at rest.

The locations of the accelerometers imply that their measurements can provide a combined displacement, resulting from the displacements in both directions and the rotation around the vertical axis of the tower.

The data collected from both the accelerometers at the far edges of the inner tube and the GPS receiver at the center of its section, shall allow the torsion detection of the tube.

The in-plane displacements, Δx and Δy , due to the pure rotation of the cross-section are simply calculated by subtracting the displacements obtained at the edges from the one simultaneously measured at the center, as follows:

$$\begin{aligned} \Delta x &= X_0 - X_p \\ \Delta y &= Y_0 - Y_p \end{aligned} \tag{5.2}$$

where X_0 and Y_0 are the displacements measured by the GPS receiver, and X_p and Y_p are the displacements calculated from the accelerometers in the corresponding directions.

As shown in Figure 5.5, the following geometrical relationships hold:

$$\begin{aligned} r \cdot \cos(\theta - \varphi) &= r \cdot \cos \theta + \Delta x \\ r \cdot \sin(\theta + \varphi) &= r \cdot \sin \theta + \Delta y \end{aligned} \quad (5.3)$$

By rearranging the two formulae of Equation (5.3), the angle of rotation, φ , can be calculated from either one of the two in-plane displacements:

$$\begin{aligned} \varphi &= \theta - \cos^{-1}\left(\cos \theta + \frac{\Delta x}{r}\right) \\ \varphi &= \sin^{-1}\left(\sin \theta + \frac{\Delta y}{r}\right) - \theta \end{aligned} \quad (5.4)$$

where r is the length of the lines drawn from the positions of the accelerometers to the center of the oval, and θ is the inclination angle of the same line with respect to the Y axis.

For the considered case-study, the values of r and θ are equal to 7303 mm and 30° , respectively, as specified in Figure 5.2.

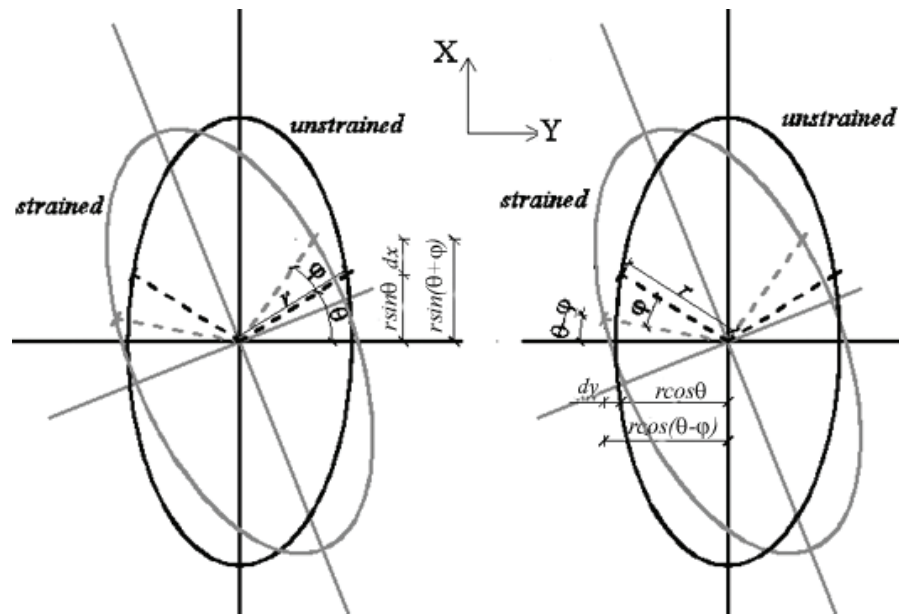


Figure 5.5. Torsional rotation of the inner tube oval section in the X - Y plane

The displacement time histories recorded by the sensors are drawn in Figures 5.6 and 5.7 for both the direction X and Y . The two graphs of Figure 5.6 refer to the displacements recorded by the GPS moving receiver; while the others two of Figure 5.7 refer to the displacements derived from the accelerations recorded by the two uni-axial accelerometers.

Since the GPS and the accelerometer signals are independently recorded, a suitable synchronization is strongly needed in order to perform a comparative analysis.

The time histories of the torsional response of the tower in terms of both the angle of rotation, φ , and the twist angle, γ , due to the event of the #Nur08 typhoon are plotted in Figures 5.8 and 5.9.

The maximum angle of rotation at the top of the GNTVT (i.e., at the height of 443m) is about 1.2° , which corresponds to a relatively low twist angle of about 0.1° . It is worth noting that using the GPS data of the rover sensor without removing the positioning errors elaborated from the measurements of the

reference unit, would have probably led to wrong values of φ and γ , which would not have been representative of the real ones (Faravelli et al., 2009).

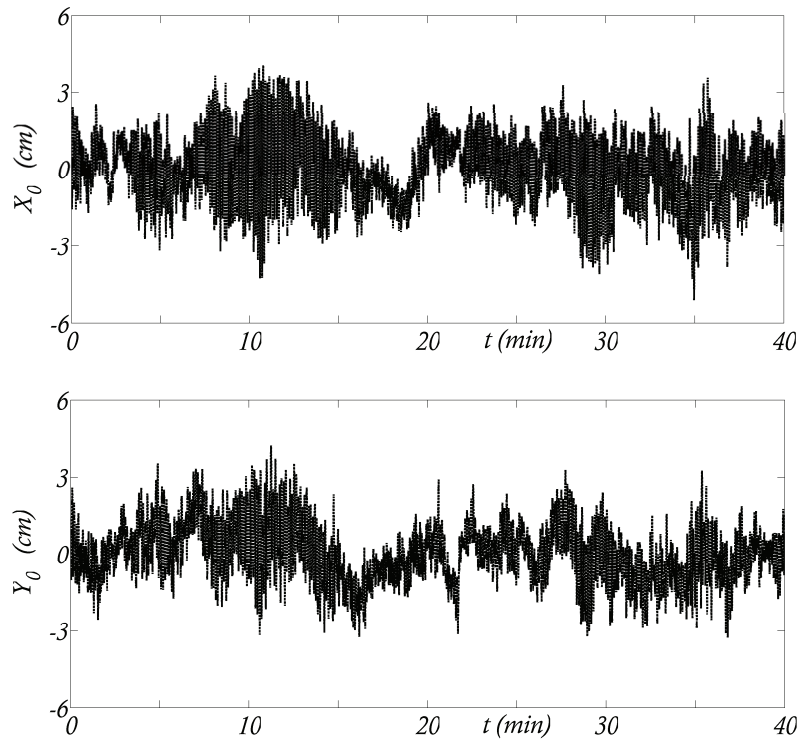


Figure 5.6. GPS in-plane displacement time histories during the #Nur08 event: along X measurements (top), along Y measurements (bottom)

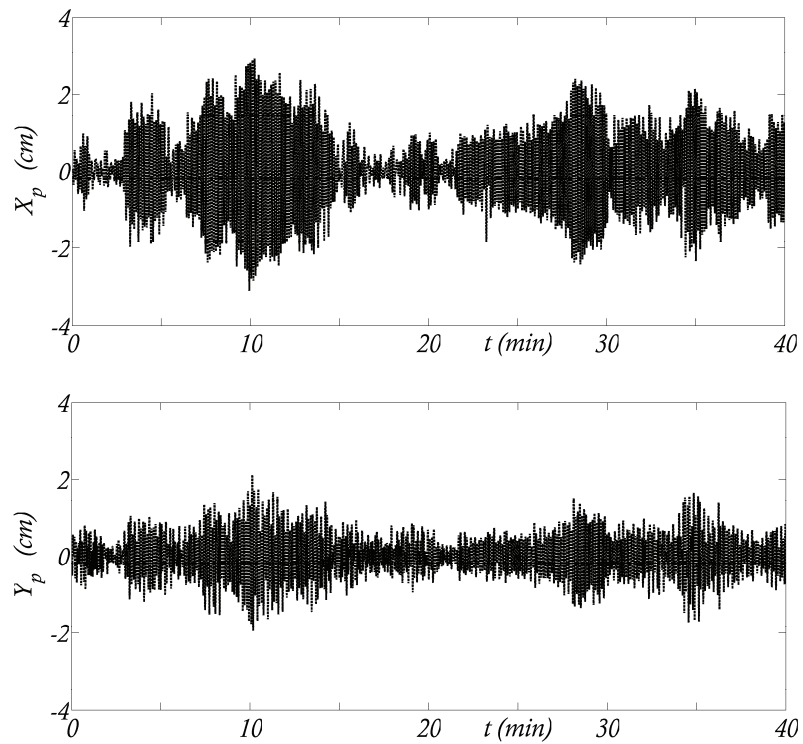


Figure 5.7. Accelerometers derived Displacements time histories elaborated from the accelerometer records collected during the #Nur08 event: along X measurements (top), along Y measurements (bottom)

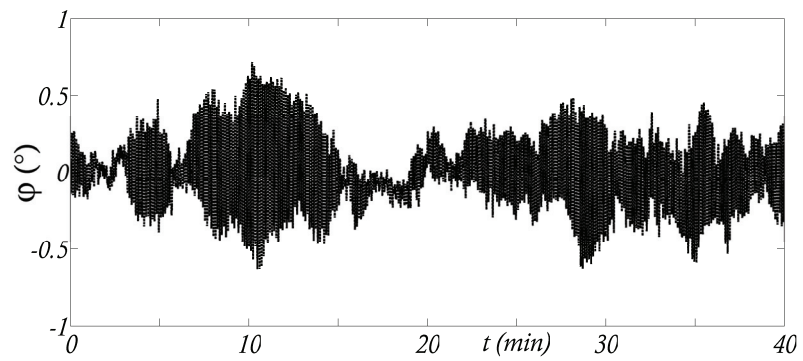


Figure 5.8. Time history angle of rotation ϕ during the #Nur08 event

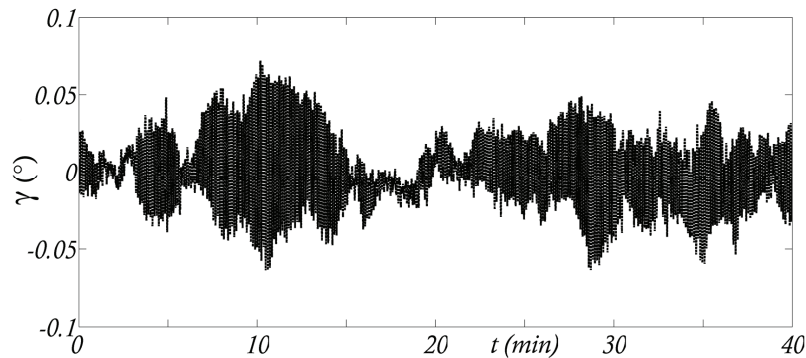


Figure 5.9. Time history of the twist angle γ during the #Nur08 event

To investigate the rule of sensors location in detecting the values of the angle of rotation, φ , its variation with the displacements derived from the accelerations recorded is plotted in Figure 5.10.

These graphs suggest that the variation of φ is more appreciable when related to the variation of the displacements along X direction, than along Y one. This could be simply due to that X direction corresponds to the longest axis of the inner tube oval cross-section.

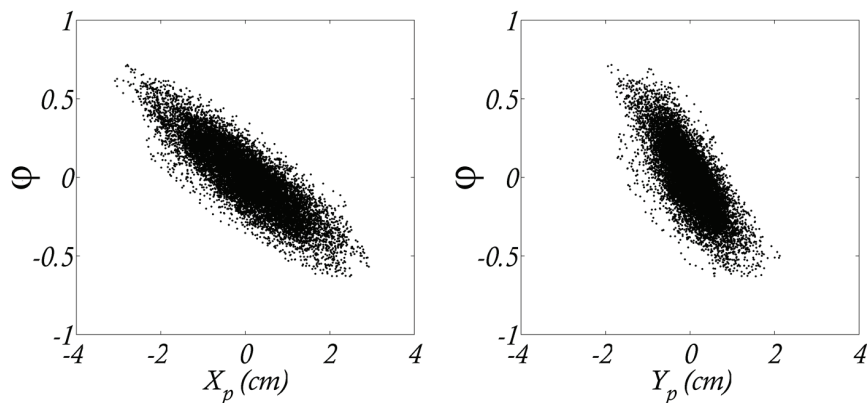


Figure 5.10. Variation of the angle of rotation φ with respect to the X (left) and Y (right) displacements derived from the accelerations measured by the accelerometers

To prove the effectiveness and the validity of the proposed procedure, the same calculation is then applied to data recorded during the Hagupit typhoon (#Hag08) on September 20, 2008. The sensors (i.e., accelerometers and GPS) locations on the inner tube are the same considered during the #Nur08 typhoon, only the height of the in construction tower was different (448m), which means only 5m more when the recording data was during the #Nur08.

The GPS data for #Hag08 event have been recorded from 1 to 5 p.m. A segment of 40 minutes is extracted from the data recorded by the GPS unit and by the accelerometers, precisely from 1.10 to 1.50 p.m..The displacement time histories recorded by the sensors are drawn in Figures 5.11 and 5.12 for both sensors in the two directions.

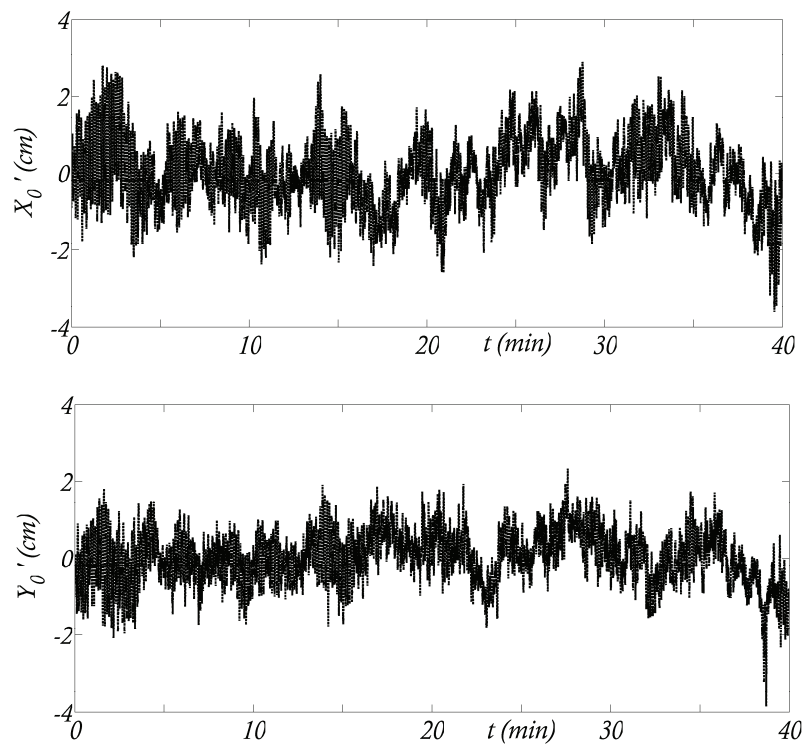


Figure 5.11. GPS in-plane displacement time histories during the #Hag08 event: along X measurements (top), along Y measurements (bottom)

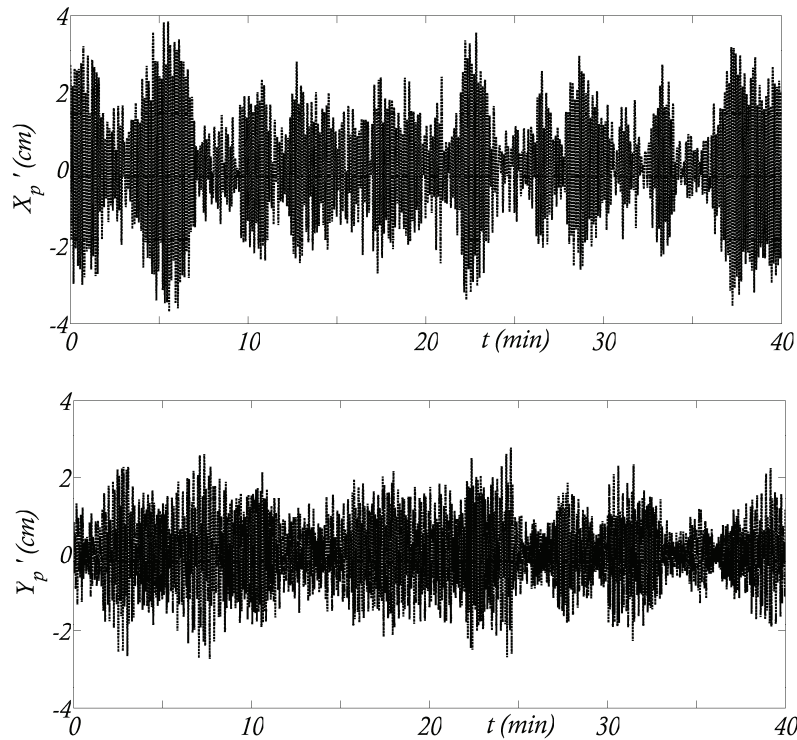


Figure 5.12. Accelerometers derived Displacements time histories elaborated from the accelerometer records collected during the #Hag08 event: along X measurements (top), along Y measurements (bottom)

The time histories of the torsional response of the tower in terms of both the angle of rotation, φ , and the twist angle, γ , due to the occurrence of the #Hag08 typhoon are plotted in Figures 5.13 and 5.14.

The maximum calculated angle of rotation at the top of the GNTVT (i.e., at the height of 448m) is about 1.4° corresponding to a twist angle of about 0.06° .

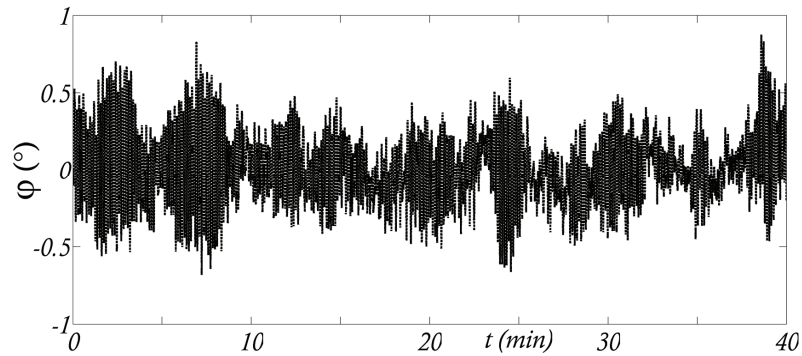


Figure 5.13. Time history angle of rotation ϕ during the #Hag08 event

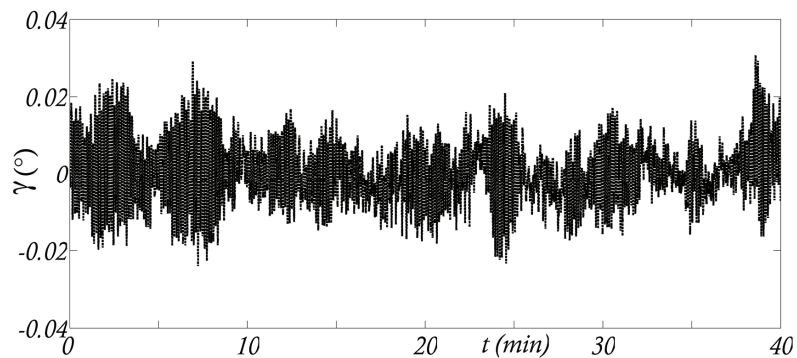


Figure 5.14. Time history of the twist angle γ during the #Hag08 event

Those values calculated from the data during the #Hag08 typhoon are in agreement with the ones obtained for the #Nur08 typhoon. Since the two wind events were having the same directions, the maximum measured speed was almost the same and the tower height was not so significantly increased (443m for the #Nur08 and 448m for the #Hag08), it derives that the values of the torsional parameters have to be almost equal.

Comparing the two groups of figures (Figures 5.13 and 5.14 and Figures 5.8 and 5.9) it could be seen that they are in good agreement, thus proving the effectiveness of the proposed calculation.

5.3 Data processing in the absence of a significant wind event

When #Nur08 and #Hag08 typhoons occurred only one GPS receiver was installed at the same height of the accelerometers (in the center of the oval cross section), while a reference one was fixed near the base of the tower. It is clear that having only one moving GPS receiver placed on the top section and located at the center of this cross section does not allow any detection of torsional movements. This is the reason of adding two uni-axial accelerometers placed at the edge of this cross section. However, in this way, the data processing during #Nur08 and #Hag08 indirectly involved all the drawbacks (the time synchronization among the others) of integrating information obtained by two kinds of devices.

Based on these considerations, a suitable configuration of GPS sensors was conceived and realized.

On March 19, 2009 (in the following #Mar09) three GPS rover receivers have been placed at the top of the tower at the current level of construction which was 450m height.

Since no strong wind events happened during the months after the installation, the data obtained were considered significant even if the tower was undergoing small oscillations produced by ambient vibrations (Casciati et al., 2009).

The #Mar09 data allow getting information on a pseudo-initial configuration in such a way that a reference configuration is identified for the torsional response of the structure.

Figure 5.15 shows the location of the base reference GPS receiver at the bottom of the tower, and of the three GPS rovers placed on the top level of the tower: two at the edges and one in the center of the section.

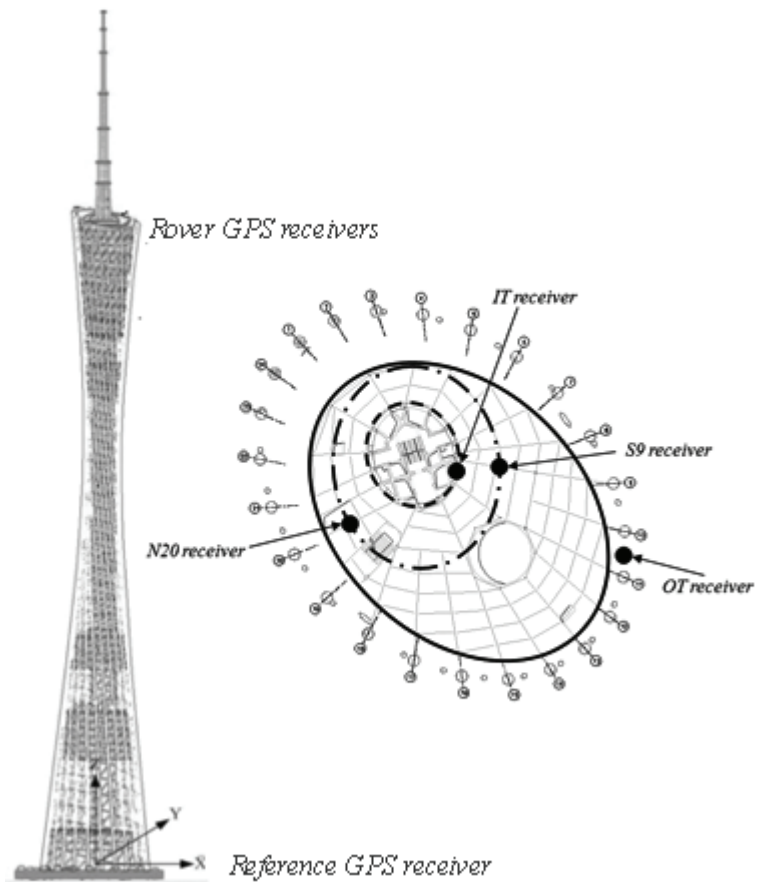


Figure 5.15. Location of the measurement points for GPS sensors (vertical and plan view)

The three top sensors of Figure 5.11 are respectively named as North20# (N20), South9# (S9) and Inner tube (IT). They are depicted in Figure 5.16 together with the reference one.

The three receivers record, at a sampling rate of 5 Hz, the North, East and vertical coordinates of the point where they are placed. The sampling rate, even if very low, is consistent with the requirement of the monitoring solutions for the tower. In fact from GPS and accelerometers data provided during ambient vibrations it can be shown that at least ten natural frequencies can be detected in

the range between 0 and 2.5Hz (i.e., the GPS Nyquist frequency), with the first natural frequency being of 0.11Hz (Ni et al., 2009). An ongoing work on the structural identification of the GNTVT from experimental data is confirming what here claimed in terms of natural frequencies of the tower detected by GPS.

A correspondence between coordinates and Cartesian axis is considered assuming that the North GPS coordinates correspond to the X -direction measurements, while the East GPS coordinates to the Y -direction. This is the same correlation adopted for the measurements taken by the two accelerometers during the #Nur08 and the #Hag08 typhoons.

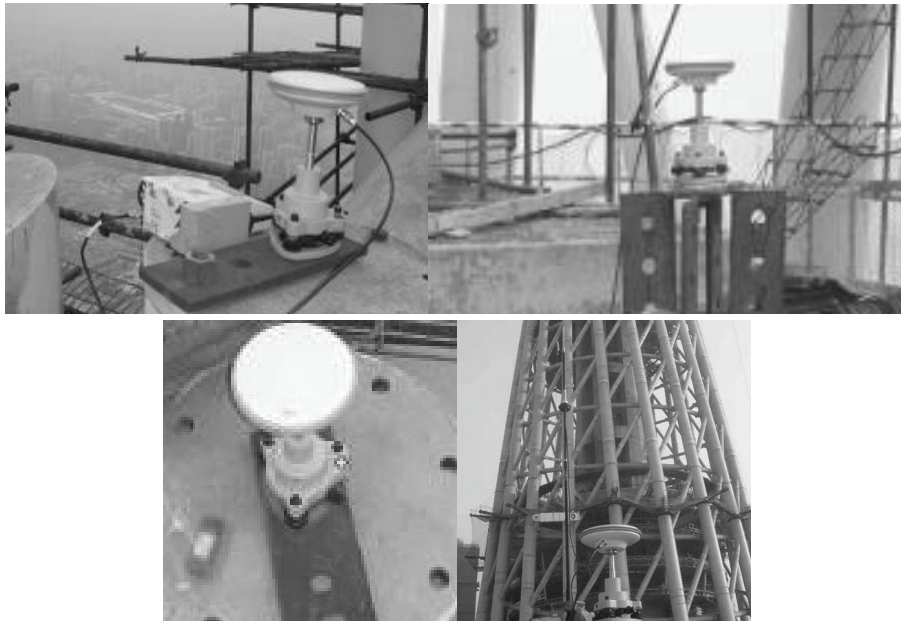


Figure 5.16. From top to bottom and form left to right: IT receiver, N20 receiver, S9 receiver and OT receiver

Before proceeding in the calculation of the torsional parameters, some observations should be highlighted if one would try to compare GPS measurements with data recorded by other sensors. In this specific case the comparison should be made between measurements taken by accelerometers

sensors during wind events with data recorded by GPS sensors in absence of a significant wind event.

The remarks are as follows:

(i) the previous set of accelerometers data during #Nur08 event were recorded in a time interval from 2 to 5 p.m., while during #Hag08 from 1 to 5 p.m..

(ii) the #Mar09 GPS data were recorded from 9 to 12 a.m, i.e., the GPS data, which are being compared with those recorded by the accelerometers, are not recorded at the same hours of the day.

(iii) the GPS accuracy, among the other, is influenced by the geometrical configuration of satellites overhead, which repeats itself every 24 hours (see Chapter 1);

(iv) the satellite configuration is strictly correlated to the GPS in-plane accuracy;

(v) taking the same time interval leads to neglect the errors in the GPS positioning which depend on the so called “geometric dilution of precision” (GDOP, see Chapter 3).

Based on these considerations, if one wants to compared sensors data (i.e., accelerometers in this case) with GPS data, the comparison has to refer to the same time interval during the day.

In the following a procedure is explained to manage the GPS data in the case they are not recorded during the same day hours of the data one wants to compare to. The case of simulating GPS measurements during the same time interval of the measurements taken during #Nur08 event is considered.

The procedure is based on the assumption that the standard deviation of GPS data recorded at two different time interval during a day is directly connected to the GDOP of the signal by the following relation:

$$\sigma^*(\rho_i^j) / \sigma'(\rho_i^j) = f_{GDOP} \quad (5.5)$$

where:

f_{GDOP} is a GDOP index;

$\sigma^*(\rho_i^j)$ represents the standard deviation of the pseudo-range measurements (i.e., the calculated distances between satellites and receivers) at a certain time interval during the sidereal day t^* ;

$\sigma'(\rho_i^j)$ represents the standard deviation of the pseudo-range measurements at a certain time interval during the day t' .

The requirement of having a GPS data record at the same time interval of the accelerometers data during the #Nur08 typhoon is satisfied by the IT sensor which data were recorded also from 2 to 5 p.m.. By calculating the standard deviation of the IT data from 2 to 5 p.m. and comparing it with the standard deviation of the IT data recorded from 9 to 12 a.m., it is shown that the two values are not exactly coincident and that their ratio defines the GDOP of the GPS signal for the two chosen time intervals.

This is demonstrated in Figure 5.17 where for the IT GPS receiver, the East and North component of the two measurements periods are plotted. The ellipse having as radius the two values of root mean square is also drawn. From the two graphs of Figure 5.17 a small but existing difference is evidenced.

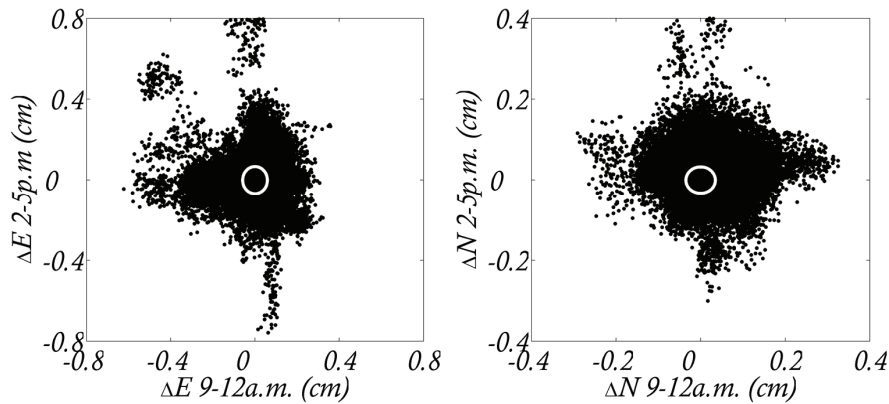


Figure 5.17. East and North comparison of two IT GPS data records

Starting from this point, the GDOP index from the 9-12a.m. measurements to the 2-5p.m. measurements for the IT GPS is calculated, and then this factor (for East component equal to 0.87 and for North component equal to 1.06) is applied also to the displacements of the N20 and N9 receivers, simulating in this way that their data would have been recorded from 2 to 5p.m. (i.e., the same time interval of the measurements taken during #Nur08 event). The factor of conversion is so seen, as previously mentioned, as the ratio of the rms values of IT recorded data between the IT 2-5p.m. data and the IT 9-12a.m. data (i.e., the GDOP index of Equation (5.5)).

By the assumptions above described the GPS data can then be compared with accelerometers data in detecting the torsional behavior of the tower.

The calculation of the torsional parameters, applied for the structural configuration unstrained by wind effects, is similar to that adopted for #Nur08 and #Hag08 typhoons. The difference is due to the change of sensors placed at the edges: two uni-axial accelerometers in the #Nur08 and #Hag08 measurements, and two GPS receivers in the #Mar09 tests. The displacements of the edge points are now the ones directly recorded by the GPS sensors instead being calculated from the accelerations recorded by the two accelerometers..

From the previous considerations derive that, in the case of #Mar09 tests, the displacements along North and along East, which are needed in the calculation of the torsional parameters, are recorded directly by the GPS sensors without requiring any integration process as happened for the recorded accelerations in the #Nur08 tests. The obvious consequence is to reduce the uncertainties in the measurements and to allow to concentrate in the analysis of which resolution can the GPS guarantee, without being the GPS accuracy corrupted by any error due to the calculation process.

The in-plane displacements, Δx and Δy , due to the pure rotation of the cross-section are simply calculated, in the same way of #Nur08 event, by subtracting the displacements obtained at the edges from the one simultaneously measured at the center, which is assumed to be the position of the inner tube receiver, as exposed in Equation (5.2), where X_0 and Y_0 are the displacements measured at

the center of rotation (i.e., IT), and X_p and Y_p are the displacements measured at the edges by S9 and N20 receiver (instead of the two accelerometers as done for the #Nur08 tests).

The angle of rotation, φ , can be calculated from either the in-plane displacements, by adopting the formula of Equation (5.4), where r is the length of the lines drawn from the positions of the edge GPS sensors to the center of the oval, and θ is the inclination angle of the same line with respect to the X axis as showed in Figure 5.18 which represents the GPS location on the outer-steel tube of the tower at the height of 450m. At this height the outer-tube section has the same oval shape of the inner-tube section, having only bigger dimensions. It is plotted horizontally just to give a better understanding of the sensors location.

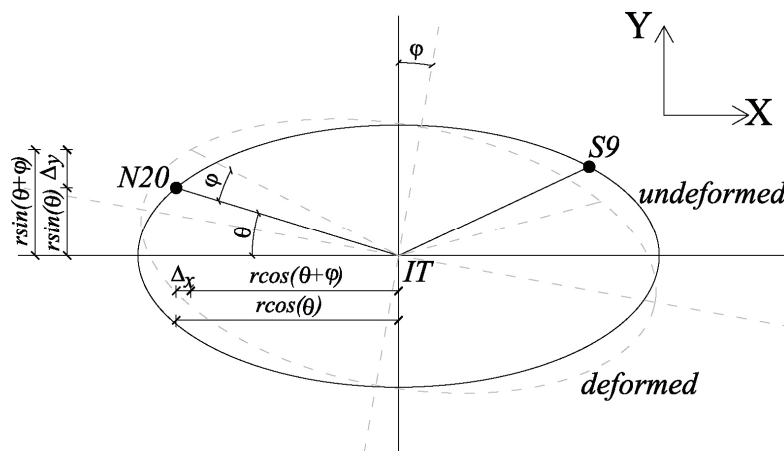


Figure 5.18. Sketch of the torsional rotation of the top in-plane elliptical section

To calculate the torsional parameters of the tower for #Mar09 experiments, a segment of 10 minutes is taken from the data recorded by each of the three GPS units from 9.00 to 9.10 a.m., and recalibrated (through the factors of conversion) as they are referring to a record from 2.00 to 2.10 p.m.. To clarify the differences between the data as recorded and the data estimated by the factors of conversion, in the plots both cases are shown.

The displacements time histories of N20 are drawn in Figure 5.19 (without the applications of the factors of conversion) and in Figure 5.20 (with the application of the factors of conversion). In each of two figures, the top plot represents the East component and the bottom plot the North one (i.e., Y and X directions respectively).

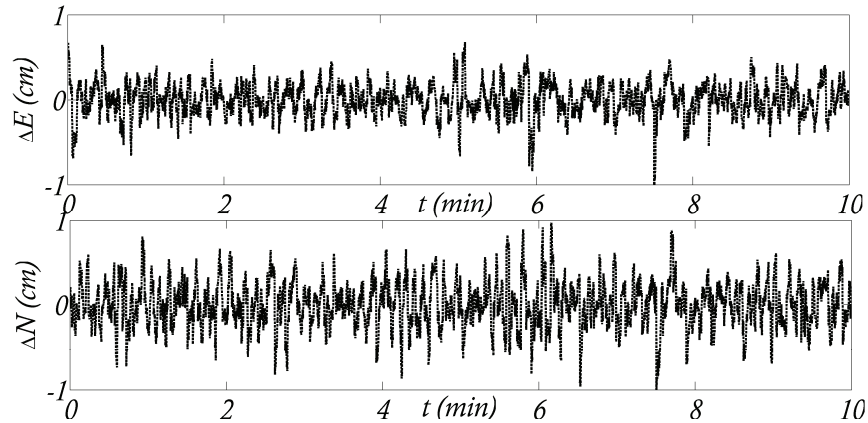


Figure 5.19. N20 GPS in-plane displacement time histories for ambient vibrations as recorded: along Y measurements (top), along X measurements (bottom)

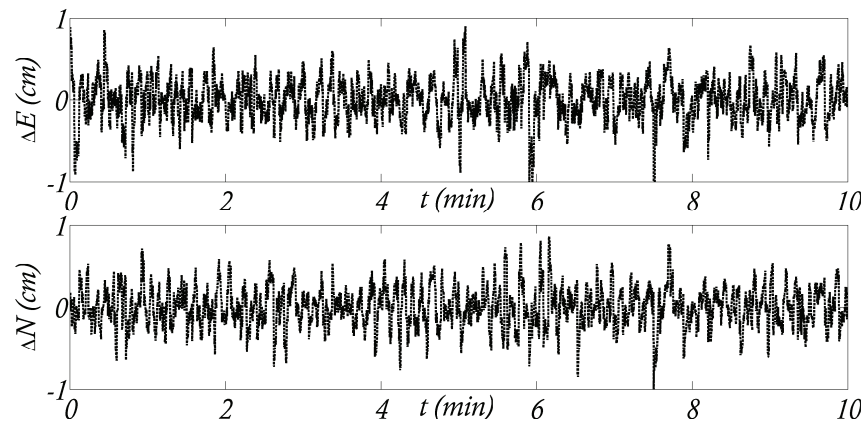


Figure 5.20. N20 GPS in-plane displacement time histories for ambient vibrations as estimated by a conversion factor: along Y measurements (top), along X measurements (bottom)

The displacements time histories of S9 are also drawn in Figure 5.21 (without the applications of the factors of conversion) and in Figure 5.22 (with the application of the factors of conversion). In each of the two figures, the top plot represents the East component and the bottom plot the North one (i.e., Y and X directions respectively).

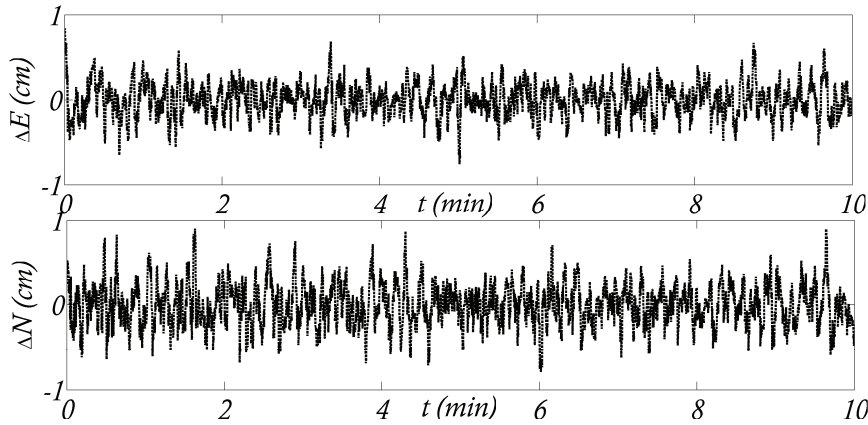


Figure 5.21. S9 GPS in-plane displacement time histories for ambient vibrations as recorded: along Y measurements (top), along X measurements (bottom)

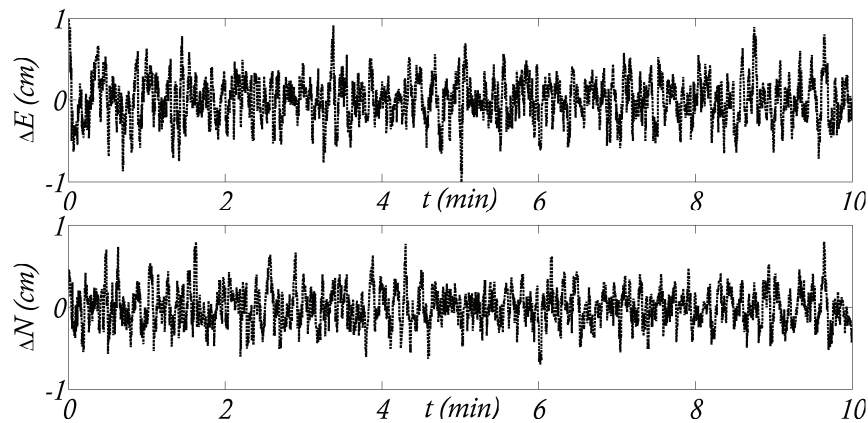


Figure 5.22. S9 GPS in-plane displacement time histories for ambient vibrations as estimated by a conversion factor: along Y measurements (top), along X measurements (bottom)

The time history of the torsional angle of rotation φ of the top in-plane section is plotted in Figure 5.23, where an extract of 10 minutes when no significant winds events occurred is showed. It is worth noting that in this calculation the displacements of S9 and N20 adopted are those calibrated by the factors of conversion.

The maximum angle of rotation is around 0.13° , which corresponds to around the 10% of the angle of rotation φ as calculated from the elaborations during the #Nur08 typhoon.

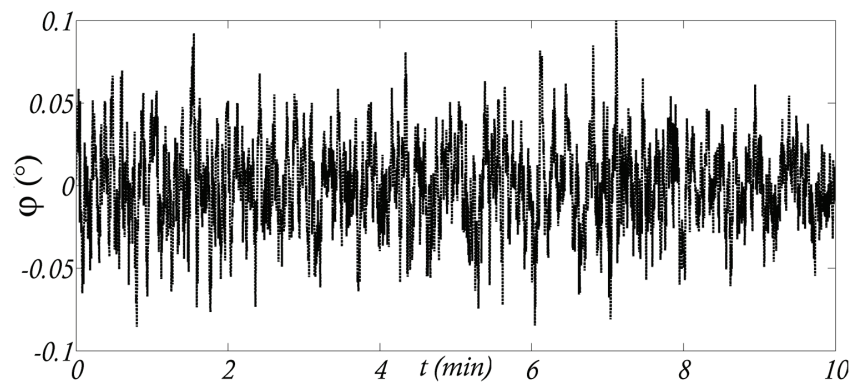


Figure 5.23. The time history of rotation angle φ for #Mar09 tests

On March 19, 2009 accelerometers data were also recorded. The location of the accelerometers was the same of that of #Nur08 and #Hag08 test, while the height was different, as the accelerometers where placed at the same level of the GPS sensors adopted in #Mar09 tests.

The possibility of having also accelerometers measurements in a clear day free of any wind event provided the ability to conduct a further investigation with the following two main purposes:

- (a) a direct comparison of the torsional angle of rotation φ and the twist angle γ in the absence of any significant wind event with those calculated for #Nur08 and #Hag08 typhoons;
- (b) an evaluation of GPS accuracy in detecting the torsional response of a flexible structure under very low vibrations due to the absence of winds.

The same procedure of #Nur08 and #Hag08 was reconsidered. The results in terms of φ and γ are reported in Figures 5.24 and 5.25, with a duration of 40 minutes; specifically from 2.10 to 2.50p.m..

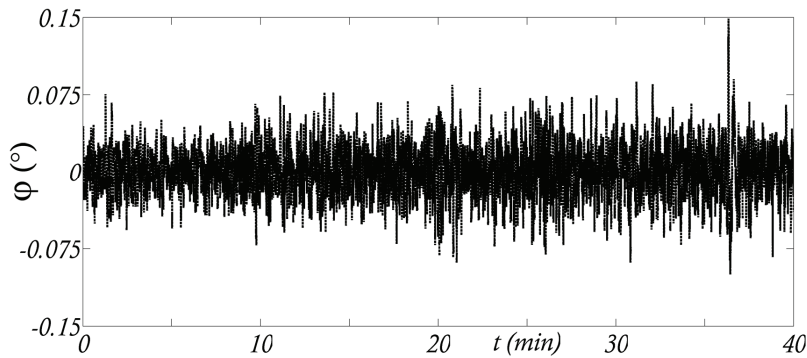


Figure 5.24. Time history of rotation angle φ for #Mar09 tests (accelerometers measurements)

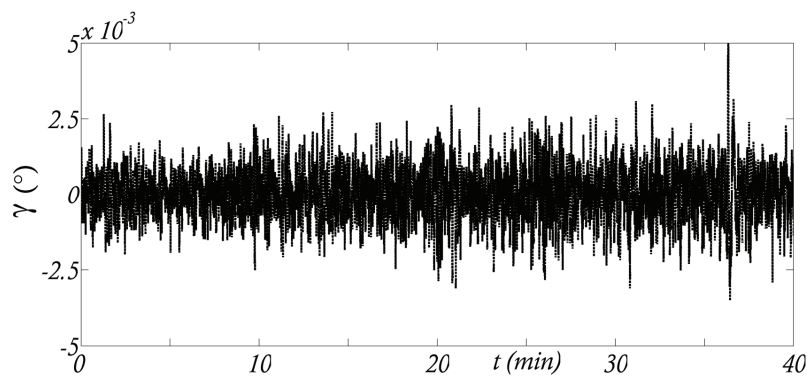


Figure 5.25. Time history of the twist angle γ for #Mar09 tests (accelerometers measurements)

The maximum angle of rotation φ as plotted in Figure 5.24 is around 0.14° , which corresponds to the maximum φ value as calculated from the three GPS measurements (0.13°). The maximum twist angle γ is around 0.007° , which is

around 10% less than the twist angle when calculated from the elaborations during the #Nur08 typhoon.

5.4 Conclusions

Chapter 5 presents a solution based on GPS and accelerometers sensors within the structural monitoring of the Guangzhou New TV Tower. The way to detect the torsional response due to typhoon wind events of this super-tall tower with inner oval cross section is analyzed under two different conditions:

- (a) during the #Nur08 and #Hag08 typhoons, when a rover GPS and two uni-axial accelerometers, placed at the top level of the tower, were installed;
- (b) during #Mar09 ambient vibrations tests, when a GPS network consisting of three rover receivers were placed at the top of the in-plane section.

The experimental measurements taken from the sensors (for the two scenarios) are analyzed to calculate two main torsional parameters, such as the angle of rotation φ of the oval cross section and the twist angle γ of the inner shaft cylinder. These two parameters are plotted as a function of time, taking into account the sensors measurements and their location, as requested by one task of the benchmark on the GNTTV.

For the typhoon events, the achievable results are affected by two effects: i) the use of two different types of sensors (accelerometers and GPS), which work independently each of the other, thus giving rise to a possible non synchronization of the recorded data; ii) the errors associated with the integration process from the accelerations measured by the accelerometers to the required displacements.

The idea is that these effects can be overcome by using several GPS sensors. The GPS topology on the plane top level of the tower is chosen as follows: one antenna is located in the centre of the inner tube and one (or more than one) at the edges (instead of accelerometers). Indeed it is required that the baselines connecting the reference and the rover(s) receivers are oriented along either the X axis or the Y axis.

The use of only GPS receivers also allows removing the suspected non synchronization of data, which may have occurred when the accelerometers had

to be considered. Furthermore, as the GPS is not only a displacement sensor but also a time sensor (see Chapter 1), this probably suggests using the GPS sensors for time synchronization.

Finally a significant purpose of this chapter is to analyze and compare the torsional behaviour of the tower with and without significant wind events.

To this aim a factitious procedure has to be applied when GPS and others sensors data are not recorded at the same time-measuring period of the day. The general proposed procedure is in this case applied to the GPS data as recorded during #Mar09 tests, by applying the following considerations:

(i) the GPS precision is influenced by the geometrical configuration of satellites overhead which is correlated to the geometric dilution of precision (GDOP);

(ii) the GDOP causes a fluctuation of the signal accuracy during the day;

(iii) this trend is the same for two different days (i.e., the GDOP factor has the same value if considering the same time interval of two different days) for the same receiver baseline configuration.

Assessing then that is not correct to compare data from GPS measurements taken in different time-measuring period of the day, it could be concluded that it is needed to convert the data recorded at rest at the same time interval of the measurements recorded during the typhoon.

Based on these assumption, the recorded GPS displacements for #Mar09 tests have been modified by applying a conversion factor, in order to recalculate the GPS displacements as they would have been recorded at the same time period (from 2.00 to 2.10p.m) of the data of #Nur08.

Measurements recorded by two uni-axial accelerometers during the #Mar09 tests have been also considered in order to prove the effectiveness of the GPS solution and to figure out a reference unstrained configuration of the torsional response of the tower.

Conclusions and Synthesis

The thesis analyzes the use of satellites systems for structural monitoring, with emphasis on the accuracy, uncertainty and reliability of the associated measurements. Among all the satellites systems, the Global Positioning System (GPS) is considered. The work is organized in five chapters.

Chapter 1 gives an overview of the GPS characteristics underling the process to calculate the satellite to user receiver distance, including the explanation of the time correlation process, the description of the signal modulation and the examination of the different sources of errors. Chapter 1 is preparatory to the development of the experimental results explained in Chapters 3, 4 and 5, as it introduces the basic concept of the measurements done by a Satellite Positioning System, with emphasis to the calculation of the three-dimensional position of points and the process of errors correction.

Chapter 2 gives the state of the art of the more significant GPS applications and solutions in Civil Engineering.

In particular this overview on GPS-based structural monitoring systems tries to focus attention on the different solutions proposed by the scientific community all over the world in the last two decades and on those aspects that are of common interest in GPS applications such as: (i) the achievable resolution, (ii) the combination of displacements amplitudes and frequencies detected, (iii) the dependence on the sampling rate and on the sensors orientation along the North or the East directions, (iv) the influence of the dilution of precision.

Chapter 3 discusses the level of accuracy that can be achieved by dual frequency GPS receivers to detect static and dynamic movements.

The results from static tests are analyzed with two precise purposes: (i) to quantify the geometric dilution of precision (GDOP) of the GPS measurements over two consecutive days (i.e., for two consecutive satellite configurations); (ii) to assess the maximum resolution that can be achieved. In particular how the accuracy of the GPS along the East, North and vertical directions can fluctuate during the day as a function of the GDOP is underlined. A significant result has been to show how the GPS measurements are strongly influenced by the orientation of the baseline connecting rover and reference receivers and how this influence is more appreciated along the East component rather than the North and the vertical ones.

A second part of chapter 3 is devoted to assessing the precision of GPS measurements during dynamic tests where movements of different amplitudes and frequency are realized by a linear actuator. The main purpose within this section has been to analyze the range of amplitudes and frequencies which can be tracked by dual-frequency high precision GPS sensors. The major outcome of these tests has been to show how the GPS accuracy depends on the combination of amplitude and rate of the imposed movements, in a range from 5 to 10mm in amplitude and with a variation from 0.1 to 4Hz in frequency.

Chapter 4 presents the results of full-scale tests for long and short duration excitations. It is devoted to investigate the effectiveness of such a full-scale implementation. The steel building which host the authors laboratory is chosen as case study. Natural (i.e., wind) and man made (i.e., movement of the internal bridge crane) dynamic actions are considered.

A first part of the chapter covers problems characterized by excitation of long duration and verifies the tracking ability of the GPS receivers for displacements induced in a steel structure by the wind actions for different wind events, for different satellites configuration and for different sampling rate of the recorded signals (from 1 to 10Hz).

A second part on the contrary concerns the detection of the response to pulse actions (short duration actions) as the movements of the bridge-crane inside the building. By comparing, both in the time and in the frequency domain, the accelerations computed from the GPS data with the accelerations directly measured by accelerometers, the potential offered by the GPS approach for monitoring dynamic displacements is emphasized. In particular a strong correspondence in the frequency domain between the GPS and the accelerometers measurements is shown.

The last part of the chapter pursues the structural identification of the building from the GPS recorded signals. The identification/validation process exploits the response to movements of the internal bridge-crane. For this purpose a FE model of the steel building is conceived and implemented. The simulations are carried out in two different scenarios of dynamical excitation induced by the bridge-crane. The results agreement in the two cases validates the FE model, thus confirming that the GPS is a promising experimental tool in the field of civil engineering.

Chapter 5 emphasizes the data processing of GPS records for a second full-scale monitoring application. The Guangzhou New TV Tower in China is considered as case study.

The way to detect the torsional response of the tower is analyzed for two different scenarios: during strong typhoon events (which are very common in that area) and during ambient vibrations. The torsional parameters (i.e., the angle of rotation of the cross section and the twist angle of the inner shaft) are calculated for both cases and then a procedure for their comparison for the two scenarios is elaborated taking into account the dependence of the GPS data on the satellite constellation configuration (as a function of the so-called “geometric dilution of precision”). The influence of the sensor locations and positions on the measurements accuracy, the integration of GPS with accelerometers, the problem of time synchronization are other interesting aspects that have been underlined.

Concluding, the main contributions of the thesis can be therefore summarized as follows:

(i) the quantization of the accuracy fluctuation during the day in terms of the geometric dilution of precision and its dependence on the orientation of the reference-rover baseline connection;

(ii) the demonstration of the frequency dependence feature of the GPS measurements for dynamic applications when small displacement amplitudes are considered;

(iii) the effectiveness of the GPS solution in both long duration (i.e., wind events) and short duration records (i.e., impulse force), for both very low and rather high frequencies;

(iv) the elaboration of a procedure that need to be considered when comparing GPS data recorded at different time-measuring period of the day or GPS data with other sensors measurements.

Biography

- A Benchmark Problem for the Structural Health Monitoring of High-Rise Slender Structures, <http://www.cse.polyu.edu.hk/benchmark/index.htm>.
- AlSaleh R., Casciati F., Fuggini C. (2009). "Detecting the torsional behavior of a tall building by GPS receivers", *Proceedings of the COMPDYN 2009, ECCOMAS Thematic Conference on Computational Methods in Structural Dynamics and Earthquake Engineering*, Rhodes, CD-ROM (article CD438).
- Ansys Inc. (2005). *ANSYS and CivilFEM 9.0 User Manual*, Madrid.
- Ashkenazi V., Dodson A. H., Moore T., Roberts G. W. (1996). "Real time OTF GPS monitoring of the Humber Bridge", *Surveying World*, vol. 4, no. 4, 26-28.
- Ashkenazi V., Dodson A. H., Moore T., Roberts G. W. (1997). "Monitoring the movement of bridges by GPS", *Proceedings of the 10th Int. Tech. Meeting of the Satellite Division of the U.S. Institute of Navigation*, Kansas City, Missouri, 1165-1172.
- Ashkenazi V., Roberts G. W. (1997). "Experimental monitoring of the Humber bridge using GPS", *Proceedings of the Institution of Civil Engineers*, vol. 120, no. 4, 177-182.
- Barnes J., Rizos C., Wang J., Meng X., Dodson A. H., Roberts G. W. (2003). "The monitoring of bridge movements using GPS and pseudolites", *Proceedings of the 11th Int. Symp. on Deformation Measurements*, Santorini, 563-572.
- Barnes J., Rizos C., Lee H. K., Roberts G. W., Meng X., Cosser E., Dodson A. H. (2005). "The integration of GPS and pseudolites for bridge monitoring", *A Window on the Future of Geodesy*, F. Sanso (ed.), IAG Symp., 128, Springer-Verlag, 83-88.
- Barnes J., Cranenbroeck J. Van. (2006). "The potential of a ground based transceivers network for water dam deformation monitoring", *Proceedings of the International Conference Hydropower*, Kunming, 765-795.

- Breuer P., Chmielewski T., Gorski P., Konopka E. (2002). "Application of GPS Technology to Measurements of Displacements of High-rise Structures Due to Weak Winds," *Journal of Wind Engineering and Industrial Aerodynamics*, 90, 223–230.
- Brown N., Troyer L., Zelzer O., Cranenbroeck J. Van. (2006). "Advances in RTK and Post Processed Monitoring with Single Frequency GPS", *Journal of Global Positioning Systems*, vol. 5, no. 1, 145-151.
- Brownjohn J. M. W., Moyo P., Rizos C., Chuan T. S. (2003a). "Practical issues in using novel sensors in SHM of civil infrastructure: Problems and solutions in implementation of GPS and fibre optics", *Proceedings of the 4th Int. Workshop on Structural Health Monitoring*, Stanford University, 499-506.
- Brownjohn J. M. W., Stringer M., Tan G.H., Poh Y.K., Ge L., Pan T.C. (2003b). "Experience with RTK-GPS system for monitoring wind and seismic effects on a tall building", *Proceedings of the 4th Int. Workshop on Structural Health Monitoring*, Stanford University.
- Brownjohn J. M. W., Rizos C., Tan G. H., Pan T. C. (2004). "Real-time long-term monitoring and static and dynamic displacements of an office tower, combining RTK GPS and accelerometer data", *Proceedings of the 1st FIG Int. Symp. on Engineering Surveys for Construction Works & Structural Eng.*, Nottingham, U.K., paper TS1.4, CD-ROM.
- Campbell S., Kwok K.C.S., Keung Y.L., Hitchcock P.A. (2006). "Full-scale Monitoring of a High-residential Building Using GPS Under Typhoon Conditions", *Proceedings of the 4th World Conference on Structural Control and Monitoring*, San Diego, paper 373.
- Casciati F., Fuggini C. (2007). "Ricevitori GPS a doppia frequenza: affidabilità di precisione nelle misure", *Proceedings of the 12th National Conference on Non-Destructive tests, Monitoring and Diagnostic (AIPnD 2007)*, Milan, CD ROM (article n°16), published online on *The e-Journal of Nondestructive Testing*, (<http://www.ndt.net>, article n° 7255).
- Casciati F., Fuggini C., Bonanno C. (2007). "Dual Frequency GPS Receivers: Reliability of Precision of the Measures", *Proceedings 4^{ème} Colloque en Interdisciplinaire en Instrumentation C2I*, Nancy, Hermes Science, 604–612.
- Casciati F., Fuggini C. (2008a). "Measuring the displacements of a steel structure by GPS units", *Proceedings of 1st International Symposium on Life-Cycle Engineering*, Varenna, Taylor & Francis, 501-506.
- Casciati F., Fuggini C. (2008b) "Monitoring an Industrial Steel Building by GPS Receivers", *Proceedings of the 4th European Workshop on Structural Health Monitoring*, Cracow, DEStech Publications Inc., 219-226.

- Casciati F., Fuggini C. (2008c). "GPS Based Structural Identification and health monitoring", *Proceedings of the Fourth European Conference on Structural Control*, St. Petersburg, 133-140.
- Casciati F., Alsaleh R., Fuggini C. (2009). "GPS-Based SHM of a tall building: torsional effects", *Proceedings of the 7th International Workshop on Structural Health Monitoring 2009*, Stanford University, Stanford, 340-347.
- Casciati F., Fuggini C. (2009a). "Towards Global Positioning System-Based Structural Health Monitoring", *Trends in Civil and Structural Engineering Computing*, Topping, B.H.V., Costa Neves, L.F., Barros R.C. (Eds), Saxe-Coburg Publications, Stirlingshire, UK, Chapter 15, 319-352.
- Casciati F., Fuggini C. (2009b). "Engineering Vibration Monitoring by GPS: Long Duration Records", *Earthquake Engineering and Engineering Vibration*, vol.8, no.3, 459-467.
- Casciati F., Fuggini C. (2009c) "GPS Based Structural Health Monitoring: Uncertainty of the Measurements", *Proceedings of the 10th International Conference on Structural Safety and Reliability (ICOSSAR2009)*, Kansai University, 2108-2114.
- Cazzaniga N.E., Pinto L. (2006), "Structural Monitoring with GPS and Accelerometers: the Chimney of the Power Plant in Piacenza", *3rd IAG Symposium on Geodesy for Geotechnical and Structural Engineering and 12th FIG Symposium on Deformation Measurements*, Baden.
- Celebi M., Prescott W., Stein R., Hudnut K., Behr J., Wilson S. (1999). "GPS monitoring of dynamic behavior long-period structures", *Earthquake Spectra*, vol. 15, 55-66.
- Celebi M. (2000). "GPS in Dynamic Monitoring of Long-period Structures", *Soil Dynamics and Earthquake Engineering*, vol. 20, 477-483.
- Celebi M., Sanli A. (2002). "GPS in pioneering dynamic monitoring of long-period structures", *Earthquake Spectra*, vol. 18, no. 1, 47-61.
- Chan W. S., Xu Y. L., Ding X. L., Dai W. J. (2006). "An integrated GPS-accelerometer data processing technique for structural deformation monitoring", *J Geodesy*, vol. 80, no. 12, 705-719.
- Chen Y., Huang D., Ding, X. (2001). "Measurement of vibrations of tall buildings with GPS: a case study", *Health Monitoring & Management of Civil Infrastructure Systems*, Chase S.B., Aktan A.E. (Eds.), vol. 4337, 477-483.
- Cheng P., Shi W. J., Zheng W. (2002). "Large Structure Health Dynamic Monitoring Using GPS Technology", *Proceedings of the FIG XXII International Congress*, Washington, TS6.2.

- Cosser E., Roberts G. W., Meng X., Dodson A. (2004). "Single Frequency GPS for Bridge Deflection Monitoring: Progress and Results", *Proceedings of the 1st FIG International Symposium on Engineering Surveys for Construction Works and Structural Engineering*, Nottingham, paper TS4.3.
- Dana P.H. (1997). "Global Positioning System (GPS) Time Dissemination for Real-time Applications, Real time Systems", *The International Journal of Time Critical Computing Systems*, vol. 12, 9-40.
- Dodson A., Meng X., Roberts G. W., Cosser E., Barnes J., Rizos C. (2003). "Integrated approach of GPS and pseudolites for bridge deformation monitoring", *Proceedings of the GNSS2003conference*, Graz, CD-ROM, paper 205.
- Duff K., Hyzak M. (1997). "Structural monitoring with GPS", *Public Roads Magazine*, vol. 60, no. 4.
- Erdogan H., Akpmar P., Gulal L., Ata E. (2007). "Monitoring the dynamic behaviors of the Bosphorus Bridge by GPS during Eurasia Marathon", *Nonlin. Processes Geophys.*, vol. 14, 513–523.
- Faravelli L., Casciati S., Fuggini C. (2009). "Full-scale experiment using GPS sensors for dynamic tests", *Proceedings of the XIX Congress AIMETA*, Ancona, CD-ROM.
- Fujino Y., Murata M., Okano S., Takeguchi M. (2000). "Monitoring system of the Akashi Kaikyo Bridge and displacement measurement using GPS", *Proceedings of the SPIE conference*, vol. 3995, 229-236.
- Ge L., Li X., Peng G. D., Rizos C., Ishikawa Y. (2002). "Intelligent skyscraper monitoring system based on GPS and Optical Fibre Sensors", *Proceedings of the 15th Int. Tech. Meeting of the Satellite Division of the U.S. Inst. of Navigation*, Portland, 896-903.
- Guo J., Ge, L. (1997). "Research of Displacement and Frequency of Tall Building under Wind Load Using GPS", *Proceedings of the 10th Int. Tech. Meeting of the Satellite Division of the U.S. Inst. of Navigation, ION GPS-97*, Kanadas City, 1385–1388.
- Guo J., Xu L., Dai L., McDonald M., Wu J., Li Y. (2005). "Application of the real-time kinematic Global Positioning System in bridge safety monitoring", *Journal of Bridge Engineering*, vol. 10, no. 2, 163-168.
- Hopfield H.S. (1969). "Two–quadratic Tropospheric Refractivity Profile for Correction Satellite Data", *Journal of Geophysical Research*, vol. 7, no. 18, 4487-4499.
- Hristopulos D.T., Mertikas S.P., Arhontakis I., Brownjohn J.M.W. (2007). "Using GPS for Monitoring Tall-building Response to Wind Loading:

- Filtering of Abrupt Changes and Low-frequency Noise, Variography and Spectral Analysis of Displacements”, *GPS Solutions*, vol. 11, 85-95.
- Kalooop M.R., Li H. (2009). “Tower Bridge Movement Analysis with GPS and Accelerometer Techniques: Case Study Yonghe Tower Bridge”, *Information technology journal*, 1-8.
- Kaplan E., Hegarty C. (2006). *Understanding GPS Principles and Applications*, Artech House, Boston, 2nd edition.
- Kijewski-Correa T.L., Kareem A. (2003a). “The height of precision”, *GPS World*, 20-34.
- Kijewski-Correa T.L., Kareem A. (2003b). “The Chicago Monitoring Project: a Fusion of Information Technologies and Advanced Sensing for Civil Infrastructures,” *Proceedings of the 1st International Conference on Structural Health Monitoring and Intelligent Infrastructure*, Tokyo, 1003-1010.
- Kijewski-Correa T.L., Kareem A., Kochly M. (2006). “Experimental Verification and Full-scale Deployment of Global Positioning Systems to Monitor the Dynamic Response of Tall Buildings”, *Journal of Structural Engineering*, vol. 132, no. 8, 1242-1253.
- Kijewski-Correa T.L., Kochly M. (2007). “Monitoring the wind-induced response of tall buildings: GPS performance and the issue of multipath effects”, *Journal of Wind Engineering and Industrial Aerodynamics*, vol. 95, 1176-1198.
- Klobuchar, J. A. (1982). “Ionospheric corrections for the single frequency user of the Global Positioning System”, *Proceedings of the National Tele-Systems Conference*, Galveston, US.
- Larocca A.P.C. (2004). “Using high-rate GPS data to monitor the dynamic behaviour of a cable-stayed bridge”, *Proceedings of the 17th Int. Tech. Meeting of the Satellite Division of the U.S. Institute of Navigation*, Long Beach, 225-234.
- Larocca A.P.C., Schaal R.E. (2005). “Millimeters in motion: Dynamic response precisely measured”, *GPS World*, vol. 16, no. 1, 16-25.
- Leica (2004). “LEICA GPS Spider-Reference Station”, *Leica Geosystems*, 1-20.
- Leica (2005). “GMX 902 User Manual”, *Leica Geosystems*, 1-32.
- Leica (2007). “Man-made structures”, *Leica Geosystems*, http://www.leica-geosystems.com/en/Man-Made-Structures_1703.htm.
- Leick A. (1995). *GPS Satellite Surveying*, John Wiley & Sons Inc., New York.
- Lekidis V., Tsakiria M., Makrab K., Karakostasb C., Klimisb N., Sous I. (2005). “Evaluation of Dynamic Response and Local Soil Effects of the

- Evripos Cablestayed Bridge Using Multi-sensor Monitoring Systems,” *Engineering Geology*, vol. 79, 43-59.
- Li X. (2004). “Integration of GPS, accelerometers and optical fibre sensors for structural deformation monitoring”, *Proceedings of the 17th Int. Tech. Meeting of the Satellite Division of the U.S. Institute of Navigation*, Long Beach, 211-224.
- Li X., Ge L., Ambikairajah E., Rizos C., Tamura Y. (2005). “Analysis of seismic response of a tall tower monitored with an integrated GPS and accelerometer system”, *Journal of Geospatial Engineering*, vol. 7, no. 1, 30-38.
- Li X., Ge L., Ambikairajah E., Rizos C., Tamura Y., Yoshida A. (2006). “Full-scale Structural Monitoring Using an Integrated GPS and Accelerometer System”, *GPS Solutions*, vol. 10, no. 4, 233-247.
- LinMot (2008). “Documentation of LinMot Configuration Software”, *LinMot User Manual*, 1-39.
- Lovse J.W., Tesky W.F., Lachapelle G. (1995). “Dynamic deformation monitoring of tall structure using GPS technology”, *Journal of Surveying Engineering*, Vol. 121, n°1, 16-22.
- Matlab (2004). *The MathWork Inc.*, Version 7 (R14).
- Meng X., Roberts G.W., Cosser E., Dodson A.H. (2003). “Real-Time bridge deflection and vibration monitoring using an integrated GPS/accelerometer/pseudolite system”, *Proceedings of the 11th Int. Symp. on Deformation Measurements*, Santorini, <http://www.fig.net/commission6/santorini/index.htm>.
- Meng X., Dodson A.H., Roberts G.W. (2007). “Detecting Bridge Dynamics with GPS and Triaxial Accelerometers”, *Engineering Structures*, vol. 29, 3178- 3184.
- Nakamura S. (2000). “GPS measurement of wind-induced suspension bridge girder displacements”, *Journal of Structural Engineering*, vol. 126, no. 12, 1413-1419.
- Ni Y. Q., Xia Y., Liao W. Y., Ko J. M. (2009) “Technology innovation in developing the structural health monitoring system for Guangzhou New TV Tower”, *Struct. Control and Health Monit.*, vol. 16, no. 1, 73-98.
- Nickitopoulou A., Protopsalti K., Kantogianni V., Triantafillidis P., Stiros S. (2003) “Experimental assessment of the accuracy of RTK-GPS for monitoring movements/oscillations of flexible engineering structures”, *Proceedings of the 11th Symposium on Deformation Measurements*, Santorini, <http://www.fig.net/commission6/santorini/index.htm>

- Nickitopoulou A., Protopsalti K., Stiros S. (2006) "Monitoring Dynamic and Quasi-static Deformations of Large Flexible Engineering Structures with GPS: Accuracy, Limitations and Promises", *Engineering Structures*, vol. 28, 1471-1482.
- Ogaja C., Rizos C., Wang J., Brownjohn J.M.W. (2001). "A dynamic GPS system for on-line structural monitoring", *Proceedings of the Int. Symp. on Kinematic Systems in Geodesy, Geomatics & Navigation*, Banff, 290-297.
- Ogaja C., Wang J., Rizos C. (2003). "Detection of wind-induced response by wavelet transformed GPS solutions", *Journal of Surveying Engineering*, vol. 129, no. 3, 99-104.
- Ogaja C., Li X., Rizos C. (2007). "Advances in Structural Monitoring with Global Positioning System Technology: 1997-2006", *Journal of Applied Geodesy*, vol. 1, no. 3, 171-179.
- Psimoulis P., Pytharouli S., Karambalis D., Stiros S. (2008). "Potential of Global Positioning System (GPS) to Measure the Frequencies of Oscillations of Engineering Structures", *Journal of Sound and Vibration*, vol. 318, 606-623.
- Psimoulis P., Stiros S. (2008) "Experimental Assessment of the Accuracy of GPS and RTS for the Determination of the Parameters of Oscillation of Major Structures", *Computer-Aided Civil and Infrastructure Engineering*, vol. 23, 389-403.
- Raziq N., Collier P. (2007). "GPS deflection monitoring of the West Gate Bridge", *Journal of Applied Geodesy*, no.1, 35-44.
- Rizos C., Li X., Ge L., Tamura Y., Yoshida A. (2008). "How far could GPS go in monitoring structural response to wind events?", *Proceedings of the 13th Symposium on Deformation Measurement and Analysis*, Lisbon, CD ROM.
- Roberts G.W., Dodson A.H., Ashkenazi V. (1999). "Twist and deflect: Monitoring motion of the Humber Bridge", *GPS World*, vol. 10, no. 10, 24-34.
- Roberts G.W., Cosser E., Meng X., Dodson A.H. (2004a). "High frequency deflection monitoring of bridges by GPS". *Journal of Global Positioning Systems*, vol. 3, no. 1-2, 226-231.
- Roberts G.W., Meng X., Dodson A.H. (2004b). "Integrating a Global Positioning System and accelerometers to monitor the deflection of bridges", *Journal of Surveying Engineering*, vol. 130, no. 2, 65-72.
- Roberts G.W., Brown C., Meng X., (2006). "Deflection monitoring and frequency analysis of the Fourth Road Bridge using GPS", *Proceedings of the 3rd IAG and 12th FIG Symposium*, Baden.

- Saastamoinen, J. (1972). "Atmospheric correction for the troposphere and stratosphere in radio ranging of satellites." *The use artificial satellites for geodesy, Geophysical Monograph*, no. 15, 247-251.
- Satirapod C., Chalermwattanachai P. (2005). "Impact of Different Tropospheric Models on GPS Baseline Accuracy: Case Study in Thailand", *Journal of Global Positioning Systems*, vol.4, no. 1-2, 36-40
- Schaal R.E., Larocca A.P.C. (2002). "A methodology to use the GPS for monitoring vertical dynamic sub-centimeter displacement", *GPS Solutions*, vol. 5, no. 3, 15-18.
- Saeky M., Hori M. (2006). "Development of an Accurate Positioning System Using Low-Cost L1 GPS receivers", *Computed-Aided Civil and Infrastructure Engineering*, vol. 21, 258-267.
- Seco A., Tirapu F., Ramirez F., Garcia B., Cabrejas J. (2007). "Assessing Building Displacement with GPS", *Building and Environment*, vol. 42, 393-399.
- Smyth A.W., Wu M., Kogan M. (2006). "Data Fusion of GPS Displacement and acceleration response measurements for large scale bridges", *Proceedings of the 4th World Conference on Structural Control and Monitoring*, San Diego, paper 279.
- Sumitro S., Wang M. L. (2005). "Sustainable structural health monitoring system", *Structural Control and Health Monitoring*, vol. 12, 445-467.
- Tamura Y., Matsui M., Pagnini L.C., Ishibashi R., Yoshida A. (2002). "Measurement of Wind Induced Response of Building Using RTK-GPS", *Journal of Wind Engineering and Industrial Aerodynamics*, vol. 90, 1783-1793.
- Tamura Y., Yoshida A. (2006). "Wind Induced Response and Integrity Monitoring of Structures by GPS", *Proceedings of the 4th World Conference on Structural Control and Monitoring*, San Diego, paper 072.
- Turner L. (2003). "Continuous GPS: Pilot Applications-Phase II (Final Report)", *California Department of Transportation*, Sacramento.
- Wong K.Y., Man K., Chan W. (2001). "Monitoring Hong Kong's bridges: Real-Time Kinematic spans the gap", *GPS World*, vol. 12, no. 7, 10-18.
- Wong K.Y. (2004). "Instrumentation and Health Monitoring of Cable-supported Bridges", *Structural Control and Health Monitoring*, vol. 11, 91-124.
- Xu L., Guo J.J., Jiang J.J. (2002). "Time-frequency Analysis of a Suspension Bridge Based on GPS", *Journal of Sound and Vibration*, vol. 254, no. 1, 105-116.
- Xu G. (2007). *GPS: Theory, Algorithms and Applications*, Springer Berlin Heidelberg New York, 2nd edition.

- Yamada H., Katsuchi H., Chanpheng T., Kusuhara S. (2006). "GPS-Based Monitoring of Wind-Induced Response of Akashi Kaikyo Bridge", *Proceedings of the 4th World Conference on Structural Control and Monitoring*, San Diego, paper 060.
- Yigit C. O., Inal C., Yetkin M. (2008). "Monitoring of tall building's dynamic behaviour using precise inclination sensors", *Proceedings of the 13th FIG Symposium on Deformation Measurements and Analysis – 4th IAG Symposium on Geodesy for Geotechnical and Structural Engineering*, Lisbon.